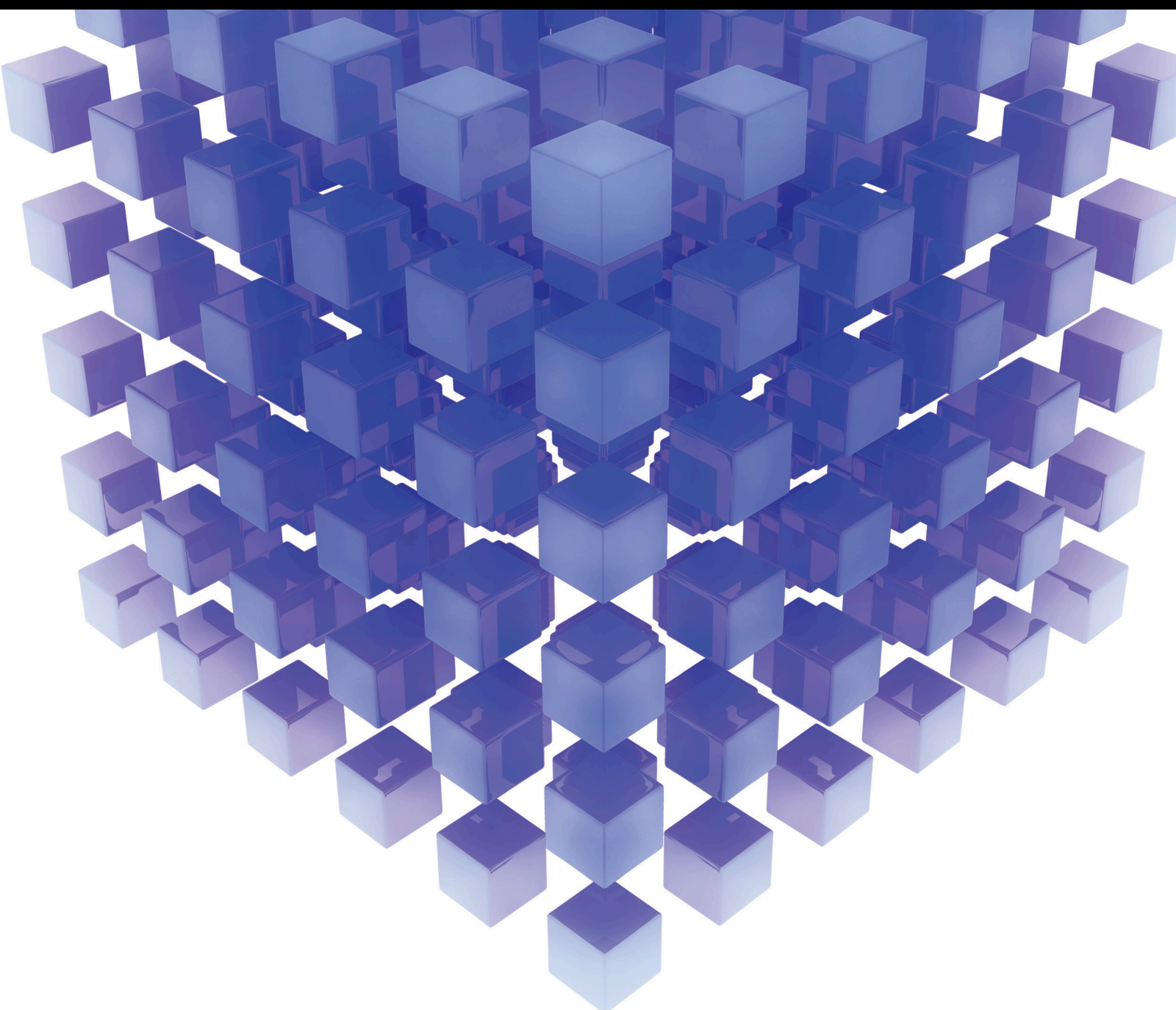


Various Approaches for Generalized Integral Transforms

Lead Guest Editor: Hwajoon Kim

Guest Editors: Arjun K. Rathie and Young Hee Geum





Various Approaches for Generalized Integral Transforms

Mathematical Problems in Engineering

Various Approaches for Generalized Integral Transforms

Lead Guest Editor: Hwajoon Kim

Guest Editors: Arjun K. Rathie and Young Hee
Geum



Copyright © 2021 Hindawi Limited. All rights reserved.

This is a special issue published in “Mathematical Problems in Engineering.” All articles are open access articles distributed under the Creative Commons Attribution License, which permits unrestricted use, distribution, and reproduction in any medium, provided the original work is properly cited.

Chief Editor

Guangming Xie, China

Editorial Board

Mohamed Abd El Aziz, Egypt
Ahmed A. Abd El-Latif, Egypt
Mahmoud Abdel-Aty, Egypt
Mohammad Yaghoub Abdollahzadeh
Jamalabadi, Republic of Korea
Rahib Abiyev, Turkey
Leonardo Acho, Spain
José Ángel Acosta, Spain
Daniela Addressi, Italy
Paolo Addresso, Italy
Claudia Adduce, Italy
Ramesh Agarwal, USA
Francesco Aggogeri, Italy
Ricardo Aguilar-Lopez, Mexico
Ali Ahmadian, Malaysia
Tarek Ahmed-Ali, France
Elias Aifantis, USA
Akif Akgul, Turkey
Guido Ala, Italy
Andrea Alaimo, Italy
Reza Alam, USA
Nicholas Alexander, United Kingdom
Salvatore Alfonzetti, Italy
Nouman Ali, Pakistan
Mohammad D. Aliyu, Canada
Juan A. Almendral, Spain
Watheq Al-Mudhafar, Iraq
Ali Saleh Alshomrani, Saudi Arabia
José Domingo Álvarez, Spain
Cláudio Alves, Portugal
Juan P. Amezquita-Sanchez, Mexico
Lionel Amodeo, France
Sebastian Anita, Romania
Renata Archetti, Italy
Muhammad Arif, Pakistan
Sabri Arik, Turkey
Francesco Aristodemo, Italy
Fausto Arpino, Italy
Alessandro Arsie, USA
Edoardo Artioli, Italy
Rashad Asharabi, Saudi Arabia
Fumihiko Ashida, Japan
Farhad Aslani, Australia
Mohsen Asle Zaem, USA

Andrea Avanzini, Italy
Richard I. Avery, USA
Viktor Avrutin, Germany
Mohammed A. Awadallah, Malaysia
Muhammad Uzair Awan, Pakistan
Francesco Aymerich, Italy
Sajad Azizi, Belgium
Michele Bacciocchi, Italy
Seungik Baek, USA
Khaled Bahlali, France
Pedro Balaguer, Spain
Stefan Balint, Romania
Ines Tejado Balsera, Spain
Alfonso Banos, Spain
Jerzy Baranowski, Poland
Tudor Barbu, Romania
Andrzej Bartoszewicz, Poland
Sergio Baselga, Spain
S. Caglar Baslamisli, Turkey
David Bassir, France
Chiara Bedon, Italy
Azeddine Beghdadi, France
Andriette Bekker, South Africa
Abdellatif Ben Makhlof, Saudi Arabia
Denis Benasciutti, Italy
Ivano Benedetti, Italy
Rosa M. Benito, Spain
Elena Benvenuti, Italy
Giovanni Berselli, Italy
Giorgio Besagni, Italy
Michele Betti, Italy
Pietro Bia, Italy
Carlo Bianca, France
Vittorio Bianco, Italy
Simone Bianco, Italy
Vincenzo Bianco, Italy
David Bigaud, France
Sardar Muhammad Bilal, Pakistan
Antonio Bilotta, Italy
Sylvio R. Bistafa, Brazil
Bartłomiej Błachowski, Poland
Chiara Boccaletti, Italy
Guido Bolognesi, United Kingdom
Rodolfo Bontempo, Italy

Alberto Borboni, Italy
Marco Bortolini, Italy
Paolo Boscariol, Italy
Daniela Boso, Italy
Guillermo Botella-Juan, Spain
Boulaïd Boulkroune, Belgium
Abdesselem Boulkroune, Algeria
Fabio Bovenga, Italy
Francesco Braghin, Italy
Ricardo Branco, Portugal
Maurizio Brocchini, Italy
Julien Bruchon, France
Matteo Bruggi, Italy
Michele Brun, Italy
Maria Elena Bruni, Italy
Vasilis Burganos, Greece
Maria Angela Butturi, Italy
Raquel Caballero-Águila, Spain
Guillermo Cabrera-Guerrero, Chile
Filippo Cacace, Italy
Pierfrancesco Cacciola, United Kingdom
Salvatore Caddemi, Italy
zuowei cai, China
Roberto Caldelli, Italy
Alberto Campagnolo, Italy
Eric Campos, Mexico
Salvatore Cannella, Italy
Francesco Cannizzaro, Italy
Maosen Cao, China
Javier Cara, Spain
Raffaele Carli, Italy
Ana Carpio, Spain
Rodrigo Carvajal, Chile
Caterina Casavola, Italy
Sara Casciati, Italy
Federica Caselli, Italy
Carmen Castillo, Spain
Inmaculada T. Castro, Spain
Miguel Castro, Portugal
Giuseppe Catalanotti, United Kingdom
Nicola Caterino, Italy
Alberto Cavallo, Italy
Gabriele Cazzulani, Italy
Luis Cea, Spain
Fatih Vehbi Celebi, Turkey
Song Cen, China
Miguel Cerrolaza, Venezuela

M. Chadli, France
Gregory Chagnon, France
Ludovic Chamoin, France
Xiaoheng Chang, China
Kuei-Lun Chang, Taiwan
Ching-Ter Chang, Taiwan
Qing Chang, USA
Kacem Chehdi, France
Peter N. Cheimets, USA
Chih-Chiang Chen, Taiwan
Xiao Chen, China
He Chen, China
Zhiwen Chen, China
Xinkai Chen, Japan
Chien-Ming Chen, China
Shyi-Ming Chen, Taiwan
Kebing Chen, China
Xue-Bo Chen, China
Xizhong Chen, Ireland
Qiang Cheng, USA
Luca Chiapponi, Italy
Ryoichi Chiba, Japan
Francisco Chicano, Spain
Nicholas Chileshe, Australia
Tirivanhu Chinyoka, South Africa
Adrian Chmielewski, Poland
Seongim Choi, USA
Ioannis T. Christou, Greece
Hung-Yuan Chung, Taiwan
Simone Cinquemani, Italy
Roberto G. Citarella, Italy
Joaquim Ciurana, Spain
John D. Clayton, USA
Francesco Clementi, Italy
Piero Colajanni, Italy
Giuseppina Colicchio, Italy
Vassilios Constantoudis, Greece
Francesco Conte, Italy
Enrico Conte, Italy
Alessandro Contento, USA
Mario Cools, Belgium
Gino Cortellessa, Italy
Juan Carlos Cortés, Spain
Carlo Cosentino, Italy
Paolo Crippa, Italy
Erik Cuevas, Mexico
Guozeng Cui, China

Maria C. Cunha, Portugal
Mehmet Cunkas, Turkey
Peter Dabnichki, Australia
Luca D'Acierno, Italy
Zhifeng Dai, China
Weizhong Dai, USA
Purushothaman Damodaran, USA
Bhabani S. Dandapat, India
Giuseppe D'Aniello, Italy
Sergey Dashkovskiy, Germany
Adiel T. de Almeida-Filho, Brazil
Fabio De Angelis, Italy
Samuele De Bartolo, Italy
Abílio De Jesus, Portugal
Pietro De Lellis, Italy
Alessandro De Luca, Italy
Stefano de Miranda, Italy
Filippo de Monte, Italy
José António Fonseca de Oliveira Correia, Portugal
Jose Renato de Sousa, Brazil
Michael Defoort, France
Alessandro Della Corte, Italy
Laurent Dewasme, Belgium
Sanku Dey, India
Gianpaolo Di Bona, Italy
Angelo Di Egidio, Italy
Roberta Di Pace, Italy
Francesca Di Puccio, Italy
Ramón I. Diego, Spain
Yannis Dimakopoulos, Greece
Rossana Dimitri, Italy
Alexandre B. Dolgui, France
José M. Domínguez, Spain
Georgios Dounias, Greece
Bo Du, China
Z. Du, China
George S. Dulikravich, USA
Emil Dumic, Croatia
Bogdan Dumitrescu, Romania
Saeed Eftekhar Azam, USA
Antonio Elipe, Spain
Anders Eriksson, Sweden
R. Emre Erkmen, Canada
Ricardo Escobar, Mexico
Francisco Periago Esparza, Spain
Gilberto Espinosa-Paredes, Mexico

Leandro F. F. Miguel, Brazil
Andrea L. Facci, Italy
Giovanni Falsone, Italy
Hua Fan, China
Nicholas Fantuzzi, Italy
Muhammad Shahid Farid, Pakistan
Mohammad Fattahi, Iran
Yann Favennec, France
Fiorenzo A. Fazzolari, United Kingdom
Giuseppe Fedele, Italy
Roberto Fedele, Italy
Zhongyang Fei, China
Mohammad Ferdows, Bangladesh
Arturo J. Fernández, Spain
Jesus M. Fernandez Oro, Spain
Massimiliano Ferraioli, Italy
Massimiliano Ferrara, Italy
Francesco Ferrise, Italy
Constantin Fetecau, Romania
Eric Feulvarch, France
Iztok Fister Jr., Slovenia
Thierry Floquet, France
Eric Florentin, France
Gerardo Flores, Mexico
Alessandro Formisano, Italy
FRANCESCO FOTI, Italy
Francesco Franco, Italy
Elisa Francomano, Italy
Juan Frausto-Solis, Mexico
Shujun Fu, China
Juan C. G. Prada, Spain
Matteo Gaeta, Italy
Mauro Gaggero, Italy
Zoran Gajic, USA
Jaime Gallardo-Alvarado, Mexico
Mosè Gallo, Italy
Akemi Gálvez, Spain
Rita Gamberini, Italy
Maria L. Gandarias, Spain
Xingbao Gao, China
Hao Gao, Hong Kong
Shangce Gao, Japan
Zhong-Ke Gao, China
Yan Gao, China
Zhiwei Gao, United Kingdom
Giovanni Garcea, Italy
José García, Chile

Luis Rodolfo Garcia Carrillo, USA
Jose M. Garcia-Aznar, Spain
Akhil Garg, China
Harish Garg, India
Alessandro Gasparetto, Italy
Gianluca Gatti, Italy
Oleg V. Gendelman, Israel
Stylianos Georgantzinou, Greece
Fotios Georgiades, India
Parviz Ghadimi, Iran
Georgios I. Giannopoulos, Greece
Agathoklis Giaralis, United Kingdom
Pablo Gil, Spain
Anna M. Gil-Lafuente, Spain
Ivan Giorgio, Italy
Gaetano Giunta, Luxembourg
Alessio Gizzi, Italy
Jefferson L.M.A. Gomes, United Kingdom
HECTOR GOMEZ, Chile
José Francisco Gómez Aguilar, Mexico
Emilio Gómez-Déniz, Spain
Antonio M. Gonçalves de Lima, Brazil
David González, Spain
Chris Goodrich, USA
Rama S. R. Gorla, USA
Veena Goswami, India
Xunjie Gou, Spain
Jakub Grabski, Poland
Antoine Grall, France
George A. Gravvanis, Greece
Fabrizio Greco, Italy
David Greiner, Spain
Jason Gu, Canada
Federico Guarracino, Italy
Michele Guida, Italy
Muhammet Gul, Turkey
Hu Guo, China
Jian-Ping Guo, China
Dong-Sheng Guo, China
Zhaoxia Guo, China
Quang Phuc Ha, Australia
Li Haitao, China
Petr Hájek, Czech Republic
Shigeyuki Hamori, Japan
Zhen-Lai Han, China
Xingsi Han, China
Weimin Han, USA

Renke Han, United Kingdom
Thomas Hanne, Switzerland
Xinan Hao, China
Mohammad A. Hariri-Ardebili, USA
Khalid Hattaf, Morocco
Xiao-Qiao He, China
Defeng He, China
Fu-Qiang He, China
Ramdane Hedjar, Saudi Arabia
Jude Hemanth, India
Reza Hemmati, Iran
Nicolae Herisanu, Romania
Alfredo G. Hernández-Díaz, Spain
M.I. Herreros, Spain
Eckhard Hitzer, Japan
Paul Honeine, France
Jaromir Horacek, Czech Republic
S. Hassan Hosseinnia, The Netherlands
Yingkun Hou, China
Xiaorong Hou, China
Lei Hou, China
Yunfeng Hu, China
Gordon Huang, Canada
Can Huang, China
Sajid Hussain, Canada
Asier Ibeas, Spain
Wubshet Ibrahim, Ethiopia
Orest V. Iftime, The Netherlands
Przemyslaw Ignaciuk, Poland
Muhammad Imran, Pakistan
Giacomo Innocenti, Italy
Emilio Insfran Pelozo, Spain
Alessio Ishizaka, France
Nazrul Islam, USA
Benoit Jung, France
Benjamin Ivorra, Spain
Breno Jacob, Brazil
Tushar Jain, India
Amin Jajarmi, Iran
Payman Jalali, Finland
Mahdi Jalili, Australia
Prashant Kumar Jamwal, Kazakhstan
Łukasz Jankowski, Poland
Fahd Jarad, Turkey
Samuel N. Jator, USA
Juan C. Jauregui-Correa, Mexico
Kandasamy Jayakrishna, India

Reza Jazar, Australia
Khalide Jbilou, France
Isabel S. Jesus, Portugal
Chao Ji, China
Linni Jian, China
Qing-Chao Jiang, China., China
Bin Jiang, China
Peng-fei Jiao, China
Emilio Jiménez Macías, Spain
Xiaoliang Jin, Canada
Maolin Jin, Republic of Korea
Zhuo Jin, Australia
Dylan F. Jones, United Kingdom
Viacheslav Kalashnikov, Mexico
Mathiyalagan Kalidass, India
Tamas Kalmar-Nagy, Hungary
Zhao Kang, China
Tomasz Kapitaniak, Poland
Julius Kaplunov, United Kingdom
Konstantinos Karamanos, Belgium
Michal Kawulok, Poland
Irfan Kaymaz, Turkey
Vahid Kayvanfar, Iran
Krzysztof Kecik, Poland
Chaudry M. Khaliq, South Africa
Mukhtaj khan, Pakistan
Abdul Qadeer Khan, Pakistan
Mostafa M. A. Khater, Egypt
Kwangki Kim, Republic of Korea
Nam-Il Kim, Republic of Korea
Philipp V. Kiryukhantsev-Korneev, Russia
P.V.V Kishore, India
Jan Koci, Czech Republic
Ioannis Kostavelis, Greece
Sotiris B. Kotsiantis, Greece
Frederic Kratz, France
Vamsi Krishna, India
Petr Krysl, USA
Edyta Kucharska, Poland
Krzysztof S. Kulpa, Poland
Kamal Kumar, India
Michal Kunicki, Poland
Cedrick A. K. Kwuimy, USA
Kyandoghere Kyamakya, Austria
Ivan Kyrchei, Ukraine
Davide La Torre, Italy
Márcio J. Lacerda, Brazil

Risto Lahdelma, Finland
Giovanni Lancioni, Italy
Jaroslaw Latalski, Poland
Antonino Laudani, Italy
Hervé Laurent, France
Aimé Lay-Ekuakille, Italy
Nicolas J. Leconte, France
Kun-Chou Lee, Taiwan
Dimitri Lefebvre, France
Eric Lefevre, France
Marek Lefik, Poland
Gang Lei, Saudi Arabia
Yaguo Lei, China
Kauko Leiviskä, Finland
Thibault Lemaire, France
afonso lemonge, Brazil
Ervin Lenzi, Brazil
Roman Lewandowski, Poland
Zhen Li, China
ChenFeng Li, China
Jun Li, China
Yang Li, China
Yueyang Li, China
Jian Li, USA
Jian Lin, China
En-Qiang Lin, USA
Zhiyun Lin, China
Yao-Jin Lin, China
Bo Liu, China
Sixin Liu, China
Wanquan Liu, China
Yu Liu, China
Heng Liu, China
Yuanchang Liu, United Kingdom
Lei Liu, China
Jianxu Liu, Thailand
Bin Liu, China
Bonifacio Llamazares, Spain
Alessandro Lo Schiavo, Italy
Jean Jacques Loiseau, France
Francesco Lolli, Italy
Paolo Lonetti, Italy
Sandro Longo, Italy
António M. Lopes, Portugal
Sebastian López, Spain
Pablo Lopez-Crespo, Spain
Cesar S. Lopez-Monsalvo, Mexico

Luis M. López-Ochoa, Spain
Ezequiel López-Rubio, Spain
Vassilios C. Loukopoulos, Greece
Jose A. Lozano-Galant, Spain
Gabriele Maria Lozito, Italy
Songtao Lu, USA
Rongxing Lu, Canada
Zhiguo Luo, China
Gabriel Luque, Spain
Valentin Lychagin, Norway
Junhai Ma, China
Dazhong Ma, China
Antonio Madeo, Italy
Alessandro Magnani, Belgium
Tahir Mahmood, Pakistan
Toqeer Mahmood, Pakistan
Fazal M. Mahomed, South Africa
Arunava Majumder, India
Paolo Manfredi, Italy
Adnan Maqsood, Pakistan
Giuseppe Carlo Marano, Italy
Damijan Markovic, France
Filipe J. Marques, Portugal
Luca Martinelli, Italy
Rodrigo Martinez-Bejar, Spain
Guiomar Martin-Herrán, Spain
Denizar Cruz Martins, Brazil
Francisco J. Martos, Spain
Elio Masciari, Italy
Franck Massa, France
Paolo Massioni, France
Alessandro Mauro, Italy
Jonathan Mayo-Maldonado, Mexico
Fabio Mazza, Italy
Pier Luigi Mazzeo, Italy
Laura Mazzola, Italy
Driss Mehdi, France
Zahid Mehmood, Pakistan
YUE MEI, China
Roderick Melnik, Canada
Xiangyu Meng, USA
Debiao Meng, China
Jose Merodio, Spain
Alessio Merola, Italy
Mahmoud Mesbah, Iran
Luciano Mescia, Italy
Laurent Mevel, France

Constantine Michailides, Cyprus
Mariusz Michta, Poland
Prankul Middha, Norway
Aki Mikkola, Finland
Giovanni Minafò, Italy
Hiroyuki Mino, Japan
Dimitrios Mitsotakis, New Zealand
Saleh Mobayen, Iran
Nikunja Mohan Modak, India
Sara Montagna, Italy
Roberto Montanini, Italy
Francisco J. Montáns, Spain
Gisele Mophou, France
Rafael Morales, Spain
Marco Morandini, Italy
Javier Moreno-Valenzuela, Mexico
Simone Morganti, Italy
Caroline Mota, Brazil
Aziz Moukrim, France
Shen Mouquan, China
Dimitris Mourtzis, Greece
Emiliano Mucchi, Italy
Taseer Muhammad, Saudi Arabia
Josefa Mula, Spain
Jose J. Muñoz, Spain
Giuseppe Muscolino, Italy
Dino Musmarra, Italy
Marco Mussetta, Italy
Ghulam Mustafa, Pakistan
Hariharan Muthusamy, India
Hakim Naceur, France
Alessandro Naddeo, Italy
Benedek Nagy, Turkey
Omar Naifar, Tunisia
Mariko Nakano-Miyatake, Mexico
Keivan Navaie, United Kingdom
Adrian Neagu, USA
Erivelton Geraldo Nepomuceno, Brazil
Luís C. Neves, United Kingdom
AMA Neves, Portugal
Dong Ngoduy, New Zealand
Nhon Nguyen-Thanh, Singapore
Papakostas Nikolaos, Ireland
Jelena Nikolic, Serbia
Tatsushi Nishi, Japan
Shanzhou Niu, China
Xesús Nogueira, Spain

Ben T. Nohara, Japan
Mohammed Nouari, France
Mustapha Nourelfath, Canada
Kazem Nouri, Iran
Ciro Núñez-Gutiérrez, Mexico
Włodzimierz Ogryczak, Poland
Roger Ohayon, France
Krzysztof Okarma, Poland
Mitsuhiro Okayasu, Japan
Diego Oliva, Mexico
Alberto Olivares, Spain
Enrique Onieva, Spain
Calogero Orlando, Italy
Sergio Ortobelli, Italy
Naohisa Otsuka, Japan
Taoreed Owolabi, Nigeria
Pawel Packo, Poland
Arturo Pagano, Italy
Roberto Palma, Spain
Alessandro Palmeri, United Kingdom
Pasquale Palumbo, Italy
Li Pan, China
Weifeng Pan, China
K. M. Pandey, India
Chandan Pandey, India
Jürgen Pannek, Germany
Elena Panteley, France
Achille Paolone, Italy
George A. Papakostas, Greece
Xosé M. Pardo, Spain
You-Jin Park, Taiwan
Manuel Pastor, Spain
Petr Páta, Czech Republic
Pubudu N. Pathirana, Australia
Surajit Kumar Paul, India
Sitek Paweł, Poland
Luis Payá, Spain
Alexander Paz, Australia
Igor Pažanin, Croatia
Libor Pekař, Czech Republic
Francesco Pellicano, Italy
Marcello Pellicciari, Italy
Bo Peng, China
Zhi-ke Peng, China
Xindong Peng, China
Zhengbiao Peng, Australia
Haipeng Peng, China

Jian Peng, China
Yuexing Peng, China
Mingshu Peng, China
Marzio Pennisi, Italy
Maria Patrizia Pera, Italy
Matjaz Perc, Slovenia
A. M. Bastos Pereira, Portugal
Ricardo Perera, Spain
F. Javier Pérez-Pinal, Mexico
Michele Perrella, Italy
Francesco Pesavento, Italy
Ivo Petras, Slovakia
Francesco Petrini, Italy
Hoang Vu Phan, Republic of Korea
Lukasz Pieczonka, Poland
Dario Piga, Switzerland
Antonina Pirrotta, Italy
Marco Pizzarelli, Italy
Javier Plaza, Spain
Goutam Pohit, India
Kemal Polat, Turkey
Dragan Poljak, Croatia
Jorge Pomares, Spain
Hiram Ponce, Mexico
Sébastien Poncet, Canada
Volodymyr Ponomaryov, Mexico
Jean-Christophe Ponsart, France
Mauro Pontani, Italy
Cornelio Posadas-Castillo, Mexico
Francesc Pozo, Spain
Aditya Rio Prabowo, Indonesia
Anchasa Pramuanjaroenkij, Thailand
Christopher Pretty, New Zealand
Leonardo Primavera, Italy
Luca Pugi, Italy
Krzysztof Puszynski, Poland
Goran D. Putnik, Portugal
Chuan Qin, China
Jianlong Qiu, China
Giuseppe Quaranta, Italy
Vitomir Racic, Italy
Ahmed G. Radwan, Egypt
Hamid Rahman, Pakistan
Carlo Rainieri, Italy
Kumbakonam Ramamani Rajagopal, USA
Venkatesan Rajinikanth, India
Ali Ramazani, USA

Higinio Ramos, Spain
Angel Manuel Ramos, Spain
Muhammad Afzal Rana, Pakistan
Amer Rasheed, Pakistan
Muhammad Rashid, Saudi Arabia
Manoj Rastogi, India
Alessandro Rasulo, Italy
S.S. Ravindran, USA
Abdolrahman Razani, Iran
Alessandro Reali, Italy
Jose A. Reinoso, Spain
Oscar Reinoso, Spain
Haijun Ren, China
X. W. Ren, China
Carlo Renno, Italy
Fabrizio Renno, Italy
Shahram Rezapour, Iran
Ricardo Riaza, Spain
Francesco Riganti-Fulginei, Italy
Gerasimos Rigatos, Greece
Francesco Ripamonti, Italy
Marcelo Raúl Risk, Argentina
Jorge Rivera, Mexico
Eugenio Roanes-Lozano, Spain
Bruno G. M. Robert, France
Ana Maria A. C. Rocha, Portugal
Luigi Rodino, Italy
Francisco Rodríguez, Spain
Rosana Rodríguez López, Spain
Alessandra Romolo, Italy
Abdolreza Roshani, Italy
Francisco Rossomando, Argentina
Jose de Jesus Rubio, Mexico
Weiguo Rui, China
Rubén Ruiz, Spain
Ivan D. Rukhlenko, Australia
Chaman Lal Sabharwal, USA
Kishin Sadarangani, Spain
Andrés Sáez, Spain
Bekir Sahin, Turkey
John S. Sakellariou, Greece
Michael Sakellariou, Greece
Salvatore Salamone, USA
Jose Vicente Salcedo, Spain
Alejandro Salcido, Mexico
Alejandro Salcido, Mexico
Salman saleem, Pakistan

Ahmed Salem, Saudi Arabia
Nunzio Salerno, Italy
Rohit Salgotra, India
Miguel A. Salido, Spain
Zabidin Salleh, Malaysia
Roque J. Saltarén, Spain
Alessandro Salvini, Italy
Abdus Samad, India
Nikolaos Samaras, Greece
Sylwester Samborski, Poland
Ramon Sancibrian, Spain
Giuseppe Sanfilippo, Italy
Omar-Jacobo Santos, Mexico
J Santos-Reyes, Mexico
José A. Sanz-Herrera, Spain
Evangelos J. Sapountzakis, Greece
Musavarah Sarwar, Pakistan
Marcelo A. Savi, Brazil
Andrey V. Savkin, Australia
Tadeusz Sawik, Poland
Roberta Sburlati, Italy
Gustavo Scaglia, Argentina
Thomas Schuster, Germany
Oliver Schütze, Mexico
Lotfi Senhadji, France
Junwon Seo, USA
Michele Serpilli, Italy
Joan Serra-Sagrasta, Spain
Silvestar Šesnić, Croatia
Erhan Set, Turkey
Gerardo Severino, Italy
Ruben Sevilla, United Kingdom
Stefano Sfarra, Italy
Mohamed Shaat, United Arab Emirates
Mostafa S. Shadloo, France
Kamal Shah, Pakistan
Leonid Shaikhet, Israel
Xingling Shao, China
Hao Shen, China
hang shen, China
Xin Pu Shen, China
Bo Shen, Germany
Dimitri O. Shepelsky, Ukraine
Weichao SHI, United Kingdom
Jian Shi, China
Suzanne M. Shontz, USA
Babak Shotorban, USA

Zhan Shu, Canada
Angelo Sifaleras, Greece
Nuno Simões, Portugal
Thanin Sitthiwirattham, Thailand
Seralathan Sivamani, India
S. Sivasankaran, Malaysia
Christos H. Skiadas, Greece
Konstantina Skouri, Greece
Neale R. Smith, Mexico
Bogdan Smolka, Poland
Delfim Soares Jr., Brazil
Alba Sofi, Italy
Francesco Soldovieri, Italy
Raffaele Solimene, Italy
Bosheng Song, China
Jussi Sopanen, Finland
Marco Spadini, Italy
Paolo Spagnolo, Italy
Bernardo Spagnolo, Italy
Ruben Specogna, Italy
Vasilios Spitas, Greece
Sri Sridharan, USA
Ivanka Stamova, USA
Rafał Stanisławski, Poland
Miladin Stefanović, Serbia
Florin Stoican, Romania
Salvatore Strano, Italy
Yakov Strelniker, Israel
Xiaodong Sun, China
Qiuye Sun, China
Qiuqin Sun, China
Zong-Yao Sun, China
Shuaishuai Sun, Australia
Suroso Suroso, Indonesia
Sergey A. Suslov, Australia
Nasser Hassen Sweilam, Egypt
Andrzej Swierniak, Poland
M Syed Ali, India
Andras Szekrenyes, Hungary
Kumar K. Tamma, USA
Yong (Aaron) Tan, United Kingdom
Marco Antonio Taneco-Hernández, Mexico
Hafez Tari, USA
Alessandro Tasora, Italy
Sergio Teggi, Italy
Ana C. Teodoro, Portugal
Efstathios E. Theotokoglou, Greece

Jing-Feng Tian, China
Alexander Timokha, Norway
Stefania Tomasiello, Italy
Gisella Tomasini, Italy
Isabella Torcicollo, Italy
Francesco Tornabene, Italy
Javier Martinez Torres, Spain
Mariano Torrisi, Italy
Thang nguyen Trung, Vietnam
Sang-Bing Tsai, China
George Tsiatas, Greece
Antonios Tsourdos, United Kingdom
Le Anh Tuan, Vietnam
Federica Tubino, Italy
Nerio Tullini, Italy
Emilio Turco, Italy
Ilhan Tuzcu, USA
Efstratios Tzirtzilakis, Greece
Filippo Ubertini, Italy
Marjan Uddin, Pakistan
Mohammad Uddin, Australia
Serdar Ulubeyli, Turkey
FRANCISCO UREÑA, Spain
Panayiotis Vafeas, Greece
Giuseppe Vairo, Italy
Eusebio Valero, Spain
Stefano Valvano, Italy
Marcello Vasta, Italy
Carlos-Renato Vázquez, Mexico
Miguel E. Vázquez-Méndez, Spain
Martin Velasco Villa, Mexico
Kalyana C. Veluvolu, Republic of Korea
Franck J. Vernerey, USA
Georgios Veronis, USA
Vincenzo Vespri, Italy
Renato Vidoni, Italy
Venkatesh Vijayaraghavan, Australia
Anna Vila, Spain
Francisco R. Villatoro, Spain
Francesca Vipiana, Italy
Stanislav Vitek, Czech Republic
Jan Vorel, Czech Republic
Michael Vynnycky, Sweden
Hao Wang, USA
Qingling Wang, China
Zenghui Wang, South Africa
C. H. Wang, Taiwan

Yong Wang, China
Guoqiang Wang, China
J.G. Wang, China
Zhenbo Wang, USA
Ji Wang, China
Shuo Wang, China
Yung-Chung Wang, Taiwan
Hui Wang, China
Zhibo Wang, China
Yongqi Wang, Germany
Xinyu Wang, China
Fu-Kwun Wang, Taiwan
Weiwei Wang, China
Dagang Wang, China
Bingchang Wang, China
Roman Wan-Wendner, Austria
Fangqing Wen, China
P.H. Wen, United Kingdom
Waldemar T. Wójcik, Poland
Wai Lok Woo, United Kingdom
Zhizheng Wu, China
Zhibin Wu, China
QiuHong Wu, China
Yuqiang Wu, China
Xianyi Wu, China
Changzhi Wu, China
Michalis Xenos, Greece
hao xiao, China
Xiao Ping Xie, China
Xue-Jun Xie, China
Qingzheng Xu, China
Lingwei Xu, China
Hang Xu, China
Zeshui Xu, China
Lei Xu, China
Qilong Xue, China
Joseph J. Yame, France
Chuanliang Yan, China
Zhiguo Yan, China
Xinggang Yan, United Kingdom
Ray-Yeng Yang, Taiwan
Weilin Yang, China
Jixiang Yang, China
Mijia Yang, USA
Min Ye, China
Jun Ye, China
Luis J. Yebra, Spain

Peng-Yeng Yin, Taiwan
Muhammad Haroon Yousaf, Pakistan
Yuan Yuan, United Kingdom
Qin Yuming, China
Abdullahi Yusuf, Nigeria
Akbar Zada, Pakistan
Elena Zaitseva, Slovakia
Arkadiusz Zak, Poland
Daniel Zaldivar, Mexico
Ernesto Zambrano-Serrano, Mexico
Francesco Zammori, Italy
Vittorio Zampoli, Italy
Rafal Zdunek, Poland
Ahmad Zeeshan, Pakistan
Ibrahim Zeid, USA
Nianyin Zeng, China
Bo Zeng, China
Junyong Zhai, China
Tongqian Zhang, China
Wenyu Zhang, China
Jian Zhang, China
Xuping Zhang, Denmark
Haopeng Zhang, USA
Kai Zhang, China
Xiaofei Zhang, China
Qian Zhang, China
Hao Zhang, China
Xianming Zhang, Australia
Yong Zhang, China
Tianwei Zhang, China
Lingfan Zhang, China
Yifan Zhao, United Kingdom
Yongmin Zhong, Australia
Jian G. Zhou, United Kingdom
Debao Zhou, USA
Zebo Zhou, China
Wu-Le Zhu, China
Quanxin Zhu, China
Gaetano Zizzo, Italy
Zhixiang Zou, China

Contents

Various Approaches for Generalized Integral Transforms

Arjun Kumar Rathie, Younghee Geum , and Hwajoon Kim 

Editorial (2 pages), Article ID 9781038, Volume 2021 (2021)

A Note on Certain Laplace Transforms of Convolution-Type Integrals Involving Product of Two Generalized Hypergeometric Functions

Arjun Kumar Rathie, Young Hee Geum, and Hwajoon Kim 

Research Article (15 pages), Article ID 8827275, Volume 2021 (2021)

Facial Image Segmentation Based on Gabor Filter

Hong-An Li , Jiangwen Fan , Jing Zhang , Zhanli Li , Dandan He , Ming Si , and Yun Zhang 

Research Article (7 pages), Article ID 6620742, Volume 2021 (2021)

Some General Integral Operator Inequalities Associated with s -Quasiconvex Functions

Young Chel Kwun, Moquddsa Zahra, Ghulam Farid , Praveen Agarwal , and Shin Min Kang 

Research Article (11 pages), Article ID 6696602, Volume 2021 (2021)

Combining Finite Element and Analytical methods to Contact Problems of 3D Structure on Soft Foundation

Chao Su, Heng Zhang , Shaopei Hu , Jiawei Bai, and Jianjian Dai

Research Article (18 pages), Article ID 8827681, Volume 2020 (2020)

Editorial

Various Approaches for Generalized Integral Transforms

Arjun Kumar Rathie,¹ Younghee Geum ,² and Hwajoon Kim ³

¹Vedant College of Engineering and Technology (Rajasthan Technical University), Bundi, Rajasthan, India

²Dankook University, Cheonan, Republic of Korea

³Kyungdong University, Yangju, Republic of Korea

Correspondence should be addressed to Hwajoon Kim; cellmath@gmail.com

Received 28 July 2021; Accepted 28 July 2021; Published 31 August 2021

Copyright © 2021 Arjun Kumar Rathie et al. This is an open access article distributed under the Creative Commons Attribution License, which permits unrestricted use, distribution, and reproduction in any medium, provided the original work is properly cited.

Integral Transform maps an equation from its original domain into another domain where it might be manipulated and solved much more easily. In this research area, our main objective of this special issue is to address some of the new and interesting engineering and applied science research problems. Although the theory of Integral Transform is not new, we think it is still worthy of further research in an application point of view, such as convolution in convolutional neural networks (CNN) or medical diagnosis image processing. Computed tomography or magnetic resonance imaging can be viewed as successful applications of the typical Integral Transform.

Theories on Integral Transforms have been studied in the form of creating a new type of transform by suitably changing the kernel. There are two views here. One is the view to see many Integral Transforms in this field as a variant of Laplace transform, and the other is to view it as a new transform. We consider the former to be a valid view.

Here, in this editorial, we describe the status of the special issue as follows.

Overall, eight research papers have been submitted to this special issue, of which four research papers have been selected for publication.

In the paper “Some General Integral Operator Inequalities Associated with φ -Quasiconvex Functions,” the authors Y. C. Kwun et al. deal with generalized integral operator inequalities which are established by using φ -quasiconvex functions. Bounds of an integral operator are established which have connections with different kinds of known fractional integral operators. All results are deducible for quasiconvex functions. Some fractional integral inequalities are deduced.

The research paper submitted by A. K. Rathie et al., entitled “A Note on Certain Laplace Transforms of Convolution-Type Integrals Involving Product of Two Generalized Hypergeometric Functions” provided as many as forty-five attractive Laplace transforms of convolution type related to the product of generalized hypergeometric functions.

In the research paper “Combining Finite Element and Analytical Methods to Contact Problems of 3D Structure on Soft Foundation,” C. Su et al. proposed a method to analyze the structural soft foundation system affected by time. The methodology is an explicit method, combining the finite element method with the analytical method. The creep deformation of the soft foundation is obtained based on Laplace transform. The structural deformation contains the statically determinate structural deformation and rigid body displacement, solved by the finite method. The contact forces are calculated by the deformation coordination equations and equilibrium equations. The methodology is validated through the augmented Lagrangian (AL) method. The results can clearly illustrate the local disengagement phenom, greatly overcome the nonconvergence of the iteration, and significantly improve the computing efficiency.

In the research paper “Facial Image Segmentation Based on Gabor Filter,” H.-A. Li et al. used the AdaBoost algorithm and the Gabor texture analysis algorithm are used to segment an image containing multiple faces, which effectively reduces the false detection rate of facial image segmentation. In facial image segmentation, the image containing face information is first analyzed for texture using the Gabor algorithm and appropriate thresholds are set with different thresholds of skin-like areas, where skin-like areas in the

image's background information are removed. Then, the AdaBoost algorithm is used to detect the face regions, and finally, the detected face regions are segmented. Experiments show that this method can quickly and accurately segment the faces in an image and effectively reduce the rate of missed and false detections.

In our view, research on the intrinsic properties of Integral Transforms, application to convolution of artificial intelligence, and research on Radon transform related to medical equipment are judged to be of high value. Finally, we believe that the results published in this special issue would be a definite contribution in the existing literature of the Integral Transform and will be useful for the mathematicians and research scholars working in this area. We look forward to seeing a lot of further research in these areas in the coming days.

Conflicts of Interest

The Guest Editors declare no conflicts of interest.

Acknowledgments

As Guest Editors of this special issue, we take this opportunity to thank all authors and learned referees/reviewers for their invaluable contributions towards the success of this special issue. We would also like to thank the Editorial Board involved in the publication of this special issue.

*Arjun Kumar Rathie
Younghee Geum
Hwajoon Kim*

Research Article

A Note on Certain Laplace Transforms of Convolution-Type Integrals Involving Product of Two Generalized Hypergeometric Functions

Arjun Kumar Rathie,¹ Young Hee Geum,² and Hwajoon Kim³ 

¹Department of Mathematics, Vedant College of Engineering and Technology, Rajasthan Technical University, Bundi 323021, India

²Dankook University, Cheonan, Republic of Korea

³Kyungdong University, Yangju, Republic of Korea

Correspondence should be addressed to Hwajoon Kim; cellmath@gmail.com

Received 30 September 2020; Accepted 22 May 2021; Published 30 May 2021

Academic Editor: Xue-Bo Chen

Copyright © 2021 Arjun Kumar Rathie et al. This is an open access article distributed under the Creative Commons Attribution License, which permits unrestricted use, distribution, and reproduction in any medium, provided the original work is properly cited.

The aim of this research paper is to provide as many as forty-five attractive Laplace transforms of convolution type related to the product of generalized hypergeometric functions. These are achieved by employing summation theorems for the series ${}_pF_{p-1}$ (for $p = 2, 3, 4$, and 5) available in the literature. The obtained research result is to provide an easier method than the existing method.

1. Introduction and Results' Required

The theory of hypergeometric and generalized hypergeometric functions [1–3] are fundamental in the field of mathematics, engineering mathematics, and mathematical physics. Most of the commonly used functions that occur in the analysis are special cases or limiting cases of ${}_2F_1$ and ${}_1F_1$.

It is well known that ${}_2F_1$ and ${}_1F_1$ defined by

$$\begin{aligned}
 {}_2F_1 \left[\begin{matrix} a, b \\ c \end{matrix} \middle| z \right] &= \sum_{n=0}^{\infty} \frac{(a)_n (b)_n}{(c)_n} \frac{z^n}{n!}, \\
 {}_1F_1 \left[\begin{matrix} a \\ c \end{matrix} \middle| z \right] &= \sum_{n=0}^{\infty} \frac{(a)_n}{(c)_n} \frac{z^n}{n!},
 \end{aligned} \tag{1}$$

where $(a)_n = \Gamma(a+n)/\Gamma(a)$ and $a \neq 0$. Applications related to the detailed content can be found in [4–7].

A natural generalization of this function can be represented by

$$\begin{aligned}
 {}_pF_q \left[\begin{matrix} (a) \\ (b) \end{matrix} \middle| z \right] &= {}_pF_q \left[\begin{matrix} a_1, \dots, a_p \\ b_1, \dots, b_q \end{matrix} \middle| z \right] \\
 &= \sum_{n=0}^{\infty} \frac{(a_1)_n \cdots (a_p)_n}{(b_1)_n \cdots (b_q)_n} \frac{z^n}{n!}.
 \end{aligned} \tag{2}$$

In the theory of hypergeometric and generalized hypergeometric functions, the following classical summation theorems for the series ${}_pF_{p-1}$ (for $p = 2, 3, 4$, and 5) play an important role [3, 4].

Gauss' summation theorem [8]:

$${}_2F_1 \left[\begin{matrix} a, b \\ c \end{matrix} \middle| 1 \right] = \frac{\Gamma(c)\Gamma(c-a-b)}{\Gamma(c-a)\Gamma(c-b)} = \Delta_1(a, b, c), \tag{3}$$

which provided $\Re(c-a-b) > 0$.

Gauss's second summation theorem [9]:

$${}_2F_1 \left[\begin{matrix} a, b \\ \frac{1}{2}(a+b+1) \end{matrix} \middle| \frac{1}{2} \right] = \frac{\Gamma(1/2)\Gamma((1/2)(a+b+1))}{\Gamma((1/2)a+(1/2))\Gamma((1/2)b+(1/2))} = \Delta_2(a, b). \quad (4)$$

Bailey's summation theorem [8]:

$${}_2F_1 \left[\begin{matrix} a, 1-a \\ b \end{matrix} \middle| \frac{1}{2} \right] = \frac{\Gamma((1/2)b)\Gamma((1/2)b+(1/2))}{\Gamma((1/2)b+(1/2)a)\Gamma((1/2)b-(1/2)a+(1/2))} = \Delta_3(a, b). \quad (5)$$

Kummer's summation theorem [8]:

$${}_2F_1 \left[\begin{matrix} a, b \\ 1+a-b \end{matrix} \middle| -1 \right] = \frac{\Gamma(1+(1/2)a)\Gamma(1+a-b)}{\Gamma(1+a)\Gamma(1+(1/2)a-b)} = \Delta_4(a, b). \quad (6)$$

Watson summation theorem [8]:

$$\begin{aligned} & {}_3F_2 \left[\begin{matrix} a, b, c \\ (1/2)(a+b+1), 2c \end{matrix} \middle| 1 \right] \\ &= \frac{\Gamma(1/2)\Gamma(c+(1/2))\Gamma((1/2)a+(1/2)b+(1/2))\Gamma(c-(1/2)a-(1/2)b+(1/2))}{\Gamma((1/2)a+(1/2))\Gamma((1/2)b+(1/2))\Gamma(c-(1/2)a+(1/2))\Gamma(c-(1/2)b+(1/2))} \\ &= \Delta_5(a, b, c), \end{aligned} \quad (7)$$

which provided $\Re(2c-a-b) > -1$.

Dixon's summation theorem [9]:

$$\begin{aligned} & {}_3F_2 \left[\begin{matrix} a, b, c \\ 1+a-b, 1+a-c \end{matrix} \middle| 1 \right] \\ &= \frac{\Gamma(1+(1/2)a)\Gamma(1+a-b)\Gamma(1+a-c)\Gamma(1+(1/2)a-b-c)}{\Gamma(1+a)\Gamma(1+(1/2)a-b)\Gamma(1+(1/2)a-c)\Gamma(1+a-b-c)} \\ &= \Delta_6(a, b, c), \end{aligned} \quad (8)$$

which provided $\Re(a-2b-2c) > -2$.

Whipple's summation theorem [9]:

$$\begin{aligned} & {}_3F_2 \left[\begin{matrix} a, 1-a, c \\ e, 1+2c-e \end{matrix} \middle| 1 \right] \\ &= \frac{2^{1-2c}\pi\Gamma(e)\Gamma(1+2c-e)}{\Gamma((1/2)a+(1/2)e)\Gamma((1/2)-(1/2)a+(1/2)e)\Gamma(c+(1/2)a-(1/2)e+(1/2))\Gamma(c-(1/2)a-(1/2)e+1)} \\ &= \Delta_7(a, c, e), \end{aligned} \quad (9)$$

which provided $\Re(c) > 0$.

Second Whipple's summation theorem [1]:

$$\begin{aligned}
 & {}_4F_3 \left[\begin{matrix} a, 1 + \frac{1}{2}a, b, c \\ \frac{1}{2}a, a - b + 1, a - c + 1 \end{matrix} \middle| -1 \right] \\
 &= \frac{\Gamma(a - b + 1)\Gamma(a - c + 1)}{\Gamma(a + 1)\Gamma(a - b - c + 1)} \\
 &= \Delta_8(a, b, c).
 \end{aligned} \tag{10}$$

Dougall's summation theorem [1]:

$$\begin{aligned}
 & {}_5F_4 \left[\begin{matrix} a, 1 + \frac{1}{2}a, c, d, e \\ \frac{1}{2}a, a - c + 1, a - d + 1, a - e + 1 \end{matrix} \middle| 1 \right] \\
 &= \frac{\Gamma(a - c + 1)\Gamma(a - d + 1)\Gamma(a - e + 1)\Gamma(a - c - d - e + 1)}{\Gamma(a + 1)\Gamma(a - d - e + 1)\Gamma(a - c - e + 1)\Gamma(a - c - d + 1)} \\
 &= \Delta_9(a, c, d, e).
 \end{aligned} \tag{11}$$

In addition to this, we have the following general result of the Laplace transform of convolution-type integrals involving the product of two generalized hypergeometric functions available in the literature, see [6, 7]:

$$\begin{aligned}
 & \int_0^\infty e^{-st} \left\{ \int_0^t \tau^{\mu-1} (t-\tau)^{\nu-1} {}_pF_q \left[\begin{matrix} (a) \\ (b) \end{matrix} \middle| k\tau \right] {}_{q'}F_{q'} \left[\begin{matrix} (a') \\ (b') \end{matrix} \middle| k'(t-\tau) \right] d\tau \right\} dt \\
 &= \Gamma(\mu)\Gamma(\nu)s^{-\mu-\nu} {}_{p+1}F_q \left[\begin{matrix} (a), \mu \\ (b) \end{matrix} \middle| \frac{k}{s} \right] {}_{q'}F_{q'} \left[\begin{matrix} (a'), \nu \\ (b') \end{matrix} \middle| \frac{k'}{s} \right].
 \end{aligned} \tag{12}$$

The aim of this note is to demonstrate how one can easily obtain in all forty-five Laplace transforms of convolution type related to the product of two generalized hypergeometric functions from the general result (12) by employing various summation theorems (3) to (11). The results obtained earlier by Milovanović et al. [1, 2] follow special cases of our main findings.

2. A Note on Certain Laplace Transforms of Convolution-Type Integrals Involving Product of Two Generalized Hypergeometric Functions

In this section, we shall establish in all forty-five Laplace transforms of convolution type related to the product of two generalized hypergeometric functions mentioned in the following theorems. All delta values that appear in this section are shown in Section 1.

Theorem 1. For $\Re(s) > 0$, $\Re(d) > 0$, $\Re(d') > 0$, $\Re(c - a - b) > 0$, and $\Re(c' - a' - b') > 0$, the following result holds true:

$$\begin{aligned}
 & \int_0^\infty e^{-st} \left\{ \int_0^t \tau^{d-1} (t-\tau)^{d'-1} {}_2F_2 \left[\begin{matrix} a, b \\ c, d \end{matrix} \middle| \tau s \right] {}_2F_2 \left[\begin{matrix} a', b' \\ c', d' \end{matrix} \middle| (t-\tau)s \right] d\tau \right\} dt \\
 &= \Gamma(d)\Gamma(d')s^{-d-d'} \Delta_1(a, b, c)\Delta_1(a', b', c').
 \end{aligned} \tag{13}$$

Theorem 2. For $\Re(s) > 0$, $\Re(d) > 0$, $\Re(d') > 0$, and $\Re(c - a - b) > 0$, the following result holds true:

$$\begin{aligned}
 & \int_0^\infty e^{-st} \left\{ \int_0^t \tau^{d-1} (t-\tau)^{d'-1} {}_2F_2 \left[\begin{matrix} a, b \\ c, d \end{matrix} \middle| \tau s \right] \times {}_2F_2 \left[\begin{matrix} a', b' \\ \frac{1}{2}(a' + b' + 1), d' \end{matrix} \middle| \frac{1}{2}(t-\tau)s \right] d\tau \right\} dt \\
 &= \Gamma(d)\Gamma(d')s^{-b-b'} \Delta_1(a, b, c)\Delta_2(a', b').
 \end{aligned} \tag{14}$$

Theorem 3. For $\Re(s) > 0$, $\Re(d) > 0$, $\Re(d') > 0$, and $\Re(c - a - b) > 0$, the following result holds true:

$$\begin{aligned}
 & \int_0^\infty e^{-st} \left\{ \int_0^t \tau^{d-1} (t-\tau)^{d'-1} {}_2F_2 \left[\begin{matrix} a, b \\ c, d \end{matrix} \middle| \tau s \right] \times {}_2F_2 \left[\begin{matrix} a', 1 - a' \\ b', d' \end{matrix} \middle| \frac{1}{2}(t-\tau)s \right] d\tau \right\} dt \\
 &= \Gamma(d)\Gamma(d')s^{-d-d'} \Delta_1(a, b, c)\Delta_3(a', b').
 \end{aligned} \tag{15}$$

Theorem 4. For $\Re(s) > 0$, $\Re(d) > 0$, $\Re(d') > 0$, and $\Re(c - a - b) > 0$, the following result holds true:

$$\int_0^\infty e^{-st} \left\{ \int_0^t \tau^{d-1} (t-\tau)^{d'-1} {}_2F_2 \left[\begin{matrix} a, b \\ c, d \end{matrix} \middle| \tau s \right] \times {}_2F_2 \left[\begin{matrix} a', b' \\ 1+a'-b', d' \end{matrix} \middle| (t-\tau)s \right] d\tau \right\} dt$$

$$= \Gamma(d)\Gamma(d')s^{-d-d'} \Delta_1(a, b, c) \Delta_4(a', b'). \quad (16)$$

Theorem 5. For $\Re(s) > 0$, $\Re(d) > 0$, $\Re(d') > 0$, $\Re(c - a - b) > 0$, and $\Re(2c' - a' - b') > -1$, the following result holds true:

$$\int_0^\infty e^{-st} \left\{ \int_0^t \tau^{d-1} (t-\tau)^{d'-1} {}_2F_2 \left[\begin{matrix} a, b \\ c, d \end{matrix} \middle| \tau s \right] \times {}_3F_3 \left[\begin{matrix} a', b', c' \\ \frac{1}{2}(a'+b'+1), 2c', d' \end{matrix} \middle| (t-\tau)s \right] d\tau \right\} dt$$

$$= \frac{\Gamma(d)\Gamma(d')}{s^{d+d'}} \Delta_1(a, b, c) \Delta_5(a', b', c'). \quad (17)$$

Theorem 6. For $\Re(s) > 0$, $\Re(d) > 0$, $\Re(d') > 0$, $\Re(c - a - b) > 0$, and $\Re(a' - 2b' - 2c') > -2$, the following result holds true:

$$\int_0^\infty e^{-st} \left\{ \int_0^t \tau^{d-1} (t-\tau)^{d'-1} {}_2F_2 \left[\begin{matrix} a, b \\ c, d \end{matrix} \middle| \tau s \right] \times {}_3F_3 \left[\begin{matrix} a', b', c' \\ 1+a'-b', 1+a'-c', d' \end{matrix} \middle| (t-\tau)s \right] d\tau \right\} dt$$

$$= \frac{\Gamma(d)\Gamma(d')}{s^{d+d'}} \Delta_1(a, b, c) \Delta_6(a', b', c'). \quad (18)$$

Theorem 7. For $\Re(s) > 0$, $\Re(d) > 0$, $\Re(d') > 0$, and $\Re(c - a - b) > 0$, the following result holds true:

$$\int_0^\infty e^{-st} \left\{ \int_0^t \tau^{d-1} (t-\tau)^{d'-1} {}_2F_2 \left[\begin{matrix} a, b \\ c, d \end{matrix} \middle| \tau s \right] \times {}_3F_3 \left[\begin{matrix} a', 1-a', c' \\ e', 1+2c'-e', d' \end{matrix} \middle| (t-\tau)s \right] d\tau \right\} dt$$

$$= \frac{\Gamma(d)\Gamma(d')}{s^{d+d'}} \Delta_1(a, b, c) \Delta_7(a', c', e'). \quad (19)$$

Theorem 8. For $\Re(s) > 0$, $\Re(d) > 0$, $\Re(d') > 0$, and $\Re(c - a - b) > 0$, the following result holds true:

$$\int_0^\infty e^{-st} \left\{ \int_0^t \tau^{d-1} (t-\tau)^{d'-1} {}_2F_2 \left[\begin{matrix} a, b \\ c, d \end{matrix} \middle| \tau s \right] \times {}_4F_4 \left[\begin{matrix} a', 1 + \frac{1}{2}a', b', c' \\ \frac{1}{2}a', a' - b' + 1, a' - c' + 1, d' \end{matrix} \middle| -(t-\tau)s \right] d\tau \right\} dt$$

$$= \frac{\Gamma(d)\Gamma(d')}{s^{d+d'}} \Delta_1(a, b, c) \Delta_8(a', b', c').$$

Theorem 9. For $\Re(s) > 0$, $\Re(d) > 0$, $\Re(f') > 0$, $\Re(c - a - b) > 0$, and $\Re(a' - c' - d' - e' + 1) > 0$, the following result holds true:

$$\int_0^\infty e^{-st} \left\{ \int_0^t \tau^{d-1} (t-\tau)^{f'-1} {}_2F_2 \left[\begin{matrix} a, b \\ c, d \end{matrix} \middle| \tau s \right] \times {}_5F_5 \left[\begin{matrix} a', 1 + \frac{1}{2}a', c', d', e' \\ \frac{1}{2}a', a' - c' + 1, a' - d' + 1, a' - e' + 1, f' \end{matrix} \middle| (t-\tau)s \right] d\tau \right\} dt$$

$$= \frac{\Gamma(d)\Gamma(f')}{s^{d+f'}} \Delta_1(a, b, c) \Delta_9(a', c', d', e').$$

Theorem 10. For $\Re(s) > 0$, $\Re(d) > 0$, and $\Re(d') > 0$, the following result holds true:

$$\int_0^\infty e^{-st} \left\{ \int_0^t \tau^{d-1} (t-\tau)^{d'-1} {}_2F_2 \left[\begin{matrix} a, b \\ \frac{1}{2}(a+b+1), d \end{matrix} \middle| \frac{1}{2}\tau s \right] \times {}_2F_2 \left[\begin{matrix} a', b' \\ \frac{1}{2}(a'+b'+1), d' \end{matrix} \middle| \frac{1}{2}(t-\tau)s \right] d\tau \right\} dt$$

$$= \frac{\Gamma(d)\Gamma(d')}{s^{d+d'}} \Delta_2(a, b) \Delta_2(a', b').$$

Theorem 11. For $\Re(s) > 0$, $\Re(d) > 0$, and $\Re(d') > 0$, the following result holds true:

$$\int_0^\infty e^{-st} \left\{ \int_0^t \tau^{d-1} (t-\tau)^{d'-1} {}_2F_2 \left[\begin{matrix} a, b \\ \frac{1}{2}(a+b+1), d \end{matrix} \middle| \frac{1}{2}\tau s \right] \times {}_2F_2 \left[\begin{matrix} a', 1 - a' \\ b', d' \end{matrix} \middle| \frac{1}{2}(t-\tau)s \right] d\tau \right\} dt$$

$$= \frac{\Gamma(d)\Gamma(d')}{s^{d+d'}} \Delta_2(a, b) \Delta_3(a', b').$$

Theorem 12. For $\Re(s) > 0$, $\Re(d) > 0$, and $\Re(d') > 0$, the following result holds true:

$$\int_0^\infty e^{-st} \left\{ \int_0^t \tau^{d-1} (t-\tau)^{d'-1} {}_2F_2 \left[\begin{matrix} a, b \\ \frac{1}{2}(a+b+1), d \end{matrix} \middle| \frac{1}{2}\tau s \right] \times {}_2F_2 \left[\begin{matrix} a', b' \\ 1+a'-b', d' \end{matrix} \middle| -(t-\tau)s \right] d\tau \right\} dt$$

$$= \frac{\Gamma(d)\Gamma(d')}{s^{d+d'}} \Delta_2(a, b) \Delta_4(a', b').$$

Theorem 13. For $\Re(s) > 0$, $\Re(d) > 0$, $\Re(d') > 0$, and $\Re(2c' - a' - b') > -1$, the following result holds true:

$$\int_0^\infty e^{-st} \left\{ \int_0^t \tau^{d-1} (t-\tau)^{d'-1} {}_2F_2 \left[\begin{matrix} a, b \\ \frac{1}{2}(a+b+1), d \end{matrix} \middle| \frac{1}{2}\tau s \right] \times {}_3F_3 \left[\begin{matrix} a', b', c' \\ \frac{1}{2}(a'+b'+1), 2c', d' \end{matrix} \middle| (t-\tau)s \right] d\tau \right\} dt$$

$$= \frac{\Gamma(d)\Gamma(d')}{s^{d+d'}} \Delta_2(a, b) \Delta_5(a', b', c').$$

Theorem 14. For $\Re(s) > 0$, $\Re(d) > 0$, $\Re(d') > 0$, and $\Re(a' - 2b' - 2c') > -2$, the following result holds true:

$$\int_0^\infty e^{-st} \left\{ \int_0^t \tau^{d-1} (t-\tau)^{d'-1} {}_2F_2 \left[\begin{matrix} a, b \\ \frac{1}{2}(a+b+1), d \end{matrix} \middle| \frac{1}{2}\tau s \right] \times {}_3F_3 \left[\begin{matrix} a', b', c' \\ 1+a'-b', 1+a'-c', d' \end{matrix} \middle| (t-\tau)s \right] d\tau \right\} dt$$

$$= \frac{\Gamma(d)\Gamma(d')}{s^{d+d'}} \Delta_2(a, b) \Delta_6(a', b', c').$$

Theorem 15. For $\Re(s) > 0$, $\Re(d) > 0$, and $\Re(d') > 0$, the following result holds true:

$$\int_0^\infty e^{-st} \left\{ \int_0^t \tau^{d-1} (t-\tau)^{d'-1} {}_2F_2 \left[\begin{matrix} a, b \\ \frac{1}{2}(a+b+1), d \end{matrix} \middle| \frac{1}{2}\tau s \right] \times {}_3F_3 \left[\begin{matrix} a', 1-a', c' \\ e', 1+2c'-e', d' \end{matrix} \middle| (t-\tau)s \right] d\tau \right\} dt$$

$$= \frac{\Gamma(d)\Gamma(d')}{s^{d+d'}} \Delta_2(a, b) \Delta_7(a', c', e').$$

Theorem 16. For $\Re(s) > 0$, $\Re(d) > 0$, and $\Re(d') > 0$, the following result holds true:

$$\int_0^\infty e^{-st} \left\{ \int_0^t \tau^{d-1} (t-\tau)^{d'-1} {}_2F_2 \left[\begin{matrix} a, b \\ \frac{1}{2}(a+b+1), d \end{matrix} \middle| \frac{1}{2}\tau s \right] \times {}_4F_4 \left[\begin{matrix} a', 1 + \frac{1}{2}a', b', c' \\ \frac{1}{2}a', a' - b' + 1, a' - c' + 1, d' \end{matrix} \middle| -(t-\tau)s \right] d\tau \right\} dt \quad (28)$$

$$= \frac{\Gamma(d)\Gamma(d')}{s^{d+d'}} \Delta_2(a, b) \Delta_8(a', b', c').$$

Theorem 17. For $\Re(s) > 0$, $\Re(d) > 0$, $\Re(f') > 0$, and $\Re(a' - c' - d' - e' + 1) > 0$, the following result holds true:

$$\int_0^\infty e^{-st} \left\{ \int_0^t \tau^{d-1} (t-\tau)^{f'-1} {}_2F_2 \left[\begin{matrix} a, b \\ \frac{1}{2}(a+b+1), d \end{matrix} \middle| \frac{1}{2}\tau s \right] \times {}_5F_5 \left[\begin{matrix} a', 1 + \frac{1}{2}a', c', d', e' \\ \frac{1}{2}a', a' - c' + 1, a' - d' + 1, a' - e' + 1, f' \end{matrix} \middle| (t-\tau)s \right] d\tau \right\} dt$$

$$= \frac{\Gamma(d)\Gamma(f')}{s^{d+f'}} \Delta_2(a, b) \Delta_9(a', c', d', e'). \quad (29)$$

Theorem 18. For $\Re(s) > 0$, $\Re(d) > 0$, and $\Re(d') > 0$, the following result holds true:

$$\int_0^\infty e^{-st} \left\{ \int_0^t \tau^{d-1} (t-\tau)^{d'-1} {}_2F_2 \left[\begin{matrix} a, 1-a \\ b, d \end{matrix} \middle| \frac{1}{2}\tau s \right] \times {}_2F_2 \left[\begin{matrix} a', 1-a' \\ b', d' \end{matrix} \middle| \frac{1}{2}(t-\tau)s \right] d\tau \right\} dt \quad (30)$$

$$= \frac{\Gamma(d)\Gamma(d')}{s^{d+d'}} \Delta_3(a, b) \Delta_3(a', b').$$

Theorem 19. For $\Re(s) > 0$, $\Re(d) > 0$, and $\Re(d') > 0$, the following result holds true:

$$\int_0^\infty e^{-st} \left\{ \int_0^t \tau^{d-1} (t-\tau)^{d'-1} {}_2F_2 \left[\begin{matrix} a, 1-a \\ b, d \end{matrix} \middle| \frac{1}{2}\tau s \right] \times {}_2F_2 \left[\begin{matrix} a', b' \\ 1+a'-b', d' \end{matrix} \middle| -(t-\tau)s \right] d\tau \right\} dt \quad (31)$$

$$= \frac{\Gamma(d)\Gamma(d')}{s^{d+d'}} \Delta_3(a, b) \Delta_4(a', b').$$

Theorem 20. For $\Re(s) > 0$, $\Re(d) > 0$, $\Re(d') > 0$, and $\Re(2c' - a' - b') > -1$, the following result holds true:

$$\int_0^\infty e^{-st} \left\{ \int_0^t \tau^{d-1} (t-\tau)^{d-1} {}_2F_2 \left[\begin{matrix} a, 1-a \\ b, d \end{matrix} \middle| \frac{1}{2} \tau s \right] \times {}_3F_3 \left[\begin{matrix} a', b', c' \\ \frac{1}{2} (a' + b' + 1), 2c', d' \end{matrix} \middle| (t-\tau)s \right] d\tau \right\} dt \quad (32)$$

$$= \frac{\Gamma(d)\Gamma(d')}{s^{d+d'}} \Delta_3(a, b) \Delta_5(a', b', c').$$

Theorem 21. For $\Re(s) > 0$, $\Re(d) > 0$, $\Re(d') > 0$, and $\Re(a' - 2b' - c') > -2$, the following result holds true:

$$\int_0^\infty e^{-st} \left\{ \int_0^t \tau^{d-1} (t-\tau)^{d-1} {}_2F_2 \left[\begin{matrix} a, 1-a \\ b, d \end{matrix} \middle| \frac{1}{2} \tau s \right] \times {}_3F_3 \left[\begin{matrix} a', b', c' \\ 1+a'-b', 1+a'-c', d' \end{matrix} \middle| (t-\tau)s \right] d\tau \right\} dt \quad (33)$$

$$= \frac{\Gamma(d)\Gamma(d')}{s^{d+d'}} \Delta_3(a, b) \Delta_6(a', b', c').$$

Theorem 22. For $\Re(s) > 0$, $\Re(d) > 0$, and $\Re(d') > 0$, the following result holds true:

$$\int_0^\infty e^{-st} \left\{ \int_0^t \tau^{d-1} (t-\tau)^{d-1} {}_2F_2 \left[\begin{matrix} a, 1-a \\ b, d \end{matrix} \middle| \frac{1}{2} \tau s \right] \times {}_3F_3 \left[\begin{matrix} a', 1-a', c' \\ e', 1+2c'-e', d' \end{matrix} \middle| (t-\tau)s \right] d\tau \right\} dt \quad (34)$$

$$= \frac{\Gamma(d)\Gamma(d')}{s^{d+d'}} \Delta_3(a, b) \Delta_7(a', c', e').$$

Theorem 23. For $\Re(s) > 0$, $\Re(d) > 0$, and $\Re(d') > 0$, the following result holds true:

$$\int_0^\infty e^{-st} \left\{ \int_0^t \tau^{d-1} (t-\tau)^{d-1} {}_2F_2 \left[\begin{matrix} a, 1-a \\ b, d \end{matrix} \middle| \frac{1}{2} \tau s \right] \times {}_4F_4 \left[\begin{matrix} a', 1 + \frac{1}{2}a', b', c' \\ \frac{1}{2}a', a' - b' + 1, a' - c' + 1, d' \end{matrix} \middle| -(t-\tau)s \right] d\tau \right\} dt \quad (35)$$

$$= \frac{\Gamma(d)\Gamma(d')}{s^{d+d'}} \Delta_3(a, b) \Delta_8(a', b', c').$$

Theorem 24. For $\Re(s) > 0$, $\Re(d) > 0$, $\Re(f') > 0$, and $\Re(a' - c' - d' - e' + 1) > 0$, the following result holds true:

$$\int_0^\infty e^{-st} \left\{ \int_0^t \tau^{d-1} (t-\tau)^{f'-1} {}_2F_2 \left[\begin{matrix} a, 1-a \\ b, d \end{matrix} \middle| \frac{1}{2} \tau s \right] \times {}_5F_5 \left[\begin{matrix} a', 1 + \frac{1}{2} a', c', d', e' \\ \frac{1}{2} a', a' - c' + 1, a' - d' + 1, a' - e' + 1, f' \end{matrix} \middle| (t-\tau)s \right] d\tau \right\} dt$$

$$= \frac{\Gamma(d)\Gamma(f')}{s^{d+f'}} \Delta_3(a, b) \Delta_9(a', c', d', e').$$

Theorem 25. For $\Re(s) > 0$, $\Re(d) > 0$, and $\Re(d') > 0$, the following result holds true:

$$\int_0^\infty e^{-st} \left\{ \int_0^t \tau^{d-1} (t-\tau)^{d'-1} {}_2F_2 \left[\begin{matrix} a, b \\ 1+a-b, d \end{matrix} \middle| -\tau s \right] \times {}_2F_2 \left[\begin{matrix} a', b' \\ 1+a'-b', d' \end{matrix} \middle| -(t-\tau)s \right] d\tau \right\} dt$$

$$= \frac{\Gamma(d)\Gamma(d')}{s^{d+d'}} \Delta_4(a, b) \Delta_4(a', b').$$

Theorem 26. For $\Re(s) > 0$, $\Re(d) > 0$, $\Re(d') > 0$, and $\Re(2c' - a' - b') > -2$, the following result holds true:

$$\int_0^\infty e^{-st} \left\{ \int_0^t \tau^{d-1} (t-\tau)^{d'-1} {}_2F_2 \left[\begin{matrix} a, b \\ 1+a-b, d \end{matrix} \middle| -\tau s \right] \times {}_3F_3 \left[\begin{matrix} a', b', c' \\ \frac{1}{2}(a'+b'+1), 2c', d' \end{matrix} \middle| (t-\tau)s \right] d\tau \right\} dt$$

$$= \frac{\Gamma(d)\Gamma(d')}{s^{d+d'}} \Delta_4(a, b) \Delta_5(a', b', c').$$

Theorem 27. For $\Re(s) > 0$, $\Re(d) > 0$, $\Re(d') > 0$, and $\Re(a' - 2b' - c') > -2$, the following result holds true:

$$\int_0^\infty e^{-st} \left\{ \int_0^t \tau^{d-1} (t-\tau)^{d'-1} {}_2F_2 \left[\begin{matrix} a, b \\ 1+a-b, d \end{matrix} \middle| -\tau s \right] \times {}_3F_3 \left[\begin{matrix} a', b', c' \\ 1+a'-b', 1+a'-c', d' \end{matrix} \middle| (t-\tau)s \right] d\tau \right\} dt$$

$$= \frac{\Gamma(d)\Gamma(d')}{s^{d+d'}} \Delta_4(a, b) \Delta_6(a', b', c').$$

Theorem 28. For $\Re(s) > 0$, $\Re(d) > 0$, and $\Re(d') > 0$, the following result holds true:

$$\int_0^\infty e^{-st} \left\{ \int_0^t \tau^{d-1} (t-\tau)^{d'-1} {}_2F_2 \left[\begin{matrix} a, b \\ 1+a-b, d \end{matrix} \middle| -\tau s \right] \times {}_3F_3 \left[\begin{matrix} a', 1-a', c' \\ e', 1+2c'-e', d' \end{matrix} \middle| (t-\tau)s \right] d\tau \right\} dt$$

$$= \frac{\Gamma(d)\Gamma(d')}{s^{d+d'}} \Delta_4(a, b) \Delta_7(a', c', e').$$

Theorem 29. For $\Re(s) > 0$, $\Re(d) > 0$, and $\Re(d') > 0$, the following result holds true:

$$\int_0^\infty e^{-st} \left\{ \int_0^t \tau^{d-1} (t-\tau)^{d'-1} {}_2F_2 \left[\begin{matrix} a, b \\ 1+a-b, d \end{matrix} \middle| -\tau s \right] \times {}_4F_4 \left[\begin{matrix} a', 1+\frac{1}{2}a', b', c' \\ \frac{1}{2}a', a'-b'+1, a'-c'+1, d' \end{matrix} \middle| -(t-\tau)s \right] d\tau \right\} dt$$

$$= \frac{\Gamma(d)\Gamma(d')}{s^{d+d'}} \Delta_4(a, b) \Delta_8(a', b', c'). \quad (41)$$

Theorem 30. For $\Re(s) > 0$, $\Re(d) > 0$, $\Re(f') > 0$, and $\Re(a' - c' - d' - e' + 1) > 0$, the following result holds true:

$$\int_0^\infty e^{-st} \left\{ \int_0^t \tau^{d-1} (t-\tau)^{f'-1} {}_2F_2 \left[\begin{matrix} a, b \\ 1+a-b, d \end{matrix} \middle| -\tau s \right] \times {}_5F_5 \left[\begin{matrix} a', 1+\frac{1}{2}a', c', d', e' \\ \frac{1}{2}a', a'-c'+1, a'-d'+1, a'-e'+1, f' \end{matrix} \middle| (t-\tau)s \right] d\tau \right\} dt$$

$$= \frac{\Gamma(d)\Gamma(f')}{s^{d+f'}} \Delta_4(a, b) \Delta_9(a', c', d', e'). \quad (42)$$

Theorem 31. For $\Re(s) > 0$, $\Re(d) > 0$, $\Re(d') > 0$, $\Re(2c - a - b) > -1$, and $\Re(2c' - a' - b') > -1$, the following result holds true:

$$\int_0^\infty e^{-st} \left\{ \int_0^t \tau^{d-1} (t-\tau)^{d'-1} {}_3F_3 \left[\begin{matrix} a, b, c \\ \frac{1}{2}(a+b+1), 2c, d \end{matrix} \middle| \tau s \right] \times {}_3F_3 \left[\begin{matrix} a', b', c' \\ \frac{1}{2}(a'+b'+1), 2c', d' \end{matrix} \middle| (t-\tau)s \right] d\tau \right\} dt$$

$$= \frac{\Gamma(d)\Gamma(d')}{s^{d+d'}} \Delta_5(a, b, c) \Delta_5(a', b', c'). \quad (43)$$

Theorem 32. For $\Re(s) > 0$, $\Re(d) > 0$, $\Re(d') > 0$, $\Re(2c - a - b) > -1$, and $\Re(a' - 2b' - c') > -2$, the following result holds true:

$$\int_0^\infty e^{-st} \left\{ \int_0^t \tau^{d-1} (t-\tau)^{d'-1} {}_3F_3 \left[\begin{matrix} a, b, c \\ \frac{1}{2}(a+b+1), 2c, d \end{matrix} \middle| \tau s \right] \times {}_3F_3 \left[\begin{matrix} a', b', c' \\ 1+a'-b', 1+a'-c', d' \end{matrix} \middle| (t-\tau)s \right] d\tau \right\} dt$$

$$= \frac{\Gamma(d)\Gamma(d')}{s^{d+d'}} \Delta_5(a, b, c) \Delta_6(a', b', c'). \quad (44)$$

Theorem 33. For $\Re(s) > 0$, $\Re(d) > 0$, $\Re(d') > 0$, and $\Re(2c' - a' - b') > -1$, the following result holds true:

$$\int_0^\infty e^{-st} \left\{ \int_0^t \tau^{d-1} (t-\tau)^{d'-1} {}_3F_3 \left[\begin{matrix} a, b, c \\ \frac{1}{2}(a+b+1), 2c, d \end{matrix} \middle| \tau s \right] \times {}_3F_3 \left[\begin{matrix} a', 1-a', c' \\ e', 1+2c'-e', d' \end{matrix} \middle| (t-\tau)s \right] d\tau \right\} dt$$

$$= \frac{\Gamma(d)\Gamma(d')}{s^{d+d'}} \Delta_5(a, b, c) \Delta_7(a', c', e').$$

Theorem 34. For $\Re(s) > 0$, $\Re(d) > 0$, $\Re(d') > 0$, and $\Re(2c - a - b) > -1$, the following result holds true:

$$\int_0^\infty e^{-st} \left\{ \int_0^t \tau^{d-1} (t-\tau)^{d'-1} {}_3F_3 \left[\begin{matrix} a, b, c \\ \frac{1}{2}(a+b+1), 2c, d \end{matrix} \middle| \tau s \right] \times {}_4F_4 \left[\begin{matrix} a', 1+\frac{1}{2}a', b', c' \\ \frac{1}{2}a', a'-b'+1, a'-c'+1, d' \end{matrix} \middle| -(t-\tau)s \right] d\tau \right\} dt$$

$$= \frac{\Gamma(d)\Gamma(d')}{s^{d+d'}} \Delta_5(a, b, c) \Delta_8(a', b', c').$$

Theorem 35. For $\Re(s) > 0$, $\Re(d) > 0$, $\Re(f') > 0$, $\Re(2c - a - b) > -1$, and $\Re(a' - c' - d' - e' + 1) > 0$, the following result holds true:

$$\int_0^\infty e^{-st} \left\{ \int_0^t \tau^{d-1} (t-\tau)^{f'-1} {}_3F_3 \left[\begin{matrix} a, b \\ \frac{1}{2}(a+b+1), 2c, d \end{matrix} \middle| \tau s \right] \times {}_5F_5 \left[\begin{matrix} a', 1+\frac{1}{2}a', c', d', e' \\ \frac{1}{2}a', a'-c'+1, a'-d'+1, a'-e'+1, f' \end{matrix} \middle| (t-\tau)s \right] d\tau \right\} dt$$

$$= \frac{\Gamma(d)\Gamma(f')}{s^{d+f'}} \Delta_5(a, b, c) \Delta_9(a', c', d', e').$$

Theorem 36. For $\Re(s) > 0$, $\Re(d) > 0$, $\Re(d') > 0$, $\Re(a - 2b - 2c) > -2$, and $\Re(a' - 2b' - c') > -2$, the following result holds true:

$$\int_0^\infty e^{-st} \left\{ \int_0^t \tau^{d-1} (t-\tau)^{d'-1} {}_3F_3 \left[\begin{matrix} a, b, c \\ 1+a-b, 1+a-c, d \end{matrix} \middle| \tau s \right] \times {}_3F_3 \left[\begin{matrix} a', b', c' \\ 1+a'-b', 1+a'-c', d' \end{matrix} \middle| (t-\tau)s \right] d\tau \right\} dt$$

$$= \frac{\Gamma(d)\Gamma(d')}{s^{d+d'}} \Delta_6(a, b, c) \Delta_6(a', b', c').$$

Theorem 37. For $\Re(s) > 0$, $\Re(d) > 0$, $\Re(d') > 0$, and $\Re(a - 2b - 2c) > -2$, the following result holds true:

$$\int_0^\infty e^{-st} \left\{ \int_0^t \tau^{d-1} (t-\tau)^{d'-1} {}_3F_3 \left[\begin{matrix} a, b, c \\ 1+a-b, 1+a-c, d \end{matrix} \middle| \tau s \right] \times {}_3F_3 \left[\begin{matrix} a', 1-a', c' \\ e', 1+2c'-e', d' \end{matrix} \middle| (t-\tau)s \right] d\tau \right\} dt$$

$$= \frac{\Gamma(d)\Gamma(d')}{s^{d+d'}} \Delta_6(a, b, c) \Delta_7(a', c', e'). \quad (49)$$

Theorem 38. For $\Re(s) > 0$, $\Re(d) > 0$, $\Re(d') > 0$, and $\Re(a - 2b - 2c) > -2$, the following result holds true:

$$\int_0^\infty e^{-st} \left\{ \int_0^t \tau^{d-1} (t-\tau)^{d'-1} {}_3F_3 \left[\begin{matrix} a, b, c \\ 1+a-b, 1+a-c, d \end{matrix} \middle| \tau s \right] \times {}_4F_4 \left[\begin{matrix} a', 1+\frac{1}{2}a', b', c' \\ \frac{1}{2}a', a'-b'+1, a'-c'+1, d' \end{matrix} \middle| -(t-\tau)s \right] d\tau \right\} dt$$

$$= \frac{\Gamma(d)\Gamma(d')}{s^{d+d'}} \Delta_6(a, b, c) \Delta_8(a', b', c'). \quad (50)$$

Theorem 39. For $\Re(s) > 0$, $\Re(d) > 0$, $\Re(f') > 0$, $\Re(a - 2b - 2c) > -2$, and $\Re(a' - c' - d' - e' + 1) > 0$, the following result holds true:

$$\int_0^\infty e^{-st} \left\{ \int_0^t \tau^{d-1} (t-\tau)^{f'-1} {}_3F_3 \left[\begin{matrix} a, b, c \\ 1+a-b, 1+a-c, d \end{matrix} \middle| \tau s \right] \times {}_5F_5 \left[\begin{matrix} a', 1+\frac{1}{2}a', c', d', e' \\ \frac{1}{2}a', a'-c'+1, a'-d'+1, a'-e'+1, f' \end{matrix} \middle| (t-\tau)s \right] d\tau \right\} dt$$

$$= \frac{\Gamma(d)\Gamma(f')}{s^{d+f'}} \Delta_6(a, b, c) \Delta_9(a', c', d', e'). \quad (51)$$

Theorem 40. For $\Re(s) > 0$, $\Re(d) > 0$, and $\Re(d') > 0$, the following result holds true:

$$\int_0^\infty e^{-st} \left\{ \int_0^t \tau^{d-1} (t-\tau)^{d'-1} {}_3F_3 \left[\begin{matrix} a, 1-a, c \\ e, 1+2c-e, d \end{matrix} \middle| \tau s \right] \times {}_3F_3 \left[\begin{matrix} a', 1-a', c' \\ e', 1+2c'-e', d' \end{matrix} \middle| (t-\tau)s \right] d\tau \right\} dt$$

$$= \frac{\Gamma(d)\Gamma(d')}{s^{d+d'}} \Delta_7(a, c, e) \Delta_7(a', c', e'). \quad (52)$$

Theorem 41. For $\Re(s) > 0$, $\Re(d) > 0$, and $\Re(d') > 0$, the following result holds true:

$$\int_0^\infty e^{-st} \left\{ \int_0^t \tau^{d-1} (t-\tau)^{d'-1} {}_3F_3 \left[\begin{matrix} a, 1-a, c \\ e, 1+2c-e, d \end{matrix} \middle| \tau s \right] \times {}_4F_4 \left[\begin{matrix} a', 1+\frac{1}{2}a', b', c' \\ \frac{1}{2}a', a'-b'+1, a'-c'+1, d' \end{matrix} \middle| -(t-\tau)s \right] d\tau \right\} dt$$

$$= \frac{\Gamma(d)\Gamma(d')}{s^{d+d'}} \Delta_7(a, c, e) \Delta_8(a', b', c').$$

Theorem 42. For $\Re(s) > 0$, $\Re(d) > 0$, $\Re(f') > 0$, and $\Re(a' - c' - d' - e' + 1) > 0$, the following result holds true:

$$\int_0^\infty e^{-st} \left\{ \int_0^t \tau^{d-1} (t-\tau)^{f'-1} {}_3F_3 \left[\begin{matrix} a, 1-a, c \\ e, 1+2c-e, d \end{matrix} \middle| \tau s \right] \times {}_5F_5 \left[\begin{matrix} a', 1+\frac{1}{2}a', c', d', e' \\ \frac{1}{2}a', a'-c'+1, a'-d'+1, a'-e'+1, f' \end{matrix} \middle| (t-\tau)s \right] d\tau \right\} dt$$

$$= \frac{\Gamma(d)\Gamma(f')}{s^{d+f'}} \Delta_7(a, c, e) \Delta_9(a', c', d', e').$$

Theorem 43. For $\Re(s) > 0$, $\Re(d) > 0$, and $\Re(d') > 0$, the following result holds true:

$$\int_0^\infty e^{-st} \left\{ \int_0^t \tau^{d-1} (t-\tau)^{d'-1} {}_4F_4 \left[\begin{matrix} a, 1+\frac{1}{2}a, b, c \\ \frac{1}{2}a, a-b+1, a-c+1, d \end{matrix} \middle| -\tau s \right] \times {}_4F_4 \left[\begin{matrix} a', 1+\frac{1}{2}a', b', c' \\ \frac{1}{2}a', a'-b'+1, a'-c'+1, d' \end{matrix} \middle| -(t-\tau)s \right] d\tau \right\} dt$$

$$= \frac{\Gamma(d)\Gamma(d')}{s^{d+d'}} \Delta_8(a, b, c) \Delta_8(a', b', c').$$

Theorem 44. For $\Re(s) > 0$, $\Re(d) > 0$, $\Re(f') > 0$, and $\Re(a' - c' - d' - e' + 1) > 0$, the following result holds true:

$$\int_0^\infty e^{-st} \left\{ \int_0^t \tau^{d-1} (t-\tau)^{f'-1} {}_4F_4 \left[\begin{matrix} a, 1+\frac{1}{2}a, b, c \\ \frac{1}{2}a, a-b+1, a-c+1, d \end{matrix} \middle| -\tau s \right] \times {}_5F_5 \left[\begin{matrix} a', 1+\frac{1}{2}a', c', d', e' \\ \frac{1}{2}a', a'-c'+1, a'-d'+1, a'-e'+1, f' \end{matrix} \middle| (t-\tau)s \right] d\tau \right\} dt$$

$$= \frac{\Gamma(d)\Gamma(f')}{s^{d+f'}} \Delta_8(a, c, e) \Delta_9(a', c', d', e').$$

Theorem 45. For $\Re(s) > 0$, $\Re(f) > 0$, $\Re(f') > 0$, $\Re(a - c - d - e + 1) > 0$, and $\Re(a' - c' - d' - e' + 1) > 0$, the following result holds true:

$$\int_0^\infty e^{-st} \left\{ \int_0^t \tau^{f-1} (t-\tau)^{f'-1} {}_5F_5 \left[\begin{matrix} a, 1 + \frac{1}{2}a, c, d, e \\ \frac{1}{2}a, a-c+1, a-d+1, a-e+1, f \end{matrix} \middle| \tau s \right] \times {}_5F_5 \left[\begin{matrix} a', 1 + \frac{1}{2}a', c', d', e' \\ \frac{1}{2}a', a'-c'+1, a'-d'+1, a'-e'+1, f' \end{matrix} \middle| (t-\tau)s \right] d\tau \right\} dt$$

$$= \frac{\Gamma(f)\Gamma(f')}{s^{f+f'}} \Delta_9(a, c, d, e) \Delta_9(a', c', d', e'). \quad (57)$$

Proof. The proofs of results (13) to (57) asserted in Theorems 1–45 are quite straight forward. For example, in order to prove result (13) asserted in Theorem 1, we proceed as follows. In the general result (9), if we get $p = q = p' = q' = 2$, $a_1 = a, a_2 = b, a'_1 = a', a'_2 = b', b_1 = c, b_2 = d, b'_1 = c', b'_2 = d', k = k' = s, \mu = d$, and $\nu = d'$, then it takes the following form:

$$\int_0^\infty e^{-st} \left\{ \int_0^t \tau^{d-1} (t-\tau)^{d'-1} {}_2F_2 \left[\begin{matrix} a, b \\ c, d \end{matrix} \middle| \tau s \right] {}_2F_2 \left[\begin{matrix} a', b' \\ c', d' \end{matrix} \middle| (t-\tau)s \right] d\tau \right\} dt$$

$$= \Gamma(d)\Gamma(d') s^{-d-d'} {}_2F_1 \left[\begin{matrix} a, b \\ c \end{matrix} \middle| 1 \right] {}_2F_1 \left[\begin{matrix} a', b' \\ c' \end{matrix} \middle| 1 \right]. \quad (58)$$

We now observe that the twice ${}_2F_1$ appearing on the right-hand side of (58) can be calculated by Gauss' summation theorem (3), and we easily arrive at the desired result (13). This completes the proof of result (13) asserted by Theorem 1. The remaining results (14)–(57) can be established in a similar way. We would like to leave the details to the interested readers. \square

3. Corollaries

In this section, we shall mention several known results of our main findings:

- In Theorems 1, 2, 4, 40, 42, and 44, if we take $d = b$ and $d' = b'$, we get the known results due to Milovanović et al. (Theorems 2.1, 2, and 2.4 in [6] and Corollary 1.3 and 1.5 in [7], respectively).
- In Theorems 3 and 11, if we take $d = b$ and $d' = 1 - a'$, we get the known results due to Milovanović et al. (Theorems 2.3 in [6] and Corollary 4 in [7], respectively).
- In Theorems 5 to 8, 13–16, and 26–29, if we take $d = b$ and $d' = c'$, we get the known results due to Milovanović et al. (Theorems 2.5 to 2.10, 2.14 to 2.16, 2.23, 2.25, and 2.29 in [6] respectively).
- In Theorems 20–23, if we take $d = 1 - a$ and $d' = c'$, we get the known results due to Milovanović et al. (Theorems 2.11 to 2.13 and 2.27 in [6], respectively).

- In Theorems 31–34, 36–38, 40, 41, and 43, if we take $d = c$ and $d' = c'$, we get the known results due to Milovanović et al. (Theorems 2.17 to 2.22, 2.31, 2.33, 2.35, and 2.37 [6], respectively).
- In Theorems 9, 17, 30, 35, 39, 42, and 44, if we take $d = b$ and $f' = c'$, we get the known results due to Milovanović et al. (Theorems 2.24, 2.26, 2.30, 2.32, 2.34, 2.36, and 2.38 in [6], respectively).
- In Theorem 24, if we take $d = 1 - a$ and $f' = c$, we get the known result due to Milovanović et al. (Theorem 2.28 in [6]).
- In Theorem 45, if we take $f = c$ and $f' = c'$, we get the known result due to Milovanović et al. (Theorem 2.39 in [6]).
- In Theorem 18, if we take $d = 1 - a$ and $d' = 1 - a'$, we get a known result due to Milovanović et al. (Corollary 2 in [7]).
- In Theorem 19, if we take $d = 1 - a$ and $d' = b'$, we get a known result due to Milovanović et al. (Corollary 6 in [7]).

4. Conclusion

In this note, our aim is to demonstrate how one can easily obtain in all forty-five attractive Laplace transforms of convolution type related to the generalized hypergeometric functions from the general result recorded in [5].

Applications related to engineering will be addressed in the next study. It is hoped that the results could be of potential use in the areas of engineering mathematics and mathematical physics.

Data Availability

No data were used to support this study.

Conflicts of Interest

The authors declare that there are no conflicts of interest regarding the publication of this paper.

References

- [1] G. V. Milovanović, R. K. Parmar, and A. K. Rathie, "Certain Laplace transforms of convolution type integrals involving product of two special ${}_pF_p$ functions," *Demonstratio Mathematica*, vol. 51, pp. 264–276, 2018.
- [2] G. Milovanovic, R. Parmar, and A. Rathie, "A study of generalized summation theorems for the series ${}_2F_1$ with an applications to Laplace transforms of convolution type integrals involving Kummer's functions ${}_1F_1$," *Applicable Analysis and Discrete Mathematics*, vol. 12, no. 1, pp. 257–272, 2018.
- [3] E. D. Rainville, *Special Functions*, Macmillan, New York, 1960.
- [4] H. Exton, *Multiple Hypergeometric Functions and Applications*, Halsted Press John Wiley & Sons, Ellis Horwood, Chichester, New York, London, Sydney and Toronto, 1976.
- [5] H. Exton, *Handbook of Hypergeometric Integrals, Theory, Applications, Tables, Computer Programs*, Halsted Press John Wiley & Sons, Ellis Horwood, Chichester, New York, Brisbane and Toronto, 1978.
- [6] L. J. Slater, *Generalized Hypergeometric Functions*, Cambridge University Press, New York, NY, USA, 1966.
- [7] L. J. Slater, *Confluent Hypergeometric Functions*, Cambridge University Press, New York, NY, USA, 1960.
- [8] C. F. Gauss, "Disquisitiones generales area seriem infinitam," Thesis, Ges. Werke Gottingen, Gottingen, 1866.
- [9] Y.-S. Kim, A. K. Rathie, and Rathie, "Applications of generalized kummer's summation theorem for the series ${}_2F_1$," *Bulletin of the Korean Mathematical Society*, vol. 46, no. 6, pp. 1201–1211, 2009.

Research Article

Facial Image Segmentation Based on Gabor Filter

Hong-An Li ¹, Jiangwen Fan ¹, Jing Zhang ¹, Zhanli Li ¹, Dandan He ², Ming Si ¹,
and Yun Zhang ¹

¹College of Computer Science and Technology, Xi'an University of Science and Technology, Xi'an 710054, China

²College of Information Engineering, Chang'an University, Xi'an 710064, China

Correspondence should be addressed to Hong-An Li; an6860@126.com

Received 19 December 2020; Revised 16 January 2021; Accepted 19 January 2021; Published 10 February 2021

Academic Editor: HwaJoon Kim

Copyright © 2021 Hong-An Li et al. This is an open access article distributed under the Creative Commons Attribution License, which permits unrestricted use, distribution, and reproduction in any medium, provided the original work is properly cited.

As an important part of face recognition, facial image segmentation has become a focus of human feature detection. In this paper, the AdaBoost algorithm and the Gabor texture analysis algorithm are used to segment an image containing multiple faces, which effectively reduces the false detection rate of facial image segmentation. In facial image segmentation, the image containing face information is first analyzed for texture using the Gabor algorithm, and appropriate thresholds are set with different thresholds of skin-like areas, where skin-like areas in the image's background information are removed. Then, the AdaBoost algorithm is used to detect face regions, and finally, the detected face regions are segmented. Experiments show that this method can quickly and accurately segment faces in an image and effectively reduce the rate of missed and false detections.

1. Introduction

With the rapid development of biometric recognition technology, face recognition [1] has been widely used in many fields. As the basic research of face recognition, facial image segmentation [2–4] is an important step in a face recognition system. Accurate and fast segmentation of the face is critical to improve the speed and accuracy of recognition. However, due to the influences of head position, occlusion, image orientation, illumination conditions and facial expression, facial segmentation is typically difficult. Early research of images containing faces primarily focused on the adjustment model, the adjustment subimage, and the deformation model. Detection methods typically detect images with frontal face regions with simple backgrounds and other unchanged conditions; thus, their detection forms are relatively fixed. Based on these facial image detection systems, even if changes in facial image detection conditions are not affected, certain system parameters must be adjusted. Then, people paid more attention to positive facial image research, facial recognition, and video coding system. In recent years, facial image segmentation has become a research hotspot. Researchers have developed many methods,

including methods that detect movement, skin color, and general information. The use of statistical methods and neural networks can find face information in complex backgrounds, markedly improving the accuracy of facial image segmentation. In addition, considerable progress has been made in the design of methods that can manage facial features with precise positions. The latest research of this project focuses on the statistical analysis model [5], the neural network learning method [6], the SVM (support vector machine) method [7], the Markov random field method [8], the BDF [9], face detection based on skin color, and other statistical information.

Currently, the rapid development of facial image segmentation and recognition has widened its possible applications. We divide existing facial image segmentation and recognition methods into three categories. The first is knowledge-based methods [10], which use surface-based rules for face recognition [11]. There are clear rules of thumb for regional facial features, and facial expressions can be used to set local features of facial features. Yang and Huang [12] used a knowledge-based hierarchical method to detect a human face and established a three-level detection system. The primary difficulty lies in transforming human

perception experience into clear rules and methods, and it is difficult to correctly detect facial areas outside these detection rules and result in feature loss. However, if these rules are too general, they can lead to error detection. In addition, the method cannot recognize all possible situations; thus, it is difficult to detect the face in different positions.

The second type is based on skin color [13]. Skin color can reveal the position of the face and is an important piece of facial information that does not depend on the details of the face. Skin color can rotate, is relatively stable, can be distinguished from the complex and diverse colors in most backgrounds, and has the advantages of pose and speed invariance. Therefore, this method is commonly used in facial image segmentation and provides good detection results for certain detection algorithms. Second, the skin is seriously disturbed by illumination, noise, and certain occlusion, and the skin color function is weakened; thus, the algorithm is difficult to use. Although skin color technology has certain limitations, it has many benefits. For example, face detection can be performed on a fine background of repeated attributes. This method does not limit the size and direction of the face, and the processing speed is relatively fast, and it is easy to define and locate the real face. Particularly in color facial image segmentation with complex and diverse colors in the background, this method can segment candidate face regions based on the different skin color thresholds, and through certain verification and face feature matching, the face region can be effectively located.

The third type is based on model matching [14]. A stored face and algorithm can be used to create a standard model [15], which describes the shape of the eyes, nose, and other facial features; or a flexible model. Then, similarities between the detection area and the standard model are calculated to determine whether the region is a face or a corresponding entity. Liang and Ai [16] used five types of face detection templates to detect facial areas. The original template was used to detect eyes, and the other four templates were used to detect facial styles with different length ratios. This method has been successfully implemented and achieved good results. However, to recognize a face in a complex background, different interventions and basic models must be developed. The hidden interference model is difficult to describe, a template that can represent different faces cannot distinguish complex backgrounds accurately, and a template that can distinguish complex backgrounds cannot represent faces accurately. Based on this method, researchers must balance model accuracy and error detection.

In order to improve the accuracy and stability of the face segmentation algorithm, this paper combined the AdaBoost algorithm [17] and Gabor filter [18] to segment the face image, and the texture of the image processed by Gabor filter is clearer, which can effectively solve the omissions and misdetection phenomenon when the AdaBoost algorithm directly segments the face. Our proposed algorithm has a significant improvement in the accuracy of face image segmentation, especially in the complex background is more obvious.

The structure of this paper is as follows: Section 1 introduces the existing facial image segmentation methods; Section 2 introduces the Haar-like feature Gabor features, and the AdaBoost algorithm; Section 3 proposes a facial image segmentation algorithm combining the Gabor filter and the AdaBoost algorithm; Section 4 presents experimental results and analyses; and Section 5 summarizes the full text.

2. Related Work

2.1. Haar Classifier. The Haar classifier is a tree-based classifier that creates a boost filter cascade classifier and primarily includes Haar-like features, integral graph method, AdaBoost algorithm, and cascading features, including the following:

- (1) Haar-like features are extracted, and the integral graph method is used to process the Haar-like features quickly
- (2) The AdaBoost algorithm is used to train the model continuously to obtain a strong classifier to distinguish a face from nonfacial information
- (3) Strong classifiers can be cascaded together by the screening cascade method, which can improve detection accuracy

A Haar-like feature is used to describe a human face. There are two rectangles (a white and black matrix), and an eigenvalue is defined as the sum of the black matrix pixels minus the sum of the white matrix pixels. These Haar eigenvalues describe changes in gray levels. Because rectangular features are only sensitive to simple graphic structures, such as edges and line segments, they can only describe the structure of a particular trend.

By changing the size and location of the model, we can list many feature elements in the image pane. The function model in Figure 1 is called a “feature prototype.” We can obtain many rectangular features by changing the position in the subwindow and the size of various templates and then calculate all eigenvalues in the subwindow based on these eigenvalues.

Figure 2 shows certain features of the face. For example, the color of the eye area in the middle is darker than that of the cheek, while the color on the right shows that the color of the bridge of the nose is lighter than that of the side of the nose. The same is true for other targets such as eyes, which can also be represented by appropriate rectangular elements. Compared to the simple use of pixels, the use of features has great advantages and yields faster computing speeds.

2.2. Gabor Filter. The Gabor transform effectively extracts spatial and local frequency information from a target region. Although the Gabor wavelet itself does not form an orthogonal basis, it may be a narrow frame under certain parameters. The Gabor wave is sensitive to the edge of the image and provides a good proportion selection characteristics and directionality. The Gabor wave is not sensitive to changes in illumination, making it widely applicable to

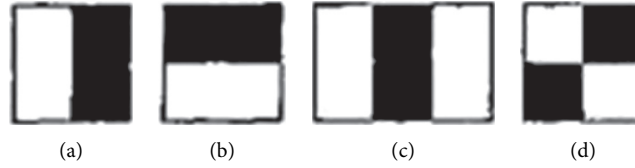


FIGURE 1: Feature prototype.

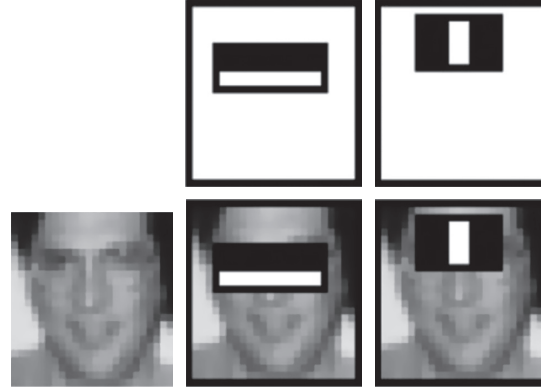


FIGURE 2: Rectangular features.

describing visual information accurately. Gabor filtering with different scales in the same direction is shown in Figure 3. Gabor filtering with different directions in the same scale is shown in Figure 4.

Gabor transforms include dividing the signal into several small time intervals and then using Fourier transform to analyze each time interval to determine the signal frequency during the corresponding time interval. The processing method includes adding a sliding window and performing Fourier transform.

If f is a concrete function, and $f \in L^2(R)$, then the Gabor transform is defined as

$$G_f(a, b, w) = \int_{-\infty}^{\infty} f(t)g_a(t - b)e^{-tw} dt, \quad (1)$$

where

$$g_a(t) = \frac{1}{2\sqrt{\pi a}} \exp\left(-\frac{t^2}{4a}\right). \quad (2)$$

Equation (1) is a Gaussian function called a window function, where $A > 0$, $b > 0$, $g_a(t - b)$ is a window function of time localization, and the parameter b is used as a parallel moving window to cover the entire time domain. If we integrate the parameter b , then we have

$$\int_{-\infty}^{\infty} G_f(a, b, w)db = \hat{f}(w), \quad w \in R. \quad (3)$$

The signal reconstruction expression is

$$f(t) = \frac{1}{2\pi} \int_{-\infty}^{\infty} \int_{-\infty}^{\infty} G_f(a, b, w)g_a(t - b)e^{tw} dwdb. \quad (4)$$

The value of the Gabor transform is Gaussian for two reasons: (1) the Fourier transform of Gaussian function

remains Gaussian function; thus, the inverse Fourier transform can also be located by the window function (i.e., the frequency-domain location); and (2) the Gabor transform is the best Fourier transform of a window. Most importantly, after the Gabor transform, a real analysis of time and frequency is performed. Thus, the Gabor transform can locate time-frequency, including all signal information concurrently, correlation information of signal change severity, frequency-domain information, and local time-domain information.

2.3. AdaBoost Algorithm. Facial image segmentation refers to the technology and process of dividing the facial image into several specific and unique regions, and identifying objects of interest in these regions. In recent years, facial image segmentation technology has been widely used in facial information processing. Facial image segmentation is an important step between facial image processing and face image analysis. Existing facial image segmentation methods can be divided into the following categories: knowledge-based, model matching, and skin color-based.

There are more types of facial image segmentation algorithms, but most are hindered by noise or background. Noise is typically difficult to distinguish from a face, which leads to low accuracy and stability. The original purpose of the AdaBoost [19] algorithm is to improve the performance of the simple classification algorithm by training various weak classifiers on the same training set and then combining these weak classifiers into a strong classifier (i.e., the final classifier) [20]. We use the AdaBoost algorithm based on Haar-like rectangle features for face detection. The AdaBoost method iteratively searches for feature vectors that can distinguish a face from background based on the edge gray features of a human face. In this iterative process, the weight

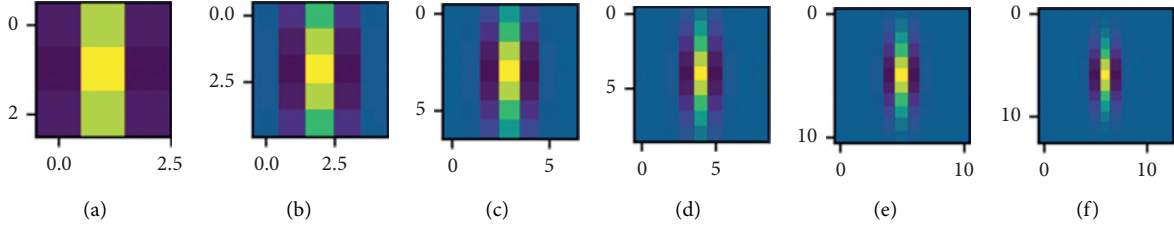


FIGURE 3: Gabor filtering with different scales in the same direction.

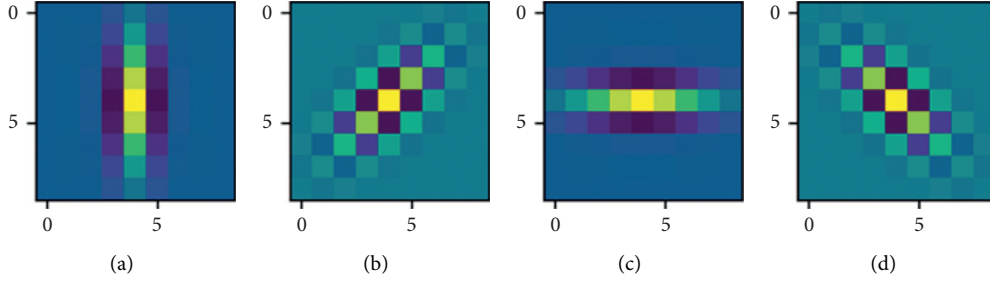


FIGURE 4: Gabor filtering in different directions under the same scale.

of this iteration is updated based on the classification accuracy of the last training set, and finally the purpose of changing the data distribution is achieved. The specific steps are as follows:

- (1) The training data set is searched, and both face regions and nonface regions are manually segmented from the image as positive and negative training sample sets, respectively.
- (2) A Haar-like feature is extracted, and its eigenvalue is used to represent the contrast between the gray level of the facial area and that of the nonface area within the rectangular range. The larger the eigenvalue, the more marked the edge features are. Then, the approximate rate is used to detect the face. The eigenvalue is defined as

$$f(r) = \left| c \times \sum_{(x,y) \in S_B} i(x,y) - \sum_{(x,y) \in S_W} i(x,y) \right|, \quad (5)$$

where $f(r)$ is the eigenvalue corresponding to the rectangular feature, $i(x,y)$ is the gray value of pixels (x,y) in the rectangle area, $\sum_{(x,y) \in S_B} i(x,y)$ is the sum of the gray levels of the face area, $\sum_{(x,y) \in S_W} i(x,y)$ is the sum of the gray levels of the background area, and c is the ratio of the size of the background area and the face area in the rectangular feature.

- (3) The classifier is selected, the weight in the iteration process is adjusted, and the weight of the correct classification samples is reduced:

$$w_{t+1,i} = w_{t,i} \beta_t^{1-\varepsilon_t}, \quad (6)$$

where $i = 1, 2, \dots, N$. When the classification is correct, the weight of ε_t decreases; otherwise, $\varepsilon_t = 1$,

and the weight value increases. The weight is updated, and iterations continue until the most effective n features are selected from the rectangular features as weak classifiers, which makes the AdaBoost algorithm integrate strong classifiers.

- (4) Because n weak classifiers may detect the same face many times, we combine the detection results from intersecting areas. We select the maximum value of four vertices as the new vertices and synthesize them into a detection result to reduce repeated face detection.

3. Facial Image Segmentation Algorithm Design

To solve the problems of false and missing detections in facial image segmentation, this paper proposes a facial image segmentation algorithm combining the Gabor filter and the AdaBoost algorithm. The AdaBoost algorithm can recognize and detect faces in an image quickly. However, when the background information of the image is complex, the face detection based on the AdaBoost algorithm will typically result in many background information sections that are similar to skin color features being detected as face information; face information may also be missed. To solve this problem, we first use the textural features of skin and the significant differences of other objects combined with Gabor texture for further analysis.

This method can be divided into two steps. First, the Gabor filter is used to obtain the texture feature map of the faces image, and then a threshold is set to extract the contour information of skin color to identify a skin-like region. In this way, black pixels can be added to the background information, which can significantly reduce the possibility of falsely detecting background information near skin color information. Second, the AdaBoost algorithm is used to segment the faces image, and the face region can be obtained. The algorithm steps are shown in Figure 5.

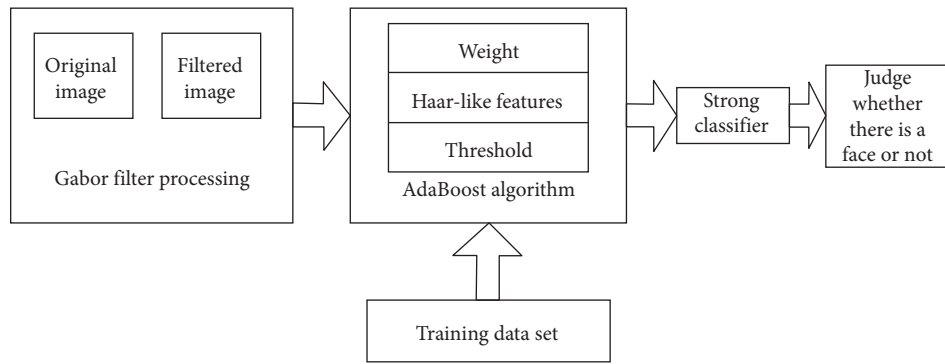


FIGURE 5: Flow chart of the algorithm.



FIGURE 6: The detection was compared to that without Gabor filtering. (a) Original image. (b) AdaBoost detection result image. (c) Gabor + AdaBoost detection result image.

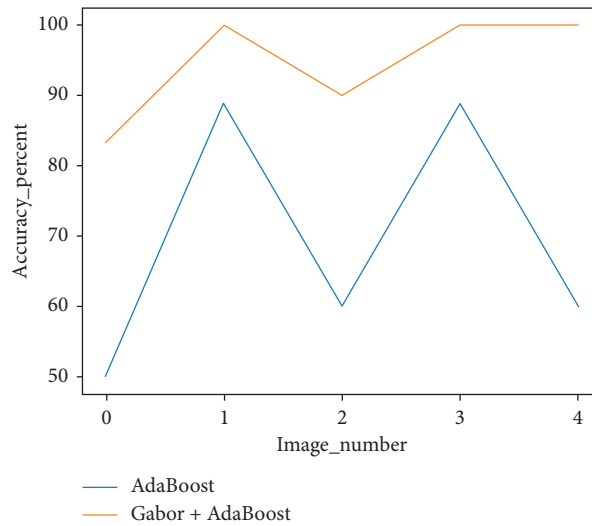


FIGURE 7: Face segmentation accuracy of experimental group and control group.

- (1) After Gabor filtering, texture features of the facial image are identified, and the contour information of skin color is extracted.
- (2) In this paper, the AdaBoost algorithm is used to extract the rectangular features in the face images. Based on the principle of minimum weighted error rate in training samples, n features that are most effective for classification are selected from the rectangular features as weak classifiers. During the iteration process, the weights are constantly modified to form a strong classifier.
- (3) The strong classifier is used for face segmentation, and the regions intersected by boundary regions are synthesized into a detection result.

4. Experiment and Analysis

4.1. Experimental Environment. To demonstrate the superiority of this algorithm, we use experimental and control groups to segment the faces image. In the experimental group, Gabor filtering was performed first, and then the AdaBoost algorithm was used for segmentation. In the control group, AdaBoost face segmentation was performed directly. The experiment was conducted on a 64 bit Windows 10 operating system with an Intel core i5-6300HQCPU@2.30 GHz2.30 GHz, 8 GB of RAM, an Nvidia GeForce GTX 960Mx, OpenCV4.0.1, and Visual Studio 2017.

4.2. Experimental Analysis. In the experiment, the Haar face feature classifier `haarcascade_frontalface_alt_XML` was trained by front face in OpenCV and then applied to positive faces images. If you want to segment the side face or other organs, OpenCV also provides a trained classifier. The experiment was divided into experimental and control groups. The design of four-direction and seven-dimension Gabor filter can filter redundant information as

much as possible. For the experimental group, the original image was filtered with a four-direction and seven-dimension Gabor filter. The four directions were 0 degrees, 45 degrees, 90 degrees, 135 degrees, and the seven scales were 1, 2, 3, 4, 5, 6, and 7 pixels, and then the filtered image was segmented with the AdaBoost algorithm. The control group directly uses the AdaBoost algorithm to segment the original image without Gabor filtering. The purpose of this experiment is to verify that our method has better detection rate and stability for face segmentation compared with AdaBoost algorithm.

For the facial image in Figure 6, we conducted 10 experiments on all experimental images, and the results of multiple experiments on each image were consistent, verifying the stability of the two methods in the experimental and control groups. In the control group without Gabor filtering, the segmentation accuracy of a human face is low, and more missed detections exist: clothes are frequently mistakenly detected as a human face. In the experimental group, spatial location and the local structure information of directional selectivity maintain the details of the image features and are not sensitive to illumination change because the Gabor filter can describe spatial frequencies well. Additionally, the experimental group after managing the Gabor filter of the images is not mistakenly identified and markedly improves the human face segmentation accuracy.

In Figure 6, we counted the face segmentation accuracy of experimental group and the control group, and Figure 7 shows the accuracy of five experiments using different methods in Figure 6, where the horizontal axis represents the picture number and the vertical axis represents the segmentation accuracy. As shown in Figure 7, the face segmentation accuracy of the experimental group is higher than that of the control group. Overall, the face segmentation accuracy of the experimental group is significantly higher than that of the control group. The comparison experiment proves the effectiveness of the method proposed in this paper.

TABLE 1: Analysis of experimental data.

Model	Total number of faces	Correct face segmentation	Number of misdetected faces	Number of missing faces	Face segmentation accuracy (%)
Our method	49	47	0	2	95.9
AdaBoost	49	34	1	15	69.4

The detection data in Figure 6 are shown in Table 1. Using AdaBoost-based face detection when the background information is complex, many background regions that are similar to skin color features will be detected as face information. In the experiment, the background is recognized as a face. The Gabor filter can describe local structure information corresponding to spatial frequency, spatial position, and direction selectivity; can retain the detailed features of the image; and is not sensitive to light changes. The accuracy of face recognition after Gabor filtering is 26.5% higher than that of direct face recognition.

5. Conclusion

To make facial image segmentation more accurate and efficient and to create a better foundation for face recognition, this study investigates a facial image segmentation algorithm based on the Gabor filter and the AdaBoost algorithm. In this method, the Gabor filter is used to filter the original images, and skin color-like regions are extracted as the final image for recognition. Then, the AdaBoost algorithm is used to recognize faces in the image. Experimental results show that the proposed method can effectively extract skin-like regions, solve the problem of missing and false detections when the AdaBoost algorithm is directly used for face segmentation, and thereby effectively improve the accuracy of facial image segmentation.

Data Availability

The image data used to support the findings of this study are included within the article.

Conflicts of Interest

The authors declare that there are no conflicts of interest regarding the publication of this article

Acknowledgments

This work was supported in part by the Natural Science Basic Research Plan in Shaanxi Province of China (2020JQ-758 and 2019JM-162).

References

- [1] X. Y. Xu, "Survey of face recognition technology," *Electronic Test*, vol. 2015, no. 5, pp. 885–894, 2015.
- [2] Y. P. Yin, Z. Ying, Z. Dan et al., "Face segmentation using CRFs based on multiple feature fusion," *Electronic Measurement Technology*, vol. 38, no. 6, pp. 54–59, 2015.
- [3] X. Wu, J. Zhao, and H. Wang, "Face segmentation based on level set and improved DBM prior shape," *Progress in Artificial Intelligence*, vol. 8, no. 46, pp. 1–13, 2019.
- [4] S. Wazarkar, B. N. Keshavamurthy, and A. Hussain, "Region-based segmentation of social images using soft KNN algorithm," *Procedia Computer Science*, vol. 125, pp. 93–98, 2018.
- [5] D. Liu, L. F. Wang, and H. F. Zhang, "Design of statistical analysis model based on big data," *Software Guide*, vol. 15, no. 7, pp. 28–30, 2016.
- [6] W. Liu, S. Liu, R. C. Bai, X. Zhou, and D. N. Zhou, "Research of mutual learning neural network training method," *Chinese Journal of Computers*, vol. 40, no. 6, pp. 1291–1308, 2017.
- [7] Y. Zhang, B. Li, H. Lu, A. Irie, and X. Ruan, "Sample-specific SVM learning for person re-identification," in *Proceedings of the 2016 IEEE Conference on Computer Vision and Pattern Recognition (CVPR)*, June 2016.
- [8] J. Z. Cao and A. G. Song, "Research on the texture image segmentation method based on Markov random field," *Chinese Journal of Scientific Instrument*, vol. 36, no. 4, pp. 776–786, 2015.
- [9] L. G. Ixaru, G. Vanden Berghe, and H. De Meyer, "Exponentially fitted variable two-step BDF algorithm for first order ODEs," *Computer Physics Communications*, vol. 150, no. 2, pp. 116–128, 2003.
- [10] J. Jun and Z. G. Lin, "A knowledge-based approach for fast human face detection," *Journal of Image and Graphics*, vol. 7, no. 1, pp. 6–10, 2002.
- [11] Y. Ming, *Research on 3D face recognition based on invariant features*, Ph.D. thesis, Beijing Jiaotong University, Beijing, China, 2012.
- [12] G. Yang and T. S. Huang, "Human face detection in a complex background," *Pattern Recognition*, vol. 27, no. 1, pp. 53–63, 1994.
- [13] Z. P. Gong, "A face detection method based on skin color," *Journal of Luohe Vocational and Technical College*, vol. 12, no. 2, pp. 42–44, 2013.
- [14] Y. Ma, *Face Detection Method Based on Color and Template Matching*, Dalian University of Technology, Dalian, China, 2006.
- [15] Z. H. Zeng and Y. M. Zhang, "3D face standard model based on OpenGL," *Mechanical Engineering and Automation*, vol. 34, no. 4, pp. 34–36, 2007.
- [16] L. H. Liang and H. Z. Ai, "Multi-template-matching based single face detection," *Journal of Image and Graphics*, vol. 4, no. 10, pp. 825–830, 1999.
- [17] J. Zhu, H. Zou, S. Rosset, and T. Hastie, "Multi-class AdaBoost," *Statistics & Its Interface*, vol. 2, no. 3, pp. 349–360, 2006.
- [18] Y. Hong-Yu, Y. U. Lei, and W. Sen, "Face recognition with Gabor texture features," *Application Research of Computers*, vol. 28, no. 10, pp. 3974–3976, 2011.
- [19] L. I. Wei, H. E. Peng-Ju, and Y. Heng, "AdaBoost pedestrian detection algorithm based on dual-threshold motion area segmentation," *Application Research of Computers*, vol. 29, no. 9, pp. 3571–3570, 2012.
- [20] S. M. Hu, D. Liang, G. Y. Yang, G.-W. Yang, and W.-Y. Zhou, "Jitter: a novel deep learning framework with meta-operators and unified graph execution," *Science China Information Sciences*, vol. 63, no. 12, pp. 1–21, 2020.

Research Article

Some General Integral Operator Inequalities Associated with φ -Quasiconvex Functions

Young Chel Kwun,¹ Moquddsa Zahra,² Ghulam Farid ,³ Praveen Agarwal ,⁴
and Shin Min Kang ⁵

¹Department of Mathematics, Dong-A University, Busan 49315, Republic of Korea

²Department of Mathematics, University of Wah, Wah Cantt, Pakistan

³Department of Mathematics, COMSATS University Islamabad, Attock Campus, Pakistan

⁴Anand International College of Engineering, Near Kanota Agra Road, Jaipur 303012, Rajasthan, India

⁵Center for General Education, China Medical University, Taichung 40402, Taiwan

Correspondence should be addressed to Ghulam Farid; faridphdsms@hotmail.com and Shin Min Kang; smkang@gnu.ac.kr

Received 21 November 2020; Revised 15 December 2020; Accepted 18 December 2020; Published 8 January 2021

Academic Editor: HwaJoon Kim

Copyright © 2021 Young Chel Kwun et al. This is an open access article distributed under the Creative Commons Attribution License, which permits unrestricted use, distribution, and reproduction in any medium, provided the original work is properly cited.

This paper deals with generalized integral operator inequalities which are established by using φ -quasiconvex functions. Bounds of an integral operator are established which have connections with different kinds of known fractional integral operators. All the results are deducible for quasiconvex functions. Some fractional integral inequalities are deduced.

1. Introduction and Preliminaries

Convex functions play a vital role in the theory of mathematical analysis. Many generalizations have been given for the convex function, for example, α -convex, m -convex, h -convex, (α, m) -convex, (h, m) -convex, s -convex, (s, m) -convex, φ -convex, and quasiconvex functions (see [1–10]). We will use φ -quasiconvex functions to study the bounds of unified integral operators, and the established results are directly related with fractional integral operators in particular cases. All the fractional integral operators defined in [11–15] satisfy the results of this paper for φ -quasiconvex functions, and also the results of [16–19] are reproduced in special cases.

Definition 1 (see [20]). A function $f: J \rightarrow \mathbb{R}$ is called convex if

$$f(tx_0 + (1-t)y_0) \leq tf(x_0) + (1-t)f(y_0), \quad t \in [0, 1], \quad (1)$$

holds $\forall x_0, y_0 \in J$, where J is an interval in \mathbb{R} .

Definition 2 (see [21]). A function $f: J \rightarrow \mathbb{R}$ is called φ -quasiconvex if

$$f(tx_0 + (1-t)y_0) \leq \max\{f(y_0), f(y_0) + \varphi(f(x_0), f(y_0))\}, \quad t \in [0, 1], \quad (2)$$

holds $\forall x_0, y_0 \in J$, where J is an interval in \mathbb{R} and $\varphi: f(J) \times f(J) \rightarrow \mathbb{R}$ is a bifunction.

For $\varphi(x_0, y_0) = x_0 - y_0$, (2) reduces to quasiconvex function. It is to be noted that every convex function is quasiconvex but converse does not hold.

Example 1 (see [22]). A function $f: [-2, 2] \rightarrow \mathbb{R}$ defined as

$$f(x) = \begin{cases} 1, & x \in [-2, -1], \\ x^2, & x \in (-1, 2], \end{cases} \quad (3)$$

is quasiconvex on $[-2, 2]$ but not a convex function on the same interval.

The aim of this paper is to establish integral inequalities by using φ -quasiconvex functions. The results will provide upper bounds of integral operators for φ -quasiconvex functions, which will behave like compact formulas that unify bounds of various kinds of operators already defined in literature. Next, we give some generalized fractional integral operators connected with the findings of this work.

Definition 3 (see [14]). Let $f \in L[x_0, y_0]$ and g be positive and increasing function on $(x_0, y_0]$, and also, let g have continuous derivative on (x_0, y_0) . The left and right fractional integrals of f with respect to g on $[x_0, y_0]$ of order λ , where $\lambda > 0$, are given as follows:

$$\begin{aligned}
 {}_g I_{x_0^+}^\lambda f(x) &= \frac{1}{\Gamma(\lambda)} \int_{x_0}^x (g(x) - g(t))^{\lambda-1} g'(t) f(t) dt, \quad x > x_0, \\
 {}_g I_{y_0^-}^\lambda f(x) &= \frac{1}{\Gamma(\lambda)} \int_x^{y_0} (g(t) - g(x))^{\lambda-1} g'(t) f(t) dt, \quad x < y_0,
 \end{aligned}
 \tag{4}$$

where

$$\Gamma(\lambda) = \int_0^\infty t^{\lambda-1} e^{-t} dt. \tag{5}$$

Definition 4 (see [23]). Let $f \in L[x_0, y_0]$ and g be positive and increasing function on $(x_0, y_0]$, and also let g have continuous derivative on (x_0, y_0) . The left and right k -fractional integrals of f with respect to g on $[x_0, y_0]$ of order λ , where $\lambda, k > 0$, are given as follows:

$$\begin{aligned}
 {}_g I_{x_0^+}^{\lambda, k} f(x) &= \frac{1}{k\Gamma_k(\lambda)} \int_{x_0}^x (g(x) - g(t))^{\lambda/k-1} g'(t) f(t) dt, \quad x > x_0, \\
 {}_g I_{y_0^-}^{\lambda, k} f(x) &= \frac{1}{k\Gamma_k(\lambda)} \int_x^{y_0} (g(t) - g(x))^{\lambda/k-1} g'(t) f(t) dt, \quad x < y_0,
 \end{aligned}
 \tag{6}$$

where

$$\Gamma_k(\lambda) = \int_0^\infty t^{\lambda-1} e^{-t^k/k} dt. \tag{7}$$

Definition 5 (see [24]). Let $f \in L_1[x_0, y_0]$ and $x \in [x_0, y_0]$; also, let $\Phi, \lambda, \varrho, \kappa, \gamma, \sigma \in \mathbb{C}$, $\Re(\lambda), \Re(\varrho), \Re(\kappa) > 0$, $\Re(\chi) > \Re(\gamma) > 0$ with $p \geq 0, \vartheta > 0$, and $0 < k \leq \vartheta + \Re(\lambda)$, then the generalized fractional integral operators ${}_{\lambda, \varrho, \kappa, \Phi, x_0^+}^{\gamma, \vartheta, k, \chi} f$ and ${}_{\lambda, \varrho, \kappa, \Phi, y_0^-}^{\gamma, \vartheta, k, \chi} f$ are defined as

$$\begin{aligned}
 \left({}_{\lambda, \varrho, \kappa, \Phi, x_0^+}^{\gamma, \vartheta, k, \chi} f \right)(x; p) &= \int_{x_0}^x (x-t)^{\varrho-1} E_{\lambda, \varrho, \kappa}^{\gamma, \vartheta, k, \chi}(\Phi(x-t)^\lambda; p) f(t) dt, \\
 \left({}_{\lambda, \varrho, \kappa, \Phi, y_0^-}^{\gamma, \vartheta, k, \chi} f \right)(x; p) &= \int_x^{y_0} (t-x)^{\varrho-1} E_{\lambda, \varrho, \kappa}^{\gamma, \vartheta, k, \chi}(\Phi(t-x)^\lambda; p) f(t) dt,
 \end{aligned}
 \tag{8}$$

where $E_{\lambda, \varrho, \kappa}^{\gamma, \vartheta, k, \chi}(t; p)$ is given by

$$E_{\lambda, \varrho, \kappa}^{\gamma, \vartheta, k, \chi}(t; p) = \sum_{n=0}^\infty \frac{\beta_p(\gamma + nk, \chi - \gamma)}{\beta(\gamma, \chi - \gamma)} \frac{(\chi)_{nk}}{\Gamma(\lambda n + \varrho)} \frac{t^n}{(\kappa)_{n\vartheta}}. \tag{9}$$

In [11], Farid defined a unified integral operator and proved the boundedness, linearity, and continuity of these integrals. It is given in the following definition.

Definition 6 (see [11]). Let $f, g: [x_0, y_0] \rightarrow \mathbb{R}$ where $0 < x_0 < y_0$ be the functions such that f is positive and integrable over $[x_0, y_0]$ and g is differentiable and strictly increasing. Also, let Ψ/x be an increasing function on $[x_0, \infty)$ and $\varrho, \kappa, \gamma, \chi \in \mathbb{C}$, $p, \lambda, \vartheta \geq 0$ and $0 < k \leq \vartheta + \lambda$. Then, for $x \in [x_0, y_0]$, the left and right integral operators are defined as

$$\left({}_g F_{\lambda, \varrho, \kappa, x_0^+}^{\Psi, \gamma, \vartheta, k, \chi} f \right)(x, \Phi; p) = \int_{x_0}^x G_x^\gamma \left(E_{\lambda, \varrho, \kappa}^{\gamma, \vartheta, k, \chi}; g; \Psi \right) g'(y) f(y) dy, \tag{10}$$

$$\left({}_g F_{\lambda, \varrho, \kappa, y_0^-}^{\Psi, \gamma, \vartheta, k, \chi} f \right)(x, \Phi; p) = \int_x^{y_0} G_x^\gamma \left(E_{\lambda, \varrho, \kappa}^{\gamma, \vartheta, k, \chi}; g; \Psi \right) g'(y) f(y) dy, \tag{11}$$

where

$$G_x^\gamma \left(E_{\lambda, \varrho, \kappa}^{\gamma, \vartheta, k, \chi}; g; \Psi \right) = \frac{\Psi(g(x) - g(y))}{g(x) - g(y)} E_{\lambda, \varrho, \kappa}^{\gamma, \vartheta, k, \chi}(\Phi(g(x) - g(y))^\lambda; p). \tag{12}$$

By making particular choices for Ψ and g and parameters involved in (9), several fractional integrals can be obtained (see [19], Remarks 6 and 7). In [19], Zhao, et al. proved the bounds of unified integral operators for quasiconvex functions stated in Theorems 1 to 4.

Theorem 1. Consider $f: [x_0, y_0] \rightarrow \mathbb{R}$ be a positive quasiconvex function and $g: [x_0, y_0] \rightarrow \mathbb{R}$ be differentiable and strictly increasing function. Also, Ψ/x be an increasing function on $[x_0, y_0]$ and $\varrho, \kappa, \gamma, \chi \in \mathbb{C}$, $p, \lambda, \nu, \vartheta \geq 0$, $0 < k \leq \vartheta + \lambda$, and $0 < k \leq \vartheta + \nu$. Then, for $x \in [x_0, y_0]$, we have

$$\begin{aligned}
 &\left({}_g F_{\lambda, \varrho, \kappa, x_0^+}^{\Psi, \gamma, \vartheta, k, \chi} f \right)(x, \Phi; p) + \left({}_g F_{\lambda, \varrho, \kappa, y_0^-}^{\Psi, \gamma, \vartheta, k, \chi} f \right)(x, \Phi; p) \\
 &\leq E_{\lambda, \varrho, \kappa}^{\gamma, \vartheta, k, \chi}(\Phi(g(x) - g(x_0))^\lambda; p) \Psi(g(x) \\
 &\quad - g(x_0)) \max\{f(x_0), f(x)\} \\
 &\quad + E_{\nu, \varrho, \kappa}^{\gamma, \vartheta, k, \chi}(\Phi(g(y_0) - g(x))^\nu; p) \Psi \\
 &\quad \cdot (g(y_0) - g(x)) \max\{f(x), f(y_0)\}.
 \end{aligned}
 \tag{13}$$

Theorem 2. Under the assumptions of Theorem 1, the following result holds:

$$\begin{aligned}
 &\left({}_g F_{\lambda, \varrho, \kappa, x_0^+}^{\Psi, \gamma, \vartheta, k, \chi} \right)(y_0, \Phi; p) + \left({}_g F_{\lambda, \varrho, \kappa, y_0^-}^{\Psi, \gamma, \vartheta, k, \chi} \right)(x_0, \Phi; p) \\
 &\leq \Psi(g(y_0) - g(x_0)) \left(E_{\lambda, \varrho, \kappa}^{\gamma, \vartheta, k, \chi}(\Phi(g(y_0) - g(x_0))^\lambda; p) \right. \\
 &\quad \left. + E_{\nu, \varrho, \kappa}^{\gamma, \vartheta, k, \chi}(\Phi(g(y_0) - g(x_0))^\nu; p) \right) \\
 &\quad \max\{f(x_0), f(y_0)\}.
 \end{aligned}
 \tag{14}$$

Theorem 3. Along with the assumptions of Theorem 1, if $f(x_0 + y_0 - x) = f(x)$, then the following result holds:

$$\begin{aligned} & f\left(\frac{x_0 + y_0}{2}\right)\left(\left({}_g F_{\nu, \varrho, \kappa, \gamma_0^-}^{\Psi, \gamma, \vartheta, k, \chi} 1\right)(x_0, \Phi; p) + \left({}_g F_{\lambda, \varrho, \kappa, x_0^+}^{\Psi, \gamma, \vartheta, k, \chi} 1\right)(y_0, \Phi; p)\right) \\ & \leq \left({}_g F_{\nu, \varrho, \kappa, \gamma_0^-}^{\Psi, \gamma, \vartheta, k, \chi} f\right)(x_0, \Phi; p) + \left({}_g F_{\lambda, \varrho, \kappa, x_0^+}^{\Psi, \gamma, \vartheta, k, \chi} f\right)(y_0, \Phi; p) \\ & \leq \Psi(g(y_0) - g(x_0))\left(E_{\lambda, \varrho, \kappa}^{\gamma, \vartheta, k, \chi}(\Phi(g(y_0) - g(x_0))^\lambda; p)\right. \\ & \quad \left.+ E_{\nu, \varrho, \kappa}^{\gamma, \vartheta, k, \chi}(\Phi(g(y_0) - g(x_0))^\nu; p)\right) \\ & \max\{f(x_0), f(y_0)\}. \end{aligned} \tag{15}$$

Theorem 4. Consider $f, g: [x_0, y_0] \rightarrow \mathbb{R}$ be two differentiable functions such that $|f'|$ is quasiconvex and g be strictly increasing for $0 < x_0 < y_0$. Also, Ψ/x be an increasing function on $[x_0, y_0]$ and $\varrho, \kappa, \gamma, \chi \in \mathbb{C}$, $p, \lambda, \nu, \vartheta \geq 0$ and $0 < k \leq \vartheta + \lambda$ and $0 < k \leq \vartheta + \nu$. Then, for $x \in (x_0, y_0)$, we have

$$\begin{aligned} & \left| \left({}_g F_{\lambda, \varrho, \kappa, x_0^+}^{\Psi, \gamma, \vartheta, k, \chi} f * g\right)(x, \Phi; p) + \left({}_g F_{\nu, \varrho, \kappa, y_0^-}^{\Psi, \gamma, \vartheta, k, \chi} f * g\right)(x, \Phi; p) \right| \\ & \leq E_{\lambda, \varrho, \kappa}^{\gamma, \vartheta, k, \chi}(\Phi(g(x) - g(x_0))^\lambda; p)\Psi(g(x) - g(x_0)) \\ & \quad \cdot \max(|f'(x_0)|, |f'(x)|) \\ & \quad + E_{\nu, \varrho, \kappa}^{\gamma, \vartheta, k, \chi}(\Phi(g(y_0) - g(x))^\nu; p)\Psi \\ & \quad \cdot (g(y_0) - g(x))\max(|f'(x)|, |f'(y_0)|), \end{aligned} \tag{16}$$

where

$$\left({}_g F_{\lambda, \varrho, \kappa, x_0^+}^{\Psi, \gamma, \vartheta, k, \chi} f * g\right)(x, \Phi; p) = \int_{x_0}^x G_x^t\left(E_{\lambda, \varrho, \kappa}^{\gamma, \vartheta, k, \chi}, g; \Psi\right)g'(t)f'(t)dt, \tag{17}$$

$$\left({}_g F_{\nu, \varrho, \kappa, y_0^-}^{\Psi, \gamma, \vartheta, k, \chi} f * g\right)(x, \Phi; p) = \int_x^{y_0} G_t^x\left(E_{\nu, \varrho, \kappa}^{\gamma, \vartheta, k, \chi}, g; \Psi\right)g'(t)f'(t)dt. \tag{18}$$

All of the above results are direct consequences of the results of this paper. Also, some of the results in papers [16–18] are very special cases. In the next section, φ -quasiconvexity has been used frequently to obtain the upper bounds and the Hadamard inequality, which gives upper as well as lower bounds of unified integral operators. Also defining convolution of two functions, some bounds have been obtained for φ -quasiconvexity of $|f'|$ of differential function f . In Section 3, some applications of the main results are given. In the whole paper, we use the notation

$$\max\{f(y_0), f(y_0) + \varphi(f(x_0), f(y_0))\} = M_\varphi^f(x_0, y_0). \tag{19}$$

2. Main Results

Theorem 5. Consider $f: [x_0, y_0] \rightarrow \mathbb{R}$ is φ -quasiconvex and positive and $g: [x_0, y_0] \rightarrow \mathbb{R}$ differentiable and strictly increasing functions. If Ψ/x is increasing function on $[x_0, y_0]$ and $\varrho, \kappa, \gamma, \chi \in \mathbb{C}$, $p, \lambda, \nu, \vartheta \geq 0$, $0 < k \leq \vartheta + \lambda$ and $0 < k \leq \vartheta + \nu$, then for $x \in [x_0, y_0]$, the following inequality holds:

$$\begin{aligned} & \left({}_g F_{\lambda, \varrho, \kappa, x_0^+}^{\Psi, \gamma, \vartheta, k, \chi} f\right)(x, \Phi; p) + \left({}_g F_{\nu, \varrho, \kappa, y_0^-}^{\Psi, \gamma, \vartheta, k, \chi} f\right)(x, \Phi; p) \\ & \leq E_{\lambda, \varrho, \kappa}^{\gamma, \vartheta, k, \chi}(\Phi(g(x) - g(x_0))^\lambda; p)\Psi \\ & \quad \cdot (g(x) - g(x_0))M_\varphi^f(x_0, x) \\ & \quad + E_{\nu, \varrho, \kappa}^{\gamma, \vartheta, k, \chi}(\Phi(g(y_0) - g(x))^\nu; p)\Psi \\ & \quad \cdot (g(y_0) - g(x))M_\varphi^f(x, y_0). \end{aligned} \tag{20}$$

Proof. For the kernel defined in (12) and the function g , we can write the following inequality:

$$G_x^t\left(E_{\lambda, \varrho, \kappa}^{\gamma, \vartheta, k, \chi}, g; \Psi\right)g'(t) \leq G_x^{x_0}\left(E_{\lambda, \varrho, \kappa}^{\gamma, \vartheta, k, \chi}, g; \Psi\right)g'(t), \tag{21}$$

$$x \in (x_0, y_0), t \in [x_0, x].$$

By using φ -quasiconvexity of f on $[x_0, x]$, one can get

$$f(t) \leq M_\varphi^f(x_0, x), \quad x \in (x_0, y_0), t \in [x_0, x]. \tag{22}$$

The following integral inequality is constituted from (21) and (22):

$$\begin{aligned} & \int_{x_0}^x G_x^t\left(E_{\lambda, \varrho, \kappa}^{\gamma, \vartheta, k, \chi}, g; \Psi\right)g'(t)f(t)dt \\ & \leq M_\varphi^f(x_0, x)G_x^{x_0}\left(E_{\lambda, \varrho, \kappa}^{\gamma, \vartheta, k, \chi}, g; \Psi\right) \int_{x_0}^x g'(t)dt. \end{aligned} \tag{23}$$

Using (10) in the left and integrating on the right side of inequality (23), we obtain the following upper bound of the left integral operator:

$$\begin{aligned} & \left({}_g F_{\lambda, \varrho, \kappa, x_0^+}^{\Psi, \gamma, \vartheta, k, \chi} f\right)(x, \Phi; p) \leq E_{\lambda, \varrho, \kappa}^{\gamma, \vartheta, k, \chi}(\Phi(g(x) - g(x_0))^\lambda; p)\Psi \\ & \quad \cdot (g(x) - g(x_0))M_\varphi^f(x_0, x). \end{aligned} \tag{24}$$

Now, following the similar technique for $t \in (x, y_0]$ and $x \in (x_0, y_0)$, we can write

$$G_t^x\left(E_{\nu, \varrho, \kappa}^{\gamma, \vartheta, k, \chi}, g; \Psi\right)g'(t) \leq G_{y_0}^x\left(E_{\nu, \varrho, \kappa}^{\gamma, \vartheta, k, \chi}, g; \Psi\right)g'(t). \tag{25}$$

Using φ -quasiconvexity for $t \in (x, y_0]$ and $x \in (x_0, y_0)$, we obtain

$$f(t) \leq M_\varphi^f(x, y_0). \tag{26}$$

The following integral inequality is constituted from (25) and (26):

$$\int_x^{y_0} G_t^x \left(E_{\nu, \varrho, \kappa}^{\gamma, \vartheta, k, \chi}, g; \Psi \right) g'(t) f(t) dt \leq G_{y_0}^x \left(E_{\nu, \varrho, \kappa}^{\gamma, \vartheta, k, \chi}, g; \Psi \right) \cdot M_\varphi^f(x, y_0) \int_x^{y_0} g'(t) dt. \quad (27)$$

Using (11) in the left and integrating on the right side of the above inequality, we obtain the following upper bound of the right integral operator:

$$\left({}_g F_{\lambda, \varrho, \kappa, \nu_0}^{\Psi, \gamma, \vartheta, k, \chi} f \right) (x; p) \leq E_{\nu, \varrho, \kappa}^{\gamma, \vartheta, k, \chi} \left(\Phi(g(y_0) - g(x))^\nu; p \right) \Psi \cdot (g(y_0) - g(x)) M_\varphi^f(x, y_0). \quad (28)$$

By summing (24) and (28), the inequality (20) can be obtained. \square

Corollary 1. Using $\lambda = \nu$ in (20), we get the following result:

$$\begin{aligned} & \left({}_g F_{\lambda, \varrho, \kappa, \nu_0}^{\Psi, \gamma, \vartheta, k, \chi} f \right) (x, \Phi; p) + \left({}_g F_{\lambda, \varrho, \kappa, \nu_0}^{\Psi, \gamma, \vartheta, k, \chi} f \right) (x, \Phi; p) \\ & \leq E_{\lambda, \varrho, \kappa}^{\gamma, \vartheta, k, \chi} \left(\Phi(g(x) - g(x_0))^\lambda; p \right) \Psi(g(x) - g(x_0)) \\ & \quad \cdot M_\varphi^f(x_0, x) \\ & \quad + E_{\lambda, \varrho, \kappa}^{\gamma, \vartheta, k, \chi} \left(\Phi(g(y_0) - g(x))^\lambda; p \right) \Psi \\ & \quad \cdot (g(y_0) - g(x)) M_\varphi^f(x, y_0). \end{aligned} \quad (29)$$

Remark 1

- (i) For $\varphi(x_0, y_0) = x_0 - y_0$ in (20), we obtain inequality (13) of Theorem 1.
- (ii) For $\varphi(x_0, y_0) = x_0 - y_0$, $\Psi(x) = x^{\lambda/k}$ for the left-hand integral and $\Psi(x) = x^{\nu/k}$ for the right-hand integral in (20) with $p = \Phi = 0$, we obtain Theorem 2.1 in [17].
- (iii) For $\lambda = \nu$ in the resulting inequality of (ii), we obtain Corollary 2.2 in [17].
- (iv) For $\varphi(x_0, y_0) = x_0 - y_0$, $\Psi(x) = x^\lambda$ for the left-hand integral and $\Psi(x) = x^\nu$ for the right-hand integral in (20) with $p = \Phi = 0$, we obtain Corollary 2.3 in [17].
- (v) Under the same assumptions as in (ii) along with g as identity function, the result (20) reduces to Corollary 2.4 in [17].
- (vi) Under the same assumptions as in (iv) along with g as identity function, the result (20) reduces to Corollary 2.5 in [17].
- (vii) Under the same assumptions as in (ii), if f is increasing on $[x_0, y_0]$, the result (20) reduces to Corollary 2.6 in [17].

(viii) Under the same assumptions as in (ii), if f is decreasing on $[x_0, y_0]$, the result (20) reduces to Corollary 2.7 in [17].

(ix) For $\lambda = \nu$ in the resulting inequality of (viii), we obtain Corollary 2.2 in [18].

Theorem 6. The following result holds under the suppositions of Theorem 5:

$$\begin{aligned} & \left({}_g F_{\lambda, \varrho, \kappa, x_0^+}^{\Psi, \gamma, \vartheta, k, \chi} f \right) (y_0, \Phi; p) + \left({}_g F_{\nu, \varrho, \kappa, y_0^-}^{\Psi, \gamma, \vartheta, k, \chi} f \right) (x_0, \Phi; p) \\ & \leq \Psi(g(y_0) - g(x_0)) \left[E_{\lambda, \varrho, \kappa}^{\gamma, \vartheta, k, \chi} \left(\Phi(g(y_0) - g(x_0))^\lambda; p \right) \right. \\ & \quad \left. + E_{\nu, \varrho, \kappa}^{\gamma, \vartheta, k, \chi} \left(\Phi(g(y_0) - g(x_0))^\nu; p \right) \right] M_\varphi^f(x_0, y_0). \end{aligned} \quad (30)$$

Proof. Using $x = y_0$ in (24) and $x = x_0$ in (28) and then adding the obtained inequalities, we get (30). \square

Corollary 2. Using $\lambda = \nu$ in (30), we get the following result:

$$\begin{aligned} & \left({}_g F_{\lambda, \varrho, \kappa, x_0^+}^{\Psi, \gamma, \vartheta, k, \chi} f \right) (y_0, \Phi; p) + \left({}_g F_{\lambda, \varrho, \kappa, y_0^-}^{\Psi, \gamma, \vartheta, k, \chi} f \right) (x_0, \Phi; p) \\ & \leq 2\Psi(g(y_0) - g(x_0)) \\ & \quad \cdot E_{\lambda, \varrho, \kappa}^{\gamma, \vartheta, k, \chi} \left(\Phi(g(y_0) - g(x_0))^\lambda; p \right) M_\varphi^f(x_0, y_0). \end{aligned} \quad (31)$$

Remark 2

- (i) For $\varphi(x_0, y_0) = x_0 - y_0$ in (30), we obtain inequality (14) of Theorem 2.
- (ii) For $\varphi(x_0, y_0) = x_0 - y_0$, $\Psi(x) = x^{\lambda/k}$ for the left-hand integral and $\Psi(x) = x^{\nu/k}$ for the right-hand integral in (30) with $p = \Phi = 0$, we obtain Theorem 3.1 in [17].
- (iii) For $\varphi(x_0, y_0) = x_0 - y_0$, $\Psi(x) = x^{\lambda/k}$ for the left-hand integral and $\Psi(x) = x^{\nu/k}$ for the right-hand integral in (31) with $p = \Phi = 0$, we obtain Corollary 3.2 in [17].
- (iv) For $\varphi(x_0, y_0) = x_0 - y_0$, replacing Φ with $\Phi' = \Phi/(y_0 - x_0)^\lambda$, $\Psi(x) = x^\lambda$ for the left-hand integral, $\Psi(x) = x^\nu$ for the right-hand integral, and g as identity function in (30), we obtain Theorem 2.1 in [18].
- (v) Under the same assumptions as in (iv) along with $\lambda = k = 1$, the result (30) reduces to Theorem 3.3 in [16].

Before proceeding to the next result, we will prove the following lemma. This lemma is necessary to prove the upcoming result.

Lemma 1. Let $f: [x_0, y_0] \rightarrow \mathbb{R}$ be φ -quasiconvex function. If $f(x) = f(x_0 + y_0 - x)$, then the following inequality holds:

$$f\left(\frac{x_0 + y_0}{2}\right) \leq M_\varphi^f(x, x), \quad x \in [x_0, y_0]. \quad (32)$$

Proof. Using φ -quasiconvexity of the function f , the upcoming inequality holds:

$$f\left(\frac{x_0 + y_0}{2}\right) \leq \max \left[\begin{array}{l} f\left(\frac{x - x_0}{y_0 - x_0}x_0 + \frac{y_0 - x}{y_0 - x_0}y_0\right), f\left(\frac{x - x_0}{y_0 - x_0}x_0 + \frac{y_0 - x}{y_0 - x_0}y_0\right) \\ + \varphi\left(f\left(\frac{x - x_0}{y_0 - x_0}y_0 + \frac{y_0 - x}{y_0 - x_0}x_0\right), f\left(\frac{x - x_0}{y_0 - x_0}x_0 + \frac{y_0 - x}{y_0 - x_0}y_0\right)\right) \end{array} \right], \quad (33)$$

$$f\left(\frac{x_0 + y_0}{2}\right) \leq M_\varphi^f(x, x_0 + y_0 - x).$$

Using $f(x_0 + y_0 - x) = f(x)$ in above inequality, we get the required inequality. \square

Remark 3. Using $\varphi(x_0, y_0) = x_0 - y_0$, (32) coincides with Lemma 1 in [19].

Theorem 7. Along with the assumptions of Theorem 5, if $f(x_0 + y_0 - x) = f(x)$ and $\varphi(x, y) = x + y$, then the following results hold:

$$\begin{aligned} & \frac{1}{3} f\left(\frac{x_0 + y_0}{2}\right) \left(\left({}_g F_{\lambda, \varrho, \kappa, x_0^+}^{\Psi, \gamma, \vartheta, k, \chi} 1 \right) (y_0, \Phi; p) + \left({}_g F_{\nu, \varrho, \kappa, y_0^-}^{\Psi, \gamma, \vartheta, k, \chi} 1 \right) (x_0, \Phi; p) \right) \\ & \leq \left({}_g F_{\lambda, \varrho, \kappa, x_0^+}^{\Psi, \gamma, \vartheta, k, \chi} f \right) (y_0, \Phi; p) + \left({}_g F_{\nu, \varrho, \kappa, y_0^-}^{\Psi, \gamma, \vartheta, k, \chi} f \right) (x_0, \Phi; p) \leq \Psi(g(y_0) - g(x_0)) \end{aligned} \quad (34)$$

$$\cdot \left(E_{\lambda, \varrho, \kappa}^{\gamma, \vartheta, k, \chi} (\Phi(g(y_0) - g(x_0))^\lambda; p) + E_{\nu, \varrho, \kappa}^{\gamma, \vartheta, k, \chi} (\Phi(g(y_0) - g(x_0))^\nu; p) \right) M_\varphi^f(x_0, y_0),$$

$$\begin{aligned} & f\left(\frac{x_0 + y_0}{2}\right) \left(\left({}_g F_{\lambda, \varrho, \kappa, x_0^+}^{\Psi, \gamma, \vartheta, k, \chi} 1 \right) (y_0, \Phi; p) + \left({}_g F_{\nu, \varrho, \kappa, y_0^-}^{\Psi, \gamma, \vartheta, k, \chi} 1 \right) (x_0, \Phi; p) \right) \\ & \leq \left({}_g F_{\lambda, \varrho, \kappa, x_0^+}^{\Psi, \gamma, \vartheta, k, \chi} f \right) (y_0, \Phi; p) + \left({}_g F_{\nu, \varrho, \kappa, y_0^-}^{\Psi, \gamma, \vartheta, k, \chi} f \right) (x_0, \Phi; p) \leq \Psi(g(y_0) - g(x_0)) \end{aligned} \quad (35)$$

$$\cdot \left(E_{\lambda, \varrho, \kappa}^{\gamma, \vartheta, k, \chi} (\Phi(g(y_0) - g(x_0))^\lambda; p) + E_{\nu, \varrho, \kappa}^{\gamma, \vartheta, k, \chi} (\Phi(g(y_0) - g(x_0))^\nu; p) \right) M_\varphi^f(x_0, y_0),$$

provided $M_\varphi^f(x, x) = f(x) + \varphi(f(x), f(x))$ or $M_\varphi^f(x, x) = f(x)$.

Proof. From the kernel defined in (12) and the function g , we can write

$$\begin{aligned} G_x^{x_0} \left(E_{\nu, \varrho, \kappa}^{\gamma, \vartheta, k, \chi}, g; \Psi \right) g'(x) & \leq G_{y_0}^{x_0} \left(E_{\nu, \varrho, \kappa}^{\gamma, \vartheta, k, \chi}, g; \Psi \right) g'(x), \\ & x \in (x_0, y_0). \end{aligned} \quad (36)$$

Using φ -quasiconvexity of f on $[x_0, y_0]$, we have

$$f(x) \leq M_\varphi^f(x_0, y_0), \quad x \in (x_0, y_0). \quad (37)$$

The following inequality is constituted from (36) and (37):

$$\begin{aligned} & \int_{x_0}^{y_0} G_x^{x_0} \left(E_{\nu, \varrho, \kappa}^{\gamma, \vartheta, k, \chi}, g; \Psi \right) g'(x) f(x) dx \\ & \leq G_{y_0}^{x_0} \left(E_{\nu, \varrho, \kappa}^{\gamma, \vartheta, k, \chi}, g; \Psi \right) M_\varphi^f(x_0, y_0) \int_{x_0}^{y_0} g'(x) dx. \end{aligned} \quad (38)$$

Using (11) in the left and integrating on the right side of the above inequality, we obtain the following upper bound of the right integral operator:

$$\begin{aligned} \left({}_g F_{\nu, \varrho, \kappa, \gamma_0}^{\Psi, \gamma, \vartheta, k, \chi} f\right)\left(x_0, \Phi; p\right) &\leq E_{\nu, \varrho, \kappa}^{\gamma, \vartheta, k, \chi}\left(\Phi\left(g\left(y_0\right)-g\left(x_0\right)\right)^{\gamma} ; p\right) \Psi \\ &\cdot\left(g\left(y_0\right)-g\left(x_0\right)\right) M_{\varphi}^f\left(x_0, y_0\right) . \end{aligned} \quad (39)$$

Also,

$$\begin{aligned} G_{y_0}^x\left(E_{\lambda, \varrho, \kappa}^{\gamma, \vartheta, k, \chi}, g ; \Psi\right) g'(x) &\leq G_{y_0}^{x_0}\left(E_{\lambda, \varrho, \kappa}^{\gamma, \vartheta, k, \chi}, g ; \Psi\right) g'(x), \\ x &\in\left(x_0, y_0\right) . \end{aligned} \quad (40)$$

From (37) and (40), we get

$$\begin{aligned} \int_{x_0}^{y_0} G_{y_0}^x\left(E_{\lambda, \varrho, \kappa}^{\gamma, \vartheta, k, \chi}, g ; \Psi\right) g'(x) f(x) dx \\ \leq G_{y_0}^{x_0}\left(E_{\lambda, \varrho, \kappa}^{\gamma, \vartheta, k, \chi}, g ; \Psi\right) M_{\varphi}^f\left(x_0, y_0\right) \int_{x_0}^{y_0} g'(x) dx . \end{aligned} \quad (41)$$

Using (10) in the left and integrating on the right side of the above inequality, we obtain the following upper bound of the left integral operator:

$$\begin{aligned} \left({}_g F_{\lambda, \varrho, \kappa, x_0^+}^{\Psi, \gamma, \vartheta, k, \chi} f\right)\left(y_0, \Phi ; p\right) &\leq E_{\lambda, \varrho, \kappa}^{\gamma, \vartheta, k, \chi}\left(\Phi\left(g\left(y_0\right)-g\left(x_0\right)\right)^{\lambda} ; p\right) \Psi \\ &\cdot\left(g\left(y_0\right)-g\left(x_0\right)\right) M_{\varphi}^f\left(x_0, y_0\right) . \end{aligned} \quad (42)$$

Now using (32) of Lemma 1, we can have

$$\begin{aligned} f\left(\frac{x_0+y_0}{2}\right) G_x^{x_0}\left(E_{\nu, \varrho, \kappa}^{\gamma, \vartheta, k, \chi}, g ; \Psi\right) g'(x) \\ \leq G_x^{x_0}\left(E_{\nu, \varrho, \kappa}^{\gamma, \vartheta, k, \chi}, g ; \Psi\right) g'(x) M_{\varphi}^f(x, x) . \end{aligned} \quad (43)$$

Case 1. If $M_{\varphi}^f(x, x) = f(x) + \varphi(f(x), f(x))$, then by using (11), $\varphi(x, y) = x + y$ in (43), and integrating over $[x_0, y_0]$, we get

$$\begin{aligned} f\left(\frac{x_0+y_0}{2}\right)\left({}_g F_{\nu, \varrho, \kappa, y_0^-}^{\Psi, \gamma, \vartheta, k, \chi} 1\right)\left(x_0, \Phi ; p\right) \\ \leq 3\left({}_g F_{\nu, \varrho, \kappa, y_0^-}^{\Psi, \gamma, \vartheta, k, \chi} f\right)\left(x_0, \Phi ; p\right) . \end{aligned} \quad (44)$$

In this case, we also have

$$\begin{aligned} f\left(\frac{x_0+y_0}{2}\right)\left({}_g F_{\lambda, \varrho, \kappa, x_0^+}^{\Psi, \gamma, \vartheta, k, \chi} 1\right)\left(y_0, \Phi ; p\right) \\ \leq 3\left({}_g F_{\lambda, \varrho, \kappa, x_0^+}^{\Psi, \gamma, \vartheta, k, \chi} f\right)\left(y_0, \Phi ; p\right) . \end{aligned} \quad (45)$$

Case 2. If $M_{\varphi}^f(x, x) = f(x)$, then by using (11) in (43), we get

$$f\left(\frac{x_0+y_0}{2}\right)\left({}_g F_{\nu, \varrho, \kappa, y_0^-}^{\Psi, \gamma, \vartheta, k, \chi} 1\right)\left(x_0, \Phi ; p\right) \leq\left({}_g F_{\nu, \varrho, \kappa, y_0^-}^{\Psi, \gamma, \vartheta, k, \chi} f\right)\left(x_0, \Phi ; p\right) . \quad (46)$$

In this case, we also have

$$f\left(\frac{x_0+y_0}{2}\right)\left({}_g F_{\lambda, \varrho, \kappa, x_0^+}^{\Psi, \gamma, \vartheta, k, \chi} 1\right)\left(y_0, \Phi ; p\right) \leq\left({}_g F_{\lambda, \varrho, \kappa, x_0^+}^{\Psi, \gamma, \vartheta, k, \chi} f\right)\left(y_0, \Phi ; p\right) . \quad (47)$$

The inequality (34) will be obtained by summing (39) with (42) and (44) with (45) and then combining the resulting inequalities. The inequality (35) will be obtained by summing (39) with (42) and (46) with (47) and then combining the resulting inequalities.

Corollary 3. For $\lambda = \nu$ in (34) and (35), we get the following results:

$$\begin{aligned} \frac{1}{3} f\left(\frac{x_0+y_0}{2}\right)\left(\left({}_g F_{\lambda, \varrho, \kappa, x_0^+}^{\Psi, \gamma, \vartheta, k, \chi} 1\right)\left(y_0, \Phi ; p\right)+\left({}_g F_{\lambda, \varrho, \kappa, y_0^-}^{\Psi, \gamma, \vartheta, k, \chi} 1\right)\left(x_0, \Phi ; p\right)\right) \\ \leq\left({}_g F_{\lambda, \varrho, \kappa, x_0^+}^{\Psi, \gamma, \vartheta, k, \chi} f\right)\left(y_0, \Phi ; p\right)+\left({}_g F_{\lambda, \varrho, \kappa, y_0^-}^{\Psi, \gamma, \vartheta, k, \chi} f\right)\left(x_0, \Phi ; p\right) \end{aligned} \quad (48)$$

$$\leq 2 \Psi\left(g\left(y_0\right)-g\left(x_0\right)\right) E_{\lambda, \varrho, \kappa}^{\gamma, \vartheta, k, \chi}\left(\Phi\left(g\left(y_0\right)-g\left(x_0\right)\right)^{\lambda} ; p\right) M_{\varphi}^f\left(x_0, y_0\right),$$

$$\begin{aligned} f\left(\frac{x_0+y_0}{2}\right)\left(\left({}_g F_{\lambda, \varrho, \kappa, x_0^+}^{\Psi, \gamma, \vartheta, k, \chi} 1\right)\left(y_0, \Phi ; p\right)+\left({}_g F_{\lambda, \varrho, \kappa, y_0^-}^{\Psi, \gamma, \vartheta, k, \chi} 1\right)\left(x_0, \Phi ; p\right)\right) \\ \leq\left({}_g F_{\lambda, \varrho, \kappa, x_0^+}^{\Psi, \gamma, \vartheta, k, \chi} f\right)\left(y_0, \Phi ; p\right)+\left({}_g F_{\lambda, \varrho, \kappa, y_0^-}^{\Psi, \gamma, \vartheta, k, \chi} f\right)\left(x_0, \Phi ; p\right) \end{aligned} \quad (49)$$

$$\leq 2 \Psi\left(g\left(y_0\right)-g\left(x_0\right)\right) E_{\lambda, \varrho, \kappa}^{\gamma, \vartheta, k, \chi}\left(\Phi\left(g\left(y_0\right)-g\left(x_0\right)\right)^{\lambda} ; p\right) M_{\varphi}^f\left(x_0, y_0\right) .$$

Remark 4.

- (i) For $\varphi(x_0, y_0) = x_0 - y_0$ in (34), we get inequality (15) of Theorem 3.
- (ii) For $\varphi(x_0, y_0) = x_0 - y_0$, $\Psi(x) = x^{\lambda/k}$ for the left-hand integral and $\Psi(x) = x^{\nu/k}$ for the right-hand integral in (34) with $p = \Phi = 0$, we obtain Theorem 2.16 in [17].
- (iii) For $\varphi(x_0, y_0) = x_0 - y_0$, $\Psi(x) = x^{\lambda/k}$ for the left-hand integral and $\Psi(x) = x^{\nu/k}$ for the right-hand integral in (48) with $p = \Phi = 0$, we obtain Corollary 2.17 in [17].
- (iv) For $\varphi(x_0, y_0) = x_0 - y_0$, $\Psi(x) = x^\lambda$ for the left-hand integral and $\Psi(x) = x^\nu$ for the right-hand integral in (34) with $p = \Phi = 0$, we obtain Corollary 2.18 in [17].
- (v) Under the same assumptions as in (ii) along with g as identity function, the result (34) reduces to Corollary 2.19 in [17].
- (vi) Under the same assumptions as in (iv) along with g as identity function, the result (34) reduces to Corollary 2.20 in [17].
- (vii) Under the same assumptions as in (ii), if f is increasing on $[x_0, y_0]$, the result (34) reduces to Corollary 2.21 in [17].
- (viii) Under the same assumptions as in (ii), if f is decreasing on $[x_0, y_0]$, the result (34) reduces to Corollary 2.22 in [17].

Theorem 8. Consider $f, g: [x_0, y_0] \rightarrow \mathbb{R}$ are two differentiable functions such that $|f'|$ is φ -quasiconvex and g is strictly increasing for $0 < x_0 < y_0$. If Ψ/x is increasing function on $[x_0, y_0]$ and $\varrho, \kappa, \gamma, \chi \in \mathbb{C}$, $p, \lambda, \nu, \vartheta \geq 0$, $0 < k \leq \vartheta + \lambda$ and $0 < k \leq \vartheta + \nu$, then for $x \in (x_0, y_0)$, the following inequality holds:

$$\begin{aligned} & \left| \left({}_g F_{\lambda, \varrho, \kappa, x_0^+}^{\Psi, \gamma, \vartheta, k, \chi} f * g \right) (x, \Phi; p) + \left({}_g F_{\nu, \varrho, \kappa, y_0^-}^{\Psi, \gamma, \vartheta, k, \chi} f * g \right) (x, \Phi; p) \right| \\ & \leq E_{\lambda, \varrho, \kappa}^{\gamma, \vartheta, k, \chi} \left(\Phi (g(x) - g(x_0))^\lambda; p \right) \Psi (g(x) - g(x_0)) \\ & \quad \cdot M_\varphi^{|f'|} (x_0, x) \\ & \quad + E_{\nu, \varrho, \kappa}^{\gamma, \vartheta, k, \chi} \left(\Phi (g(y_0) - g(x))^\nu; p \right) \Psi \\ & \quad \cdot (g(y_0) - g(x)) M_\varphi^{|f'|} (x, y_0), \end{aligned} \tag{50}$$

where $({}_g F_{\lambda, \varrho, \kappa, x_0^+}^{\Psi, \gamma, \vartheta, k, \chi} f * g)(x, \Phi; p)$ and $({}_g F_{\nu, \varrho, \kappa, y_0^-}^{\Psi, \gamma, \vartheta, k, \chi} f * g)(x, \Phi; p)$ are defined in (17) and (18).

Proof. The φ -quasiconvexity of $|f'|$ implies the following inequality:

$$|f'(t)| \leq M_\varphi^{|f'|} (x_0, x), \quad t \in [x_0, x], \quad x \in (x_0, y_0), \tag{51}$$

which is equivalent to

$$-\left(M_\varphi^{|f'|} (x_0, x) \right) \leq f'(t) \leq M_\varphi^{|f'|} (x_0, x). \tag{52}$$

First consider

$$f'(t) \leq M_\varphi^{|f'|} (x_0, x). \tag{53}$$

The following inequality is constituted from (21) and (53):

$$\begin{aligned} & \int_{x_0}^x G_x^t \left(E_{\lambda, \varrho, \kappa}^{\gamma, \vartheta, k, \chi}, g; \Psi \right) g'(t) f'(t) dt \\ & \leq M_\varphi^{|f'|} (x_0, x) G_x^{x_0} \left(E_{\lambda, \varrho, \kappa}^{\gamma, \vartheta, k, \chi}, g; \Psi \right) \int_{x_0}^x g'(t) dt, \end{aligned} \tag{54}$$

from which we get

$$\begin{aligned} & \left({}_g F_{\lambda, \varrho, \kappa, x_0^+}^{\Psi, \gamma, \vartheta, k, \chi} f * g \right) (x, \Phi; p) \leq E_{\lambda, \varrho, \kappa}^{\gamma, \vartheta, k, \chi} \left(\Phi (g(x) - g(x_0))^\lambda; p \right) \Psi \\ & \quad \cdot (g(x) - g(x_0)) M_\varphi^{|f'|} (x_0, x). \end{aligned} \tag{55}$$

Now, we consider

$$-\left(M_\varphi^{|f'|} (x_0, x) \right) \leq f'(t). \tag{56}$$

Using (21) and (56), we get

$$\begin{aligned} & \left({}_g F_{\lambda, \varrho, \kappa, x_0^+}^{\Psi, \gamma, \vartheta, k, \chi} f * g \right) (x, \Phi; p) \geq -E_{\lambda, \varrho, \kappa}^{\gamma, \vartheta, k, \chi} \left(\Phi (g(x) - g(x_0))^\lambda; p \right) \Psi \\ & \quad \cdot (g(x) - g(x_0)) M_\varphi^{|f'|} (x_0, x). \end{aligned} \tag{57}$$

Now, again using φ -quasiconvexity of $|f'|$, we have

$$|f'(t)| \leq M_\varphi^{|f'|} (x, y_0), \quad t \in (x, y_0], \quad x \in (x_0, y_0). \tag{58}$$

Similarly using (25) and (58), one can obtain

$$\begin{aligned} & \left({}_g F_{\nu, \varrho, \kappa, y_0^-}^{\Psi, \gamma, \vartheta, k, \chi} f * g \right) (x, \Phi; p) \leq E_{\nu, \varrho, \kappa}^{\gamma, \vartheta, k, \chi} \left(\Phi (g(y_0) - g(x))^\nu; p \right) \Psi \\ & \quad \cdot (g(y_0) - g(x)) M_\varphi^{|f'|} (x, y_0), \end{aligned} \tag{59}$$

$$\begin{aligned} & \left({}_g F_{\nu, \varrho, \kappa, y_0^-}^{\Psi, \gamma, \vartheta, k, \chi} f * g \right) (x, \Phi; p) \geq -E_{\nu, \varrho, \kappa}^{\gamma, \vartheta, k, \chi} \\ & \quad \cdot \left(\Phi (g(y_0) - g(x))^\nu; p \right) \Psi (g(y_0) - g(x)) M_\varphi^{|f'|} (x, y_0). \end{aligned} \tag{60}$$

The inequality (50) will be obtained by summing (55), (57), (59), and (60). \square

Corollary 4. For $\lambda = \nu$ in (50), we get the following result:

$$\begin{aligned} & \left| \left({}_g F_{\lambda, \varrho, \kappa, x_0^+}^{\Psi, \gamma, \vartheta, k, \chi} f * g \right) (x, \Phi; p) + \left({}_g F_{\lambda, \varrho, \kappa, y_0^-}^{\Psi, \gamma, \vartheta, k, \chi} f * g \right) (x, \Phi; p) \right| \\ & \leq E_{\lambda, \varrho, \kappa}^{\gamma, \vartheta, k, \chi} \left(\Phi (g(x) - g(x_0))^{\lambda}; p \right) \Psi (g(x) - g(x_0)) M_{\varphi}^{|f'|} \\ & \quad \cdot (x_0, x) \\ & \quad + E_{\lambda, \varrho, \kappa}^{\gamma, \vartheta, k, \chi} \left(\Phi (g(y_0) - g(x))^{\lambda}; p \right) \Psi \\ & \quad \cdot (g(y_0) - g(x)) M_{\varphi}^{|f'|} (x, y_0). \end{aligned} \quad (61)$$

Remark 5.

- (i) For $\varphi(x_0, y_0) = x_0 - y_0$ in (50), we obtain inequality (16) of Theorem 4.
- (ii) For $\varphi(x_0, y_0) = x_0 - y_0$, $\Psi(x) = x^{\lambda/k}$ for the left-hand integral and $\Psi(x) = x^{\nu/k}$ for right-hand integral in (50) with $p = \Phi = 0$, we obtain Theorem 2.8 in [17].
- (iii) For $\varphi(x_0, y_0) = x_0 - y_0$, $\Psi(x) = x^{\lambda/k}$ for the left-hand integral and $\Psi(x) = x^{\nu/k}$ for the right-hand integral in (61) with $p = \Phi = 0$, we obtain Corollary 2.9 in [17].
- (iv) For $\varphi(x_0, y_0) = x_0 - y_0$, $\Psi(x) = x^{\lambda}$ for the left-hand integral and $\Psi(x) = x^{\nu}$ for the right-hand integral in (50) with $p = \Phi = 0$, we obtain Corollary 2.10 in [17].
- (v) Under the same assumptions as in (ii) along with g as identity function, the result (50) reduces to Corollary 2.11 in [17].
- (vi) Under the same assumptions as in (iv) along with g as identity function, the result (50) reduces to Corollary 2.12 in [17].
- (vii) Under the same assumptions as in (ii), if f is increasing on $[x_0, y_0]$, the result (50) reduces to Corollary 2.13 in [17].
- (viii) Under the same assumptions as in (ii), if f is decreasing on $[x_0, y_0]$, the result (50) reduces to Corollary 2.14 in [17].
- (ix) Under the same assumptions as in (ii), if in addition we put $x = x_0$ and $x = y_0$ in the left- and right-hand integrals, respectively, we obtain Theorem 3.2 in [17].
- (x) For $\lambda = \nu$ in the resulting inequality of (ix), we obtain Corollary 3.5 in [17].
- (xi) For $\lambda = k = 1$ in the resulting inequality of (x), we obtain Corollary 3.6 in [17].

3. Applications

In this section, we present some results by applying theorems of previous section.

Proposition 1. The following result holds under the suppositions of Theorem 5:

$$\begin{aligned} \Gamma(\varrho) & \left(\left({}_g^{\varrho} I_{x_0^+} f \right) (x) + \left({}_g^{\varrho} I_{y_0^-} f \right) (x) \right) \leq (g(x) - g(x_0))^{\varrho} \\ & \cdot M_{\varphi}^f(x_0, x) + (g(y_0) - g(x))^{\varrho} M_{\varphi}^f(x, y_0). \end{aligned} \quad (62)$$

Proof. For $\Psi(t) = t^{\varrho}$, $\varrho > 0$ and $p = \Phi = 0$, $\lambda = \nu$ with Ψ/t is increasing for $\varrho \geq 1$ in the proof of Theorem 5 we get (62). \square

Proposition 2. The following result holds under the suppositions of Theorem 5:

$$\begin{aligned} \left({}_{x_0^+} I_{\Psi} f \right) (x) + \left({}_{y_0^-} I_{\Psi} f \right) (x) & \leq \Psi(x - x_0) M_{\varphi}^f(x_0, x) \\ & + \Psi(y_0 - x) M_{\varphi}^f(x, y_0). \end{aligned} \quad (63)$$

Proof. Using g as identity function, $\Phi = p = 0$, and $\lambda = \nu$ in the proof of Theorem 5, we get inequality (63). \square

Corollary 5. For $\Psi(t) = \Gamma(\varrho)t^{\varrho/k}/k\Gamma_k(\varrho)$ in Theorem 5, the following bound for $\varrho \geq k$ is satisfied:

$$\begin{aligned} \left({}_g^{\varrho} I_{x_0^+}^k f \right) (x) + \left({}_g^{\varrho} I_{y_0^-}^k f \right) (x) & \leq \frac{1}{k\Gamma_k(\varrho)} \left[(g(x) - g(x_0))^{\varrho/k} \right. \\ & \left. \cdot M_{\varphi}^f(x_0, x) + (g(y_0) - g(x))^{\varrho/k} M_{\varphi}^f(x, y_0) \right]. \end{aligned} \quad (64)$$

Corollary 6. Using $\Psi(t) = t^{\varrho}$ in (63), fractional integrals ${}^{\varrho} I_{x_0^+} f(x)$ and ${}^{\varrho} I_{y_0^-} f(x)$ defined in [14] are obtained which satisfy the following bound:

$$\begin{aligned} \Gamma(\varrho) & \left(\left({}^{\varrho} I_{x_0^+} f \right) (x) + \left({}^{\varrho} I_{y_0^-} f \right) (x) \right) \leq (x - x_0)^{\varrho} M_{\varphi}^f(x_0, x) \\ & + (y_0 - x)^{\varrho} M_{\varphi}^f(x, y_0). \end{aligned} \quad (65)$$

Corollary 7. Using $\Psi(t) = \Gamma(\varrho)t^{\varrho/k}/k\Gamma_k(\varrho)$ in (63), fractional integral operators ${}^{\varrho} I_{x_0^+}^k f(x)$ and ${}^{\varrho} I_{y_0^-}^k f(x)$ given in [26] are obtained which satisfy the following bound:

$$\begin{aligned} \left({}^{\varrho} I_{x_0^+}^k f \right) (x) + \left({}^{\varrho} I_{y_0^-}^k f \right) (x) & \leq \frac{1}{k\Gamma_k(\varrho)} \left[(x - x_0)^{\varrho/k} M_{\varphi}^f(x_0, x) \right. \\ & \left. + (y_0 - x)^{\varrho/k} M_{\varphi}^f(x, y_0) \right]. \end{aligned} \quad (66)$$

Corollary 8. Using $\Psi(t) = t^{\varrho}$, $\varrho > 0$, and $g(x) = x^{\varepsilon}/\varepsilon$, $\varepsilon > 0$, in (10) and (11), respectively, with $p = \Phi = 0$, then fractional

integral operators $({}^\varepsilon I_{x_0^+}^\varrho f)(x)$ and $({}^\varepsilon I_{y_0^-}^\varrho f)(x)$ given in [27] are obtained which satisfy the following bound:

$$\begin{aligned} & \left({}^\varepsilon I_{x_0^+}^\varrho f \right) (x) + \left({}^\varepsilon I_{y_0^-}^\varrho f \right) (x) \leq \frac{1}{\varepsilon^\varrho \Gamma(\varrho)} \left[(x^\varepsilon - x_0^\varepsilon)^\varrho M_\varphi^f(x_0, x) \right. \\ & \left. + (y_0^\varepsilon - x^\varepsilon)^\varrho M_\varphi^f(x, y_0) \right]. \end{aligned} \tag{67}$$

Corollary 9. Using $\Psi(t) = t^\varrho, \varrho > 0$, and $g(x) = x^{s+1}/s + 1, s > 0$, in (10) and (11), respectively, with $p = \Phi = 0$, then fractional integral operators $({}^s I_{x_0^+}^\varrho f)(x)$ and $({}^s I_{y_0^-}^\varrho f)(x)$ are obtained which satisfy the following bound:

$$\begin{aligned} & \left({}^s I_{x_0^+}^\varrho f \right) (x) + \left({}^s I_{y_0^-}^\varrho f \right) (x) \leq \frac{1}{(s+1)^\varrho \Gamma(\varrho)} \left[(x^{s+1} - x_0^{s+1})^\varrho \right. \\ & \left. \cdot M_\varphi^f(x_0, x) + (y_0^{s+1} - x^{s+1})^\varrho M_\varphi^f(x, y_0) \right]. \end{aligned} \tag{68}$$

Corollary 10. Using $\Psi(t) = \Gamma(\varrho)t^{\varrho/k}/k\Gamma_k(\varrho)$ and $g(x) = x^{s+1}/s + 1, s > 0$ in (10) and (11), respectively, with $p = \Phi = 0$, then fractional integral operators $({}^k I_{x_0^+}^\varrho f)(x)$ and $({}^k I_{y_0^-}^\varrho f)(x)$ given in [28] are obtained which satisfy the following bound:

$$\begin{aligned} & \left({}^s I_{x_0^+}^\varrho f \right) (x) + \left({}^s I_{y_0^-}^\varrho f \right) (x) \leq \frac{1}{(s+1)^{\varrho/k} k \Gamma_k(\varrho)} \\ & \cdot \left[(x^{s+1} - x_0^{s+1})^{\varrho/k} M_\varphi^f(x_0, x) + (y_0^{s+1} - x^{s+1})^{\varrho/k} M_\varphi^f(x, y_0) \right]. \end{aligned} \tag{69}$$

Corollary 11. Using $\Psi(t) = t^\varrho, \varrho > 0, g(x) = x^{\beta+s}/\beta + s, \beta, s > 0$, in (10) and (11), respectively, with $p = \Phi = 0$, fractional integral operators $({}^\beta I_{x_0^+}^\varrho f)(x)$ and $({}^\beta I_{y_0^-}^\varrho f)(x)$ are obtained given in [13] which satisfy the following bound:

$$\begin{aligned} & \left({}^\beta I_{x_0^+}^\varrho f \right) (x) + \left({}^\beta I_{y_0^-}^\varrho f \right) (x) \leq \frac{1}{(\beta+s)^\varrho \Gamma(\varrho)} \\ & \cdot \left[(x^{\beta+s} - x_0^{\beta+s})^\varrho M_\varphi^f(x_0, x) + (y_0^{\beta+s} - x^{\beta+s})^\varrho M_\varphi^f(x, y_0) \right]. \end{aligned} \tag{70}$$

Corollary 12. Using $\Psi(t) = t^\varrho, \varrho > 0, g(x) = (x - x_0)^\varepsilon/\varepsilon$ in (10), and $g(x) = -(y_0 - x)^\varepsilon/\varepsilon$ in (11), where $\varepsilon > 0$ with $p = \Phi = 0$, then following fractional integral operators are obtained given in [12]:

$$\begin{aligned} & \left(F_{\lambda, \delta, \kappa, x_0^+}^{t^\varrho, \gamma, \vartheta, \kappa, \chi} f \right) (x) = \left({}^\varepsilon I_{x_0^+}^\varrho f \right) (x) = \frac{\varepsilon^{1-\varrho}}{\Gamma(\varrho)} \int_{x_0}^x ((x - x_0)^\varepsilon - (t - x_0)^\varepsilon)^{\varrho-1} (t - x_0)^{\varepsilon-1} f(t) dt, \\ & \left(F_{\lambda, \delta, \kappa, y_0^-}^{t^\varrho, \gamma, \vartheta, \kappa, \chi} f \right) (x) = \left({}^\varepsilon I_{y_0^-}^\varrho f \right) (x) = \frac{\varepsilon^{1-\varrho}}{\Gamma(\varrho)} \int_x^{y_0} ((y_0 - x)^\varepsilon - (y_0 - t)^\varepsilon)^{\varrho-1} (y_0 - t)^{\varepsilon-1} f(t) dt. \end{aligned} \tag{71}$$

Furthermore, the following bound is also satisfied:

$$\begin{aligned} & \left({}^\varepsilon I_{x_0^+}^\varrho f \right) (x) + \left({}^\varepsilon I_{y_0^-}^\varrho f \right) (x) \leq \frac{1}{\varepsilon^\varrho \Gamma(\varrho)} \\ & \cdot \left[(x - x_0)^{\varepsilon\varrho} M_\varphi^f(x_0, x) + (y_0 - x)^{\varepsilon\varrho} M_\varphi^f(x, y_0) \right]. \end{aligned} \tag{72}$$

Corollary 13. For $\Psi(t) = \Gamma(\varrho)t^{\varrho/k}/k\Gamma_k(\varrho), \varrho > k$ and $g(x) = (x - x_0)^\varepsilon/\varepsilon$ in (10) and $g(x) = -(y_0 - x)^\varepsilon/\varepsilon$ in (11), where $\varepsilon > 0$ with $p = \Phi = 0$, then the following fractional integral operators are obtained given in [29]:

$$\begin{aligned} & \left(F_{\lambda, \delta, \kappa, x_0^+}^{(\Gamma(\varrho)t^{\varrho/k}/k\Gamma_k(\varrho)), \gamma, \vartheta, \kappa, \chi} f \right) (x) = \left({}^\varepsilon I_{x_0^+}^\varrho f \right) (x) = \frac{\varepsilon^{1-(\varrho/k)}}{k\Gamma_k(\varrho)} \int_{x_0}^x ((x - x_0)^\varepsilon - (t - x_0)^\varepsilon)^{(\varrho/k)-1} (t - x_0)^{\varepsilon-1} f(t) dt, \\ & \left(F_{\lambda, \delta, \kappa, y_0^-}^{(\Gamma(\varrho)t^{\varrho/k}/k\Gamma_k(\varrho)), \gamma, \vartheta, \kappa, \chi} f \right) (x) = \left({}^\varepsilon I_{y_0^-}^\varrho f \right) (x) = \frac{\varepsilon^{1-(\varrho/k)}}{k\Gamma_k(\varrho)} \int_x^{y_0} ((y_0 - x)^\varepsilon - (y_0 - t)^\varepsilon)^{(\varrho/k)-1} (y_0 - t)^{\varepsilon-1} f(t) dt. \end{aligned} \tag{73}$$

Furthermore, the following bound is also satisfied:

$$\begin{aligned} & \left({}^\varepsilon I_{x_0^+}^\varrho f \right) (x) + \left({}^\varepsilon I_{y_0^-}^\varrho f \right) (x) \leq \frac{1}{\varepsilon^{\varrho/k} k \Gamma_k(\varrho)} \left[(x - x_0)^{\varepsilon\varrho/k} M_\varphi^f(x_0, x) + (y_0 - x)^{\varepsilon\varrho/k} M_\varphi^f(x, y_0) \right]. \end{aligned} \tag{74}$$

Similar bounds can be obtained for Theorems 7 and 8 which we leave for the reader.

4. Concluding Remarks

A notion namely φ -quasiconvexity is studied under an integral operator that associates with different kinds of operators independently defined by various authors during the last two decades. The consequences of the results are compiled in the form of corollaries and remarks. Although some of the particular cases are analyzed in Section 3 by applying Theorem 5, the reader can further compute more results as desired by applying other theorems.

Data Availability

There are no additional data required for the finding of results of this paper.

Disclosure

There is no funding available for the publication of this paper.

Conflicts of Interest

The authors declare that there are no conflicts of interest.

Authors' Contributions

All authors have equal contribution in this article.

Acknowledgments

This work was supported by the Dong-A University Research Fund.

References

- [1] G. Adilov and I. Yesilce, "On generalization of the concept of convexity," *Hacetatepe Journal of Mathematics and Statistics*, vol. 41, no. 5, pp. 723–730, 2012.
- [2] G. Adilov and I. Yesilce, " B^{-1} -Convex sets and B^{-1} -Measurable maps," *Numerical Functional Analysis and Optimization*, vol. 33, no. 2, pp. 131–141, 2012.
- [3] G. A. Anastassiou, "Generalized fractional Hermite-Hadamard inequalities involving m -convexity and (s,m) -convexity," *Series: Mathematics and Informatics*, vol. 28, no. 2, pp. 107–126, 2013.
- [4] W. Bricc and C. Horvath, "B-Convexity," *Optimization*, vol. 53, no. 2, pp. 103–127, 2004.
- [5] M. Bombardelli and S. Varošanec, "Properties of h -convex functions related to the Hermite-Hadamard-Fejér inequalities," *Computers & Mathematics with Applications*, vol. 58, no. 9, pp. 1869–1877, 2009.
- [6] H. Hudzik and L. Maligranda, "Some remarks on s -convex functions," *Aequationes Mathematicae*, vol. 48, no. 1, pp. 100–111, 1994.
- [7] Y. C. Kwun, M. Zahra, G. Farid, S. Zainab, and S. M. Kang, "On a unified integral operator for φ -convex functions," *Advances in Difference Equations*, vol. 297, 2020.
- [8] V. G. Mihesan, "A generalization of convexity," in *Proceedings of the Seminar on Functional Equations, Approx. And Convex*, Cluj-Napoca, Romania, 1993.
- [9] M. E. Özdemir, A. O. Akdemri, and E. Set, "On (h,m) -convexity and Hadamard type inequalities," *Journal of Mathematics and Mechanics*, vol. 8, no. 1, pp. 51–58, 2016.
- [10] S.-M. Yuan and Z.-M. Liu, "Some properties of α -convex and α -quasiconvex functions with respect to n -symmetric points," *Applied Mathematics and Computation*, vol. 188, no. 2, pp. 1142–1150, 2007.
- [11] G. Farid, "Existence of an integral operator and its consequences in fractional and conformable integrals," *Open Journal of Mathematical Sciences*, vol. 3, no. 1, pp. 210–216, 2019.
- [12] F. Jarad, E. Ugurlu, T. Abdeljawad, and D. Baleanu, "On a new class of fractional operators," *Advances in Difference Equations*, vol. 2017, p. 247, 2017.
- [13] T. U. Khan and M. A. Khan, "Generalized conformable fractional operators," *Journal of Computational and Applied Mathematics*, vol. 346, pp. 378–389, 2019.
- [14] A. A. Kilbas, H. M. Srivastava, and J. J. Trujillo, *Theory And Applications Of Fractional Differential Equations*, Vol. 204, Elsevier, New York, NY, USA, 2006.
- [15] G. Rahman, D. Baleanu, M. A. Qurashi, S. D. Purohit, S. Mubeen, and M. Arshad, "The extended Mittag-Leffler function via fractional calculus," *Journal of Nonlinear Science and Applications*, vol. 10, pp. 4244–4253, 2013.
- [16] S. S. Dragomir and C. E. M. Pearce, "Quasi-convex functions and Hadamard's inequality," *Bulletin of the Australian Mathematical Society*, vol. 57, no. 3, pp. 377–385, 1998.
- [17] G. Farid, C. Y. Jung, S. Ullah, W. Nazeer, M. Waseem, and S. M. Kang, "Some generalized k -fractional integral inequalities for quasi-convex functions," *Journal of Computational Analysis and Applications*, vol. 29, no. 3, pp. 454–467, 2021.
- [18] S. Ullah, G. Farid, K. A. Khan, A. Waheed, and S. Mehmood, "Generalized fractional inequalities for quasi-convex functions," *Advance Difference Equations*, vol. 15, 2019.
- [19] D. Zhao, G. Farid, M. Zeb, S. Ahmad, and K. Mahreen, "On boundedness of unified integral operators for quasiconvex functions," *Advance Difference Equations*, vol. 38, 2020.
- [20] A. W. Roberts and D. E. Varberg, *Convex Functions*, Academic Press, New York, NY, USA, 1973.
- [21] M. E. Gordji, M. R. Delavar, and M. D. L. Sen, "On φ -convex functions," *Journal of Mathematical Inequalities*, vol. 10, no. 1, pp. 173–183, 2016.
- [22] D. A. Ion, "Some estimates on the Hermite-Hadamard inequality through quasi-convex functions," *Analele Universitatii din Craiova. Seria Matematica*, vol. 34, pp. 82–87, 2007.
- [23] Y. C. Kwun, G. Farid, W. Nazeer, S. Ullah, and S. M. Kang, "Generalized Riemann-Liouville k -fractional integrals associated with Ostrowski type inequalities and error bounds of Hadamard inequalities," *IEEE Access*, vol. 6, 2018.
- [24] M. Andrić, G. Farid, and J. Pečarić, "A further extension of Mittag-Leffler function," *Fractional Calculus and Applied Analysis*, vol. 21, no. 5, pp. 1377–1395, 2018.
- [25] Y. C. Kwun, G. Farid, W. Nazeer, S. Ullah, K. Mahreen, and S. M. Kang, "Inequalities for a unified integral operator and associated results in fractional integrals," *IEEE Access*, vol. 7, 2019.
- [26] S. Mubeen and G. M. Habibullah, " κ -fractional integral and application," *International Journal of Contemporary Mathematical Sciences*, vol. 7, pp. 89–94, 2012.

- [27] H. Chen and U. N. Katugampola, "Hermite-Hadamard and Hermite-Hadamard-Fejér type inequalities for generalized fractional integrals," *Journal of Mathematical Analysis and Applications*, vol. 446, no. 2, pp. 1274–1291, 2017.
- [28] M. Z. Sarikaya, Z. Dahmani, M. E. Kiris, and F. Ahmad, " (k, s) -Riemann-Liouville fractional integral and applications," *Hacettepe Journal of Mathematics and Statistics*, vol. 1, no. 45, pp. 77–89, 2016.
- [29] S. Habib, S. Mubeen, and M. N. Naeem, "Chebyshev type integral inequalities for generalized k -fractional conformable integrals," *Journal of Inequalities and Special Functions*, vol. 9, no. 4, pp. 53–65, 2018.

Research Article

Combining Finite Element and Analytical methods to Contact Problems of 3D Structure on Soft Foundation

Chao Su, Heng Zhang , Shaopei Hu , Jiawei Bai, and Jianjian Dai

College of Water Conservancy and Hydropower Engineering, Hohai University, Nanjing 210098, China

Correspondence should be addressed to Heng Zhang; zhangheng@hhu.edu.cn

Received 17 September 2020; Revised 5 October 2020; Accepted 7 October 2020; Published 30 October 2020

Academic Editor: HwaJoon Kim

Copyright © 2020 Chao Su et al. This is an open access article distributed under the Creative Commons Attribution License, which permits unrestricted use, distribution, and reproduction in any medium, provided the original work is properly cited.

The computational efficiency and nonconvergence of the iteration are two main difficulties in contact problems, especially in the creep of the foundation. This paper proposes a method to analyze the structural soft foundation system affected by time. The methodology is an explicit method, combining the finite element method with the analytical method. The creep deformation of soft foundation is obtained based on Laplace transforms. The structural deformation contains the statically determinate structural deformation and rigid body displacement, solved by the finite method. The contact forces are calculated by the deformation coordination equations and equilibrium equations. The methodology is validated through augmented Lagrangian (AL) method. The results can clearly illustrate the local disengagement phenome, greatly overcome the nonconvergence of the iteration, and significantly improve computing efficiency.

1. Introduction

Hydraulic structures in plain areas are mostly built on soft soil which have high water content, low strength, and low bearing capacity. It often needs taking measures to strengthen the foundation during the construction period. The soil layer bottom of the foundation is the bottleneck controlling the bearing capacity and also the main place where the creep occurs [1]. The creep property results in the significant alteration of the foundation deformation, which leads to the uneven settlement in the upper structure [2]. In contrast to traditional problem of beam or plate on an elastic foundation, the influence of creep can be recognized as a necessary long-term stability method to analyze stress state of the structure [3]. Long-term monitoring data show that the creep deformation continues to increase during the operation period, and it can reach more than twice at the end of construction period [4]. The creep creates unique contact changing laws of the soft foundation and is cognized as the most serious factor that directly affects stress redistribution of the structure. In addition, the computational efficiency and calculation accuracy of the contact forces also face great challenge.

In structural soft foundation system, the contact surfaces are deterministic and searching of contact surfaces is not necessary. Contact forces are time-sensitive and spatiality-nonlinear. Therefore, the contact problem can be simplified to finding the solution of contact forces, which mainly include analytical method, direct iterative method, mathematical programming method, penalty method, augmented Lagrangian method, and contact element method. In 1881, Hertz obtained an analytical solution in two contact bodies [5]. Signorini added the general formulation and defined it as a unilateral contact problem [6]. Winkler established the liner relationship between contact forces and deflection deformation, and got the analytical solution of contact problem in beam on elastic foundation [7]. Analytical method is still studied today and is widely used to solve the problem of dynamic load in rail transportation [8, 9]. The direct iterative method is numerical. For typical example, Francavilla obtained flexibility matrices in terms of contact forces at possible contact surfaces of two bodies and solved the quasilinear problem [10]. The direct iterative method has a clear concept, but the computational complexity is heavy owing to large quantities of the possible contact forces. In mathematical programming method, it is regarded as linear

complementarity problem (LCP) or parametric linear complementarity problem (PLCP). Anders and Gunnar formulated the contact problems including varying contact surfaces and friction through the mathematical programming method [11, 12]. The advantage of the penalty method is imposing the contact conditions without increasing the number of variables. A penalty term is used to enforce the contact constraints. Luenberger discussed the ill-conditioned numerical problem caused by large values for penalty parameters [13]. Augmented Lagrangian method combines the penalty method and the Lagrangian method. It transforms the problem of original constraints into optimization so that it is well suited to the method of finite element and widely used in related software. Simo proposed the technique updating Lagrangian multipliers with penalty parameters to inherit the advantage of Lagrangian method [14]. Contact element method describes the contact behavior in interfaces. It expresses the contact stresses regarded as a function of the relative displacements in the mean planes of the microscopically rough surfaces. In another word, it assumes that the interface is a kind of element type and has constitutive laws. Goodman proposed the four-node planar and nonthickness contact surface element [15].

A series of studies in contact problems of beam on elastic foundation make excellent contributions to long-span engineering programs [8]. It assumes that the reactive force of the foundation carrying a loaded beam at every point is proportional to the corresponding deflection of the beam [7]. Higher-order nonlinear partial differential equation can be used to reflect the contact phenomena [16, 17]. Through these researches, Gao considered the beam and foundation as two different element types, and each can use an own type of finite element [18]. This idea inspires us to study further. The key to contact problem lies in finding the solution of unilateral problems. The structure and soft foundation are two different contacting bodies, and each can be solved independently. Therefore, when the time-affection relationship of soft foundation is established, the same of the contact problems can be solved.

The creep deformation of soft foundation has received extensive attention. Any foundation needs to quantitatively describe soil structure, rheological characteristic, spatial distribution, and mechanical property, evaluating accurately the bearing capacity, the effective stress, and settlement deformation. Terzaghi and Biot derived the three-dimensional consolidation equations based on the principle of effective stress [19, 20]. These equations have been well applied in complex foundation so far [21–23]. Singh adopted creep rate and creep function to construct a famous empirical creep model [24]. When the characterization of deformation is obtained, it is necessary to develop viscoelastic or elastic-viscoplastic constitutive theories based on micromechanics. The component models are applied to describe the rheological property and comprised of varying Hooke units and Kelvin units, such as the Kelvin model, the Maxwell model, and the Burgers model [25, 26]. Some elastic-viscoplastic constitutive models are built based on the Can-Clay creep model and modified Can-Clay creep model [27, 28]. Furthermore, Lee proposed an analytical method to

solve the viscoelastic deformation by Laplace transform [29]. This analytical method has few parameters and can be easily used in soft foundation. Therefore, this method can be used to describe the contact forces and deformation of the soft foundation in the unilateral constraint problem.

In this paper, the contact problem is considered as a unilateral constraint problem. This paper introduces a methodology to analyze the time affection on structural soft foundation system. The methodology is presented as a numerical implementation and combining finite element method with analytical method. It aims to solve the contact problem and focus on the contact forces varying with time. In this methodology, the finite element method is used to solve the structure deformation. The analytical method is based on the Maxwell model and Lee's theory, extended to three dimensions and applied to the soft foundation. Then, the deformation coordination equation and force-method asymmetric matrix equation for quasilinear problems of the contact surface can be established. The contact situations, contact forces, and deformation at each time increment step are determined finally.

2. Analysis of the Problem Formulations

Similar to the direct method, contact forces are split into forces and reaction forces in the structural soft foundation system [7]. Therefore, the contact problems of the structural soft foundation system are divided into two unilateral constraint problems. As Figure 1 shows, contact forces are treated as unknown variables and act on the structure and foundation separately. The deformation coordination equations of contact surface can be put on solving the contact forces. Then, these contact forces can act on the structure, and the stress state of the structure is obtained.

The deformation of structure contains the statically determinate structural deformation and rigid body displacement. The force method based on the Boltzmann superposition principle is used to solve the statically determinate structural deformation. Firstly, the basic deformation caused by each unit force of contact surface is calculated. Secondly, the deformation caused by external forces of contact surface is calculated. Thirdly, the statically determinate structural deformation is shown as

$$U_{st} = U_{f0} + \delta_1 \times X_1 + \dots + \delta_n \times X_n, \quad (1)$$

where U_{st} is the deformation obtained by all forces in the statically determinate structural system; U_{f0} is the deformation obtained by the external forces; $\delta_1 \dots \delta_n$ are the deformation obtained by each unit force separately; and $X_1 \dots X_n$ are the unknown contact forces.

The rigid body displacement of the structure can be shown by the deformation of six supports. Through the Lee's method, the deformation of contact surface can also be shown by n contact force on the soft foundation multiplied by the deformation caused by the corresponding unit force. A total of $n + 6$ variables are formed. It still needs to add the force and bending moment equilibrium equations. Finally, the contact surface equations include n deformation

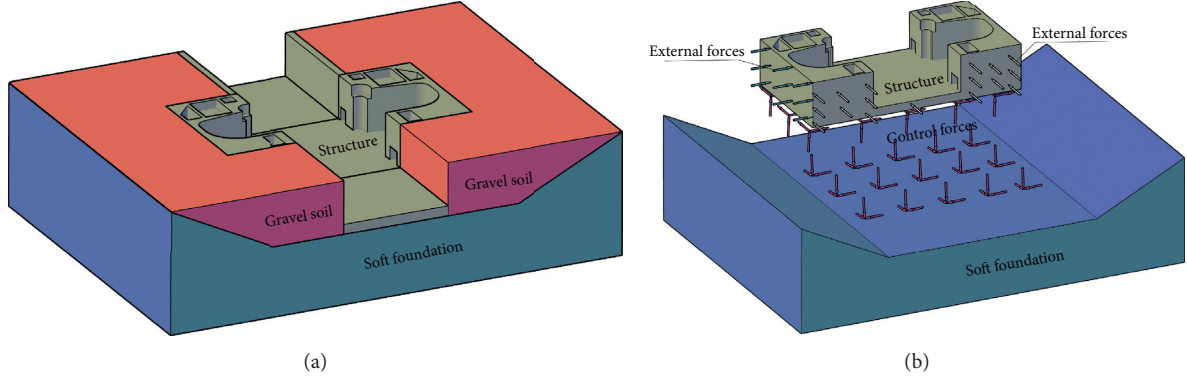


FIGURE 1: Structural soft foundation system. (a) Structure and soft foundation. (b) Load combination.

coordination equations and 6 equilibrium equations. It can be simplified as follows:

$$\begin{cases} U_{st} + U_{rb} = U_{sf}, \\ \sum F_x = 0; \sum F_y = 0; \sum F_z = 0, \\ \sum M_x = 0; \sum M_y = 0; \sum M_z = 0, \end{cases} \quad (2)$$

where U_{rb} is the rigid body displacement of structural contact surface; U_{st} is the contact surface deformation of soft foundation; and $\sum F = 0$ $\sum M = 0$ are composited by the forces and bending moments in three directions. The deformation coordination equations of the contact surface are built in the first line in (2). The force and bending moment equilibrium equations in three directions are added. The contact forces and rigid body displacement are calculated. Then, the stress state of the structure can be calculated.

3. Analytical Solution of Soft Foundation

The analytical solution of viscoelastic deformation is obtained by Lee's method. Taking Kelvin model as an example, the elastic solution of a semi-infinite space body subjected to concentrated load is integrated to derive the solution of distributed force based on the principle of superposition. Then, the viscoelastic deformation in the Laplace space is obtained based on the elastic-viscoelastic correspondence principle. Finally, the solution of the viscoelastic deformation under distributed force can be obtained by inverse Laplace transformation.

As shown in Figure 2, there is a rectangle with length a and width b on the boundary of the semi-infinite foundation. The normal uniform load (Figure 2(a)) and tangential uniform load (Figure 2(b)) are concentration of $1/ab$. They act on the rectangle. The elastic deformation acted normal concentrated force is shown:

$$\begin{cases} u_{zz} = \frac{(1+\mu)P}{2\pi ER} \left[2(1-\mu) + \frac{z^2}{R^2} \right], \\ u_{zr} = \frac{(1+\mu)P}{2\pi ER} \left[\frac{rz}{R^2} - \frac{(1-2\mu)r}{R+z} \right], \end{cases} \quad (3)$$

where u_{zr} is the radial deformation; u_{zz} is the normal deformation; P is the normal concentrated force; R is the distance from a point to the origin of coordinates; r is the distance from a point to the normal line; E is the elasticity modulus; and μ is Poisson's ratio. (3) has no solution when $R=0$ so that unit distribution force is considered. The normal differential force dP shown based on Lagrangian coordinate system is $d\eta d\xi/ab$. The elastic deformation acted normal concentrated force is shown:

$$\begin{cases} \delta_{zz} = \frac{1-\mu^2}{ab\pi E} \int_{\eta=x-(a/2)}^{\eta=x+(a/2)} \int_{\xi=y-(b/2)}^{\xi=y+(b/2)} \frac{d\xi d\eta}{\sqrt{\xi^2 + \eta^2}}, \\ \delta_{zx} = \frac{(1+\mu)(2\mu-1)}{ab\pi E} \int_{\eta=x-(a/2)}^{\eta=x+(a/2)} \int_{\xi=y-(b/2)}^{\xi=y+(b/2)} \frac{d\xi d\eta}{\sqrt{\xi^2 + \eta^2}} \frac{x}{\sqrt{x^2 + y^2}}, \\ \delta_{zy} = \frac{(1+\mu)(2\mu-1)}{ab\pi E} \int_{\eta=x-(a/2)}^{\eta=x+(a/2)} \int_{\xi=y-(b/2)}^{\xi=y+(b/2)} \frac{d\xi d\eta}{\sqrt{\xi^2 + \eta^2}} \frac{y}{\sqrt{x^2 + y^2}}, \end{cases} \quad (4)$$

where δ_{zx} , δ_{zy} , δ_{zz} are the deformation in x , y , z directions under unit distribution force in z direction. According to elastic-viscoelastic correspondence principle, after Laplace transforms, the viscoelastic deformation formula is obtained:

$$\begin{cases} \delta_{zz}(s) = \frac{1-[\mu(s)]^2}{ab\pi[E(s)]} \frac{e^{-ts}}{s} F_k, \\ \delta_{zx}(s) = \frac{(1+[\mu(s)])(2[\mu(s)]-1)}{ab\pi[E(s)]} \frac{e^{-ts}}{s} \frac{x}{\sqrt{x^2 + y^2}} F_k, \\ \delta_{zy}(s) = \frac{(1+[\mu(s)])(2[\mu(s)]-1)}{ab\pi[E(s)]} \frac{e^{-ts}}{s} \frac{y}{\sqrt{x^2 + y^2}} F_k, \end{cases} \quad (5)$$

where $F_k = \int_{\eta=x-(a/2)}^{\eta=x+(a/2)} \int_{\xi=y-(b/2)}^{\xi=y+(b/2)} d\xi d\eta / \sqrt{\xi^2 + \eta^2}$ is obtained by the numerical integration method.

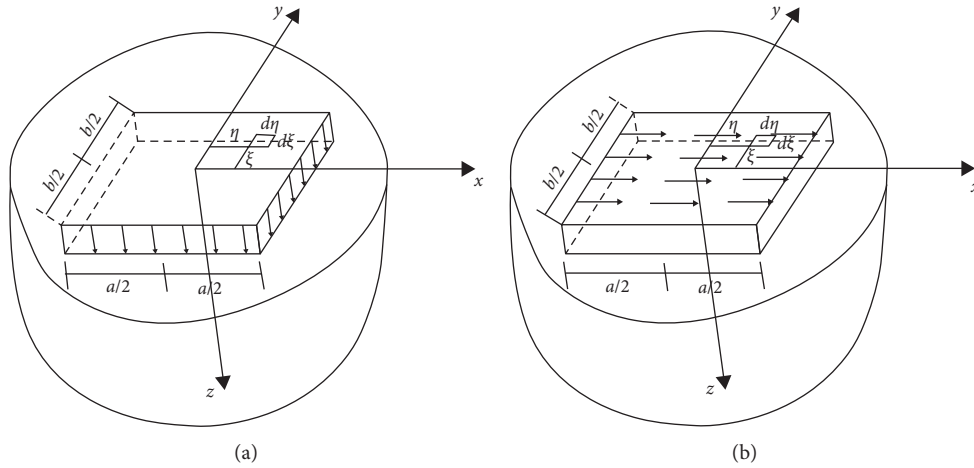


FIGURE 2: Normal and tangential uniform loads act on space semi-infinite foundation. (a) Normal uniform load. (b) Tangential uniform load.

Kelvin viscoelastic solution is derived by inverse Laplace transformation.

$$\left\{ \begin{array}{l} \delta_{zz} = \left[\left(\frac{3}{6K + 2G_1} \right) \left(1 - e^{-((6K+2G_1)/2\eta_1)} \right) + \frac{1}{2G_1} \left(1 - e^{-G_1/\eta_1} \right) \right] \frac{F_k}{2ab\pi}, \\ \delta_{zx} = \left(\frac{-3}{6K + 2G_1} \right) \left(1 - e^{-((6K+2G_1)/2\eta_1)} \right) \frac{F_k}{2ab\pi} \frac{x}{\sqrt{x^2 + y^2}}, \\ \delta_{zy} = \left(\frac{-3}{6K + 2G_1} \right) \left(1 - e^{-((6K+2G_1)/2\eta_1)} \right) \frac{F_k}{2ab\pi} \frac{y}{\sqrt{x^2 + y^2}}, \end{array} \right. \quad (6)$$

where K is the bulk modulus; G_1 is the shear stiffness; and η_1 is the coefficient of viscosity. Tangential load causes the

deformation; the elastic deformation is shown in the following equation [30]:

$$\left\{ \begin{array}{l} u_{xx} = \frac{(1 + \mu)P}{2\pi ER} \left\{ 1 + \frac{x^2}{R^2} + (1 - 2\mu) \left[\frac{R}{R + z} - \frac{x^2}{(R + z)^2} \right] \right\}, \\ u_{xy} = \frac{(1 + \mu)P}{2\pi ER} \left[\frac{xy}{R^2} - \frac{(1 - 2\mu)xy}{(R + z)^2} \right], \\ u_{xz} = \frac{(1 + \mu)P}{2\pi ER} \left[\frac{xy}{R^2} + \frac{(1 - 2\mu)x}{R + z} \right]. \end{array} \right. \quad (7)$$

Through the Laplace transformation and inverse Laplace transformation, the viscoelastic deformation can also be solved and shown in the following equation:

$$\left\{ \begin{aligned} \delta_{xx} &= \frac{1}{2\pi ab} \left[\frac{1}{2G_1} \left(e^{-(G_1/\eta_1)t} \right) + \frac{3}{6K + 2G_1} \left(e^{-((6K+2G_1)/2\eta_1)t} \right) \right] F_k + \frac{1}{2\pi ab} \left[\frac{1}{2G_1} \left(e^{-(G_1/\eta_1)t} \right) - \frac{3}{6K + 2G_1} \left(e^{-((6K+2G_1)/2\eta_1)t} \right) \right] x^2 F_g, \\ \delta_{xy} &= \frac{xy F_g}{2\pi ab} \left[\frac{1}{2G_1} \left(e^{-(G_1/\eta_1)t} \right) - \frac{3}{6K + 2G_1} \left(e^{-((6K+2G_1)/2\eta_1)t} \right) \right], \\ \delta_{xz} &= \frac{x F_i}{2\pi ab} \left[\frac{3}{6K + 2G_1} \left(e^{-((6K+2G_1)/2\eta_1)t} \right) \right]. \end{aligned} \right. \quad (8)$$

$$\left\{ \begin{aligned} F_i &= \int_{\eta=x-(a/2)}^{\eta=x+(a/2)} \int_{\xi=y-(b/2)}^{\xi=y+(b/2)} d\xi d\eta / \sqrt{\xi^2 + \eta^2} \\ F_g &= \int_{\eta=x-(a/2)}^{\eta=x+(a/2)} \int_{\xi=y-(b/2)}^{\xi=y+(b/2)} d\xi d\eta / (\sqrt{\xi^2 + \eta^2})^{3/2} \end{aligned} \right.$$
 is obtained by the numerical integration method, where δ_{xx} , δ_{xy} , δ_{xz} are the deformation in x , y , z directions under unit distribution

force in x direction. The analytical solution of viscoelastic deformation based on the Maxwell model can be calculated by MATLAB. The process is given in the appendix. The final equation is shown as follows:

$$\left\{ \begin{aligned} \delta_{xx} &= \frac{4G_3 F_i 3KF_i - 2G_3 F_g x^2 + 3KF_g x^2}{4G_3 ab\pi (G_3 + 3K)} - \frac{3\eta_1 e(t(G_2 G_3 + 3G_2 K)/G_2 \eta_1 + G_3 \eta_1 + 3K \eta_1)(G_2 F_i - G_2 F_g x^2)}{4ab\pi (G_3 + 3K)(G_2 \eta_1 + G_3 \eta_1 + 3K \eta_1)} \\ &\quad - \frac{\eta_1 e((G_2 G_3 t)/G_2 \eta_1 + G_3 \eta_1)(G_2 F_g x^2 + G_2 F_i)}{4G_3 ab\pi (G_2 \eta_1 + G_3 \eta_1)}, \\ \delta_{xy} &= \frac{3G_2 \eta_1 F_g x y e(t(G_2 G_3 + 3G_2 K)/(G_2 \eta_1 + G_3 \eta_1 + 3K \eta_1))}{4ab\pi (G_3 + 3K)(G_2 \eta_1 + G_3 \eta_1 + 3K \eta_1)} - \frac{F_g x y (2G_3 - 3K)}{4G_3 ab\pi (G_3 + 3K)} - \frac{(G_2 \eta_1 F_g x y e(G_2 G_3 t)/(G_2 \eta_1 + G_3 \eta_1))}{4G_3 ab\pi (G_2 \eta_1 + G_3 \eta_1)}, \\ \delta_{xz} &= \frac{3F_i x}{4ab\pi (G_3 + 3K)} - \frac{3G_2 \eta_1 F_g x y e(t(G_2 G_3 + 3G_2 K)/(G_2 \eta_1 + G_3 \eta_1 + 3K \eta_1))}{4ab\pi (G_3 + 3K)(G_2 \eta_1 + G_3 \eta_1 + 3K \eta_1)}, \\ \delta_{zx} &= \frac{3G_2 \eta_1 F_g x y e(t(G_2 G_3 + 3G_2 K)/(G_2 \eta_1 + G_3 \eta_1 + 3K \eta_1))}{4ab\pi (G_3 + 3K)(G_2 \eta_1 + G_3 \eta_1 + 3K \eta_1)} - \frac{3F_i x}{4ab\pi \sqrt{x^2 + y^2} (G_3 + 3K)}, \\ \delta_{zy} &= \frac{3G_2 \eta_1 F_g x y e(t(G_2 G_3 + 3G_2 K)/(G_2 \eta_1 + G_3 \eta_1 + 3K \eta_1))}{4ab\pi \sqrt{x^2 + y^2} (G_3 + 3K)(G_2 \eta_1 + G_3 \eta_1 + 3K \eta_1)} - \frac{3F_i y}{4ab\pi \sqrt{x^2 + y^2} (G_3 + 3K)}, \\ \delta_{zz} &= \frac{F_i (4G_3 + 3K)}{4G_3 ab\pi (G_3 + 3K)} - \frac{3G_2 \eta_1 F_g x y e(t(G_2 G_3 + 3G_2 K)/(G_2 \eta_1 + G_3 \eta_1 + 3K \eta_1))}{4ab\pi \sqrt{x^2 + y^2} (G_3 + 3K)(G_2 \eta_1 + G_3 \eta_1 + 3K \eta_1)} - \frac{G_2 \eta_1 F_k e((G_2 G_3 t)/(G_2 \eta_1 + G_3 \eta_1))}{4ab\pi (G_2 \eta_1 + G_3 \eta_1)}, \end{aligned} \right. \quad (9)$$

where G_2 , G_3 are the parameters of shear stiffness. The deformation at any point of the contact surface on soft foundation acted on a force can be shown as

$$\begin{bmatrix} U_{sfx} \\ U_{sfy} \\ U_{sfz} \end{bmatrix} = \begin{bmatrix} \delta_{xx} & \delta_{yx} & \delta_{zx} \\ \delta_{xy} & \delta_{yy} & \delta_{zy} \\ \delta_{xz} & \delta_{yz} & \delta_{zz} \end{bmatrix} \begin{bmatrix} F_x \\ F_y \\ F_z \end{bmatrix}, \quad (10)$$

where U_{sfx} , U_{sfy} , and U_{sfz} are the deformation of soft foundation in three directions. F_x , F_y , and F_z are the contact forces of soft foundation in three directions. (10) shows the deformation of a single point under a distribution force. The real contact surface deformation is more complicated.

4. Structure Deformation

4.1. Statically Determinate Structural Deformation. The contact forces are treated as unknown variables and act on the structure and foundation separately. As Figure 3 shows, in order to ensure the structure statically determinate, the structure has six constraints on the contact surface. It is divided into multiple hexahedrons. Each unit distribution force acts on the bottom of underside element. Note that the unit distribution force acting on the contact surface separating two adjacent volume elements in the structure and the soft foundation must be equal and opposite. The resultant point of distributed force is under the bottom of element. The deformation of the resultant point can be shown by deformation of element nodes. The equation is as follows:

$$\begin{bmatrix} u \\ v \\ w \end{bmatrix} = \begin{bmatrix} N_1 & 0 & 0 & \dots & N_4 & 0 & 0 \\ 0 & N_1 & 0 & \dots & 0 & N_4 & 0 \\ 0 & 0 & N_1 & \dots & 0 & 0 & N_4 \end{bmatrix} q^e, \quad (11)$$

where N_1, N_2, N_3, N_4 are the shape function of the four nodes which are at the bottom of the hexahedron element and q^e is the deformation of element. The programming of these deformations can be finished with DLOAD subroutine and UTRACLOAD subroutine in Abaqus. The DLOAD subroutine is used to get the solution of the deformation acted by each unit distribution force in z -axis direction. The UTRACLOAD subroutine is used to get the solution of the deformation acted by each unit distribution force in x and y direction. The $xleft$, $xright$, $yleft$, and $yright$ are the four boundaries of the unit distributed force. The $xstart$, $xend$, $ystart$, and $yend$ are the first and final coordinates of the unit distributed force. The $T_user(1)$, $T_user(2)$, and $T_user(3)$ are the direction of the unit distribution force. The v and time are the speed and time of the unit distributed force. The $coord(1)$ and $coord(2)$ are the x and y coordinates of each position of the contact surface. It determines where the unit distributed force is applied and where the force is zero. Figure 4 shows the flow chart of subroutines in Abaqus. (1) All parameters are input in the subroutine. (2) The parameters of $xleft$, $xright$, $yleft$, and $yright$ are updated. (3) The position of force is determined. (4) The time is updated and the above process is repeated.

A unit distributed force moves from the bottom of the first element to the bottom of the last element on the underside element. The deformation during the movement is recorded. According to equation (11), the deformation of the resultant point is calculated by numerical software. Then, the statically determinate structural deformation can also be expressed in the same form as (10).

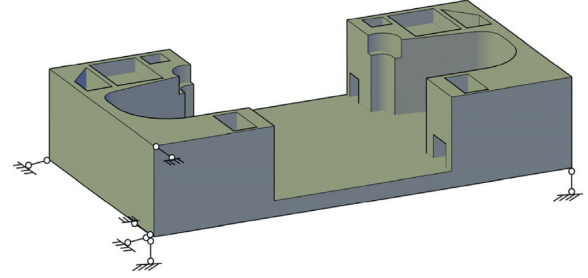


FIGURE 3: Statically determinate structure deformation.

5. Rigid Body Displacement

The rigid body displacement of statically determinate structure can be described by Cauchy equations. It means that the strain of the structure is zero. For infinitesimal motion, the relationship between strain and displacement is

$$\begin{cases} \varepsilon_x = \frac{\partial u}{\partial x}, \varepsilon_y = \frac{\partial v}{\partial y}, \varepsilon_z = \frac{\partial w}{\partial z}, \\ \gamma_{yz} = \frac{\partial w}{\partial y} + \frac{\partial v}{\partial z}, \gamma_{zx} = \frac{\partial u}{\partial z} + \frac{\partial w}{\partial x}, \gamma_{xy} = \frac{\partial v}{\partial x} + \frac{\partial u}{\partial y}, \\ \varepsilon_x = \varepsilon_y = \varepsilon_z = \gamma_{yz} = \gamma_{zx} = \gamma_{xy} = 0, \end{cases} \quad (12)$$

where $\varepsilon_x, \varepsilon_y, \varepsilon_z$ are the normal strain in x, y, z directions and $\gamma_{yz}, \gamma_{zx}, \gamma_{xy}$ are the shearing strain in x, y, z directions. Solving the above formulas, the rigid body displacement can be obtained as

$$\begin{cases} u = u_0 + \varphi_y z - \varphi_z y, \\ v = v_0 + \varphi_z x - \varphi_x z, \\ w = w_0 + \varphi_x y - \varphi_y x, \end{cases} \quad (13)$$

where u, v, w are the rigid body displacement in x, y, z directions; $\varphi_x, \varphi_y, \varphi_z$ are the rigid body rotation angles in x, y, z directions; and u_0, v_0, w_0 are the translational deformations in x, y, z directions. These equations can be comprehended through geometric transformation in Figure 5. It is important that the sign of rigid body rotation angles follows the right hand's spiral rule. When $z=0$, the equation shows the deformation of undersurface. (13) can be simplified as linear matrix equation:

$$\begin{bmatrix} u \\ v \\ w \end{bmatrix} = \begin{bmatrix} 1 & 0 & 0 & 0 & 0 & -y \\ 0 & 1 & 0 & 0 & 0 & x \\ 0 & 0 & 1 & y & x & 0 \end{bmatrix} \begin{bmatrix} u_0 \\ v_0 \\ w_0 \\ \varphi_x \\ \varphi_y \\ \varphi_z \end{bmatrix}. \quad (14)$$

After the statically determinate structural deformation and rigid body displacement are obtained, the contact surface deformation can be described as the sum of them in the structure.

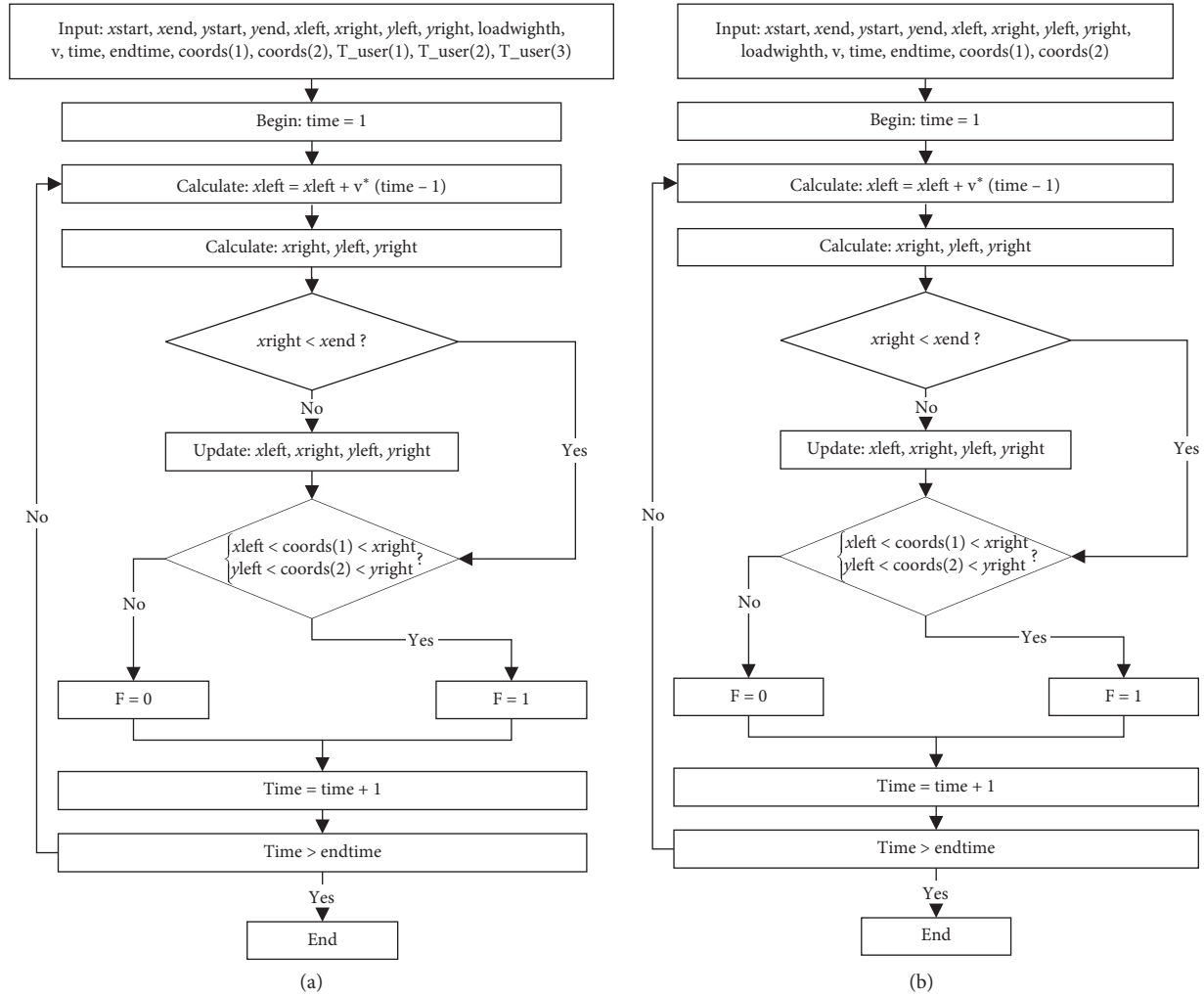


FIGURE 4: Flow chart of subroutines in Abaqus. (a) UTRACLOAD subroutine. (b) DLOAD subroutine.

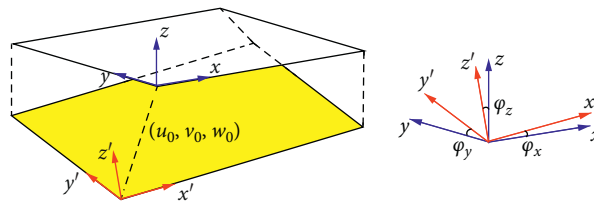


FIGURE 5: Rigid body displacement of contact surface.

6. Force Equilibrium Equations and Bending Moment Equilibrium Equations

By means of rational mechanics, the force equilibrium equations and bending moment equilibrium equations of 3D

structure can be elucidated in three directions. These equations are as follows:

$$\begin{cases} \sum_{k=1}^n X_k + F_x = 0, \sum_{k=1}^n Y_k + F_y = 0, \sum_{k=1}^n Z_k + F_z = 0, \left(\sum_{k=1}^n b_k Z_k - \sum_{k=1}^n c_k Y_k \right) + (y_F F_z - z_F F_y) = 0, \left(\sum_{k=1}^n c_k X_k - \sum_{k=1}^n a_k Z_k \right) \\ + (z_F F_x - x_F F_z) = 0, \left(\sum_{k=1}^n a_k Y_k - \sum_{k=1}^n b_k X_k \right) + (x_F F_y - y_F F_x) = 0, \end{cases} \quad (15)$$

where $\sum_{k=1}^n X_k$, $\sum_{k=1}^n Y_k$, $\sum_{k=1}^n Z_k$ are the sum of contact forces in x , y , z directions; a_k , b_k , c_k are the coordinates of the contact forces' functional point; x_F , y_F , z_F are the

coordinates of the external forces' functional point; and F_x , F_y , F_z are the external forces in x , y , z directions. When $c=0$, (15) can be simplified as linear matrix equation:

$$\begin{bmatrix} 1 & \dots & 1 & 0 & \dots & 0 & 0 & \dots & 0 \\ 0 & \dots & 0 & 1 & \dots & 1 & 0 & \dots & 0 \\ 0 & \dots & 0 & 0 & \dots & 0 & 1 & \dots & 1 \\ 0 & \dots & 0 & 0 & \dots & 0 & b_1 & \dots & b_n \\ 0 & \dots & 0 & 0 & \dots & 0 & -a_1 & \dots & -a_n \\ -b_1 & \dots & -b_n & a_1 & \dots & a_n & 0 & \dots & 0 \end{bmatrix} \begin{bmatrix} X_1 \\ \dots \\ X_n \\ Y_1 \\ \dots \\ Y_n \\ Z_1 \\ \dots \\ Z_n \end{bmatrix} = \begin{bmatrix} -F_x \\ -F_y \\ -F_z \\ -y_F F_z + z_F F_y \\ -z_F F_x + x_F F_z \\ -x_F F_y + y_F F_x \end{bmatrix}. \quad (16)$$

7. Mixed Finite Element Methodology

Through the analysis of Sections 3, the time affection of soft foundation can be resolved. When the parameters of foundation are determined, the contact forces can be discussed. This contact problem is solved based on the deformation coordination equations.

The eight-node isoparametric elements are used to make the structure discrete. Three connecting rods at the bottom center point of the underside element are set along the x , y , and z directions. They are used to connect the structure with

foundation. The increment of the normal deformation Δz and the increment of the rigid body rotation angles $\Delta\varphi_x$, $\Delta\varphi_y$ are taken as unknown quantities. Taking time step l for example, the finite element method is used to obtain the deformation of nodes and the deflection of the bottom center point of the underside elements. The deformation and deflection are caused by the external loads and unit link force. The normal incremental equation of structure on viscoelastic foundation is solved by combining finite element with the analytical method. It is shown as

$$\begin{cases} \sum_{k=1}^n \delta_{ki}^{(l)} \Delta Z_k^{(l)} + \Delta z + b_i \Delta\varphi_x - a_i \Delta\varphi_y + \Delta_{ip}^{(l)} = 0, \\ n \text{ formulas in total, } i = 1, 2, \dots, n, \\ \sum_{k=1}^n \Delta Z_k^{(l)} + \sum \Delta F_z^{(l)} = 0, \\ \sum_{k=1}^n b_k \Delta Z_k^{(l)} + \sum \Delta M_x^{(l)} = 0, \\ \sum_{k=1}^n a_k \Delta Z_k^{(l)} + \sum \Delta M_y^{(l)} = 0, \end{cases} \quad (17)$$

where $\delta_{ki}^{(l)}$ is the deformation of i position under unit distribution force acting on k position in z direction in the time step l ; $\Delta_{ip}^{(l)}$ is the deformation of i position under external forces at z direction in the time step l ; a_i is the coordinate of y -axis at i position in the time step l ; b_i is the coordinate of x -axis at i position in the time step l ; $\Delta Z_k^{(l)}$ is the element connecting rod force at z direction in the time step l ; $\Delta F_z^{(l)}$ is

the composition of forces at z direction in the time step l ; $\Delta M_x^{(l)}$, $\Delta M_y^{(l)}$ are the composition of bending moments at x and y directions in the time step l . The basic unknown quantities can be solved by the Gaussian elimination with partial pivoting method. Then, the increment of each unknown quantity of the system in the time step is obtained. The equations of contact surface in three-dimensional are also shown as

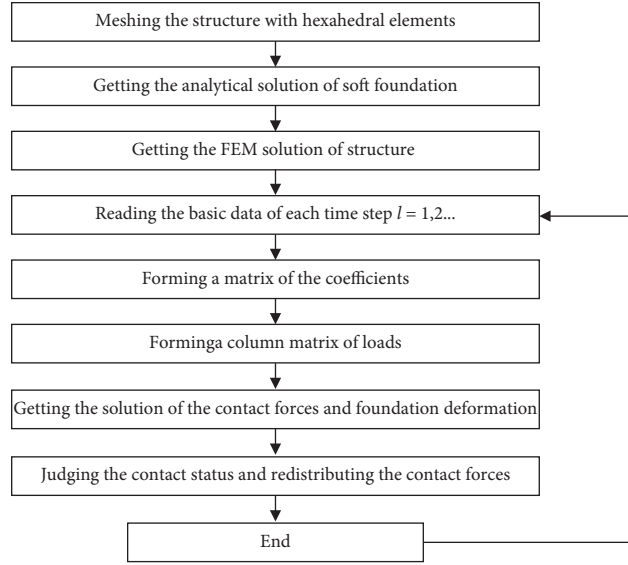


FIGURE 6: Program flow chart.

$$\left\{ \begin{array}{l}
 \sum_{k=1}^n \left[\delta_{xxki}^{(l)} \Delta X_k^{(l)} + \delta_{yyki}^{(l)} \Delta Y_k^{(l)} + \delta_{zxki}^{(l)} \Delta Z_k^{(l)} \right] + (\Delta x^{(l)} - b_i \Delta \varphi_z^{(l)}) + \Delta_{ipx}^{(l)} = 0, \\
 \sum_{k=1}^n \left[\delta_{xyki}^{(l)} \Delta X_k^{(l)} + \delta_{yyki}^{(l)} \Delta Y_k^{(l)} + \delta_{zyki}^{(l)} \Delta Z_k^{(l)} \right] + (\Delta y^{(l)} - a_i \Delta \varphi_z^{(l)}) + \Delta_{ipy}^{(l)} = 0, \\
 \sum_{k=1}^n \left[\delta_{xzki}^{(l)} \Delta X_k^{(l)} + \delta_{yzki}^{(l)} \Delta Y_k^{(l)} + \delta_{zzki}^{(l)} \Delta Z_k^{(l)} \right] + (\Delta z^{(l)} + a_i \Delta \varphi_x^{(l)} - b_i \Delta \varphi_y^{(l)}) + \Delta_{ipz}^{(l)} = 0, \\
 3n \text{ formulas in total, } i = 1, 2, \dots, n, \\
 \sum_{k=1}^n \Delta X_k^{(l)} + \sum \Delta F_x^{(l)} = 0, \\
 \sum_{k=1}^n \Delta Y_k^{(l)} + \sum \Delta F_y^{(l)} = 0, \\
 \sum_{k=1}^n \Delta Z_k^{(l)} + \sum \Delta F_z^{(l)} = 0, \\
 \sum_{k=1}^n a_k \Delta Z_k^{(l)} + \sum \Delta M_x^{(l)} = 0, \\
 \sum_{k=1}^n b_k \Delta Z_k^{(l)} + \sum \Delta M_y^{(l)} = 0, \\
 \sum_{k=1}^n b_k \Delta X_k^{(l)} + \sum_{k=1}^n a_k \Delta Y_k^{(l)} + \sum \Delta M_z^{(l)} = 0, \\
 \delta_{mki}^{(l)} = \delta_{stmki}^{(l)} + \delta_{sfmki}^{(l)}, m = xx, yx, zx, xy, yy, zy, xz, yz, zz,
 \end{array} \right. \quad (18)$$

where $\delta_{mki}^{(l)}$ is the deformation of i position under unit distribution force acting on k position at m -axis direction in the time step l ; $\delta_{sfmki}^{(l)}$, $\delta_{stmki}^{(l)}$ are the deformation of foundation and structure under unit distribution force; $\Delta X_k^{(l)}$, $\Delta Y_k^{(l)}$, $\Delta Z_k^{(l)}$ are the contact forces at k position in x , y , and z directions in the time step l .

The program flow chart is shown in Figure 6. (1) The structure is meshed with hexahedral elements and the position of each connecting rod on the contact surface is set. (2) The analytical solution for soft foundation of each unit distribution force and FEM solution for the structure are obtained. (3) The coefficient matrix and typical

equation are formed. (4) The increment of contact forces and foundation deformation are solved. (5) The contact state is judged and the redistribution of contact forces are calculated.

8. Model Validation

8.1. Example 1. The model validation can be finished through comparative analysis of our method and the augmented Lagrangian (AL) method. The augmented Lagrangian (AL) method is calculated by Abaqus. The time affection of soft foundation is described by Maxwell

UMAT [31]. The length, width, and height of structure is separately 10 m, 6 m, and 3 m. The pressure acting on the upper surface in z direction is 1000 Pa. The pressure acting on the left surface in x direction is 500 Pa. The total time is 1200 d. The time increment is 30 d. The structure can be dispersed into multiple hexahedrons. The labels of the bottom center point of the underside element on the contact surface are 1, 2,...,240. Each label has three degrees of freedom (DOF). There is a total of 720 contact forces in three DOF. From (18), the contact forces equations are shown at time step l :

$$\begin{bmatrix}
 \delta_{xx,1,1} & \dots & \delta_{xx,240,1} & \delta_{yx,1,1} & \dots & \delta_{yx,240,1} & \delta_{zx,1,1} & \dots & \delta_{zx,240,1} & 1 & 0 & 0 & 0 & 0 & -b|_{x=0.25} \\
 \dots & y=0.25 \\
 \delta_{xx,1,240} & \dots & \delta_{xx,240,240} & \delta_{yx,1,240} & \dots & \delta_{yx,240,240} & \delta_{zx,1,240} & \dots & \delta_{zx,240,240} & 1 & 0 & 0 & 0 & 0 & -b|_{x=9.75} \\
 \dots & y=5.75 \\
 \delta_{xy,1,1} & \dots & \delta_{xy,240,1} & \delta_{yy,1,1} & \dots & \delta_{yy,240,1} & \delta_{zy,1,1} & \dots & \delta_{zy,240,1} & 0 & 1 & 0 & 0 & 0 & a|_{x=0.25} \\
 \dots & y=0.25 \\
 \delta_{xy,1,240} & \dots & \delta_{xy,240,240} & \delta_{yy,1,240} & \dots & \delta_{yy,240,240} & \delta_{zy,1,240} & \dots & \delta_{zy,240,240} & 0 & 1 & 0 & 0 & 0 & a|_{x=9.75} \\
 \dots & y=5.75 \\
 \delta_{xz,1,1} & \dots & \delta_{xz,240,1} & \delta_{yz,1,1} & \dots & \delta_{yz,240,1} & \delta_{zz,1,1} & \dots & \delta_{zz,240,1} & 0 & 0 & 1 & b|_{x=9.75} & a|_{x=9.75} & 0 \\
 \dots & y=5.75 & y=5.75 & \\
 \delta_{xz,1,240} & \dots & \delta_{xz,240,240} & \delta_{yz,1,240} & \dots & \delta_{yz,240,240} & \delta_{yz,1,240} & \dots & \delta_{zz,240,240} & 0 & 0 & 1 & b|_{x=9.75} & -a|_{x=9.75} & 0 \\
 \dots & y=2.75 & y=2.75 & \\
 1 & \dots & 1 & 0 & \dots & 0 & 0 & \dots & 0 & 0 & 0 & 0 & 0 & 0 & 0 \\
 0 & \dots & 0 & 1 & \dots & 1 & 0 & \dots & 0 & 0 & 0 & 0 & 0 & 0 & 0 \\
 0 & \dots & 0 & 0 & \dots & 0 & 1 & \dots & 0 & 0 & 0 & 0 & 0 & 0 & 0 \\
 0 & \dots & 0 & 0 & \dots & 0 & a|_{x=0.25} & \dots & 0 & 0 & 0 & 0 & 0 & 0 & 0 \\
 \dots & \dots & \dots & \dots & \dots & \dots & y=0.25 & \dots & \\
 0 & \dots & 0 & 0 & \dots & 0 & -a|_{x=9.75} & \dots & 0 & 0 & 0 & 0 & 0 & 0 & 0 \\
 \dots & \dots & \dots & \dots & \dots & \dots & y=2.75 & \dots & \\
 -b|_{x=0.25} & \dots & -b|_{x=9.75} & a|_{x=0.25} & \dots & a|_{x=9.75} & 0 & \dots & 0 & 0 & 0 & 0 & 0 & 0 & 0 \\
 y=0.25 & & y=5.75 & y=0.25 & & y=2.75 & & & & & & & & & &
 \end{bmatrix}
 \begin{bmatrix}
 X_1 \\
 \dots \\
 X_{240} \\
 Y_1 \\
 \dots \\
 Y_{240} \\
 Z_1 \\
 \dots \\
 Z_{240} \\
 l_1 \\
 l_2 \\
 l_3 \\
 l_4 \\
 l_5 \\
 l_6
 \end{bmatrix}
 =
 \begin{bmatrix}
 -\Delta_{1,x} \\
 \dots \\
 -\Delta_{240,x} \\
 -\Delta_{1,y} \\
 \dots \\
 -\Delta_{240,y} \\
 Z_1 \\
 \dots \\
 -\Delta_{240,z} \\
 -F_x \\
 -F_y \\
 -F_z \\
 -y_F F_z \\
 x_F F_z \\
 -x_F F_y + y_F F_x
 \end{bmatrix},
 \tag{19}$$

$$\begin{bmatrix}
 A & B \\
 C & 0
 \end{bmatrix}
 \begin{bmatrix}
 F \\
 G
 \end{bmatrix}
 =
 \begin{bmatrix}
 D \\
 E
 \end{bmatrix},
 \tag{20}$$

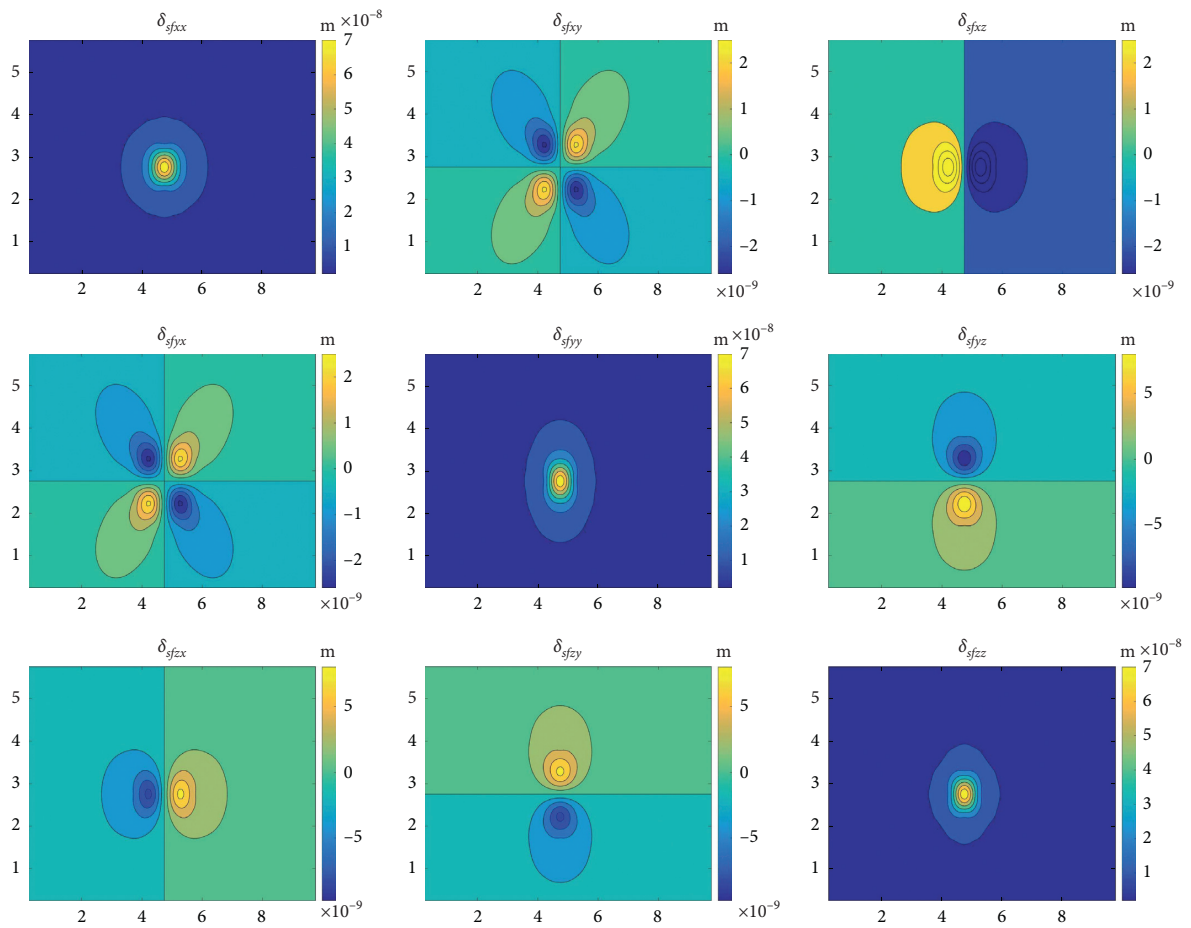
where a, b is the coordinate of center point in x and y directions, respectively. The matrices in (19) can be portioned into seven blocks in (20) for programming, as shown in (20). The block A stands for the sum of the deformation of structure and foundation resulted by unit distribution force. The block B^*G stands for the rigid body displacement. The

block C^*F stands for the external forces and bending moment. The parameters of structure and foundation are shown in Table 1.

Figure 7 shows the deformation of soft foundation in three directions under unit distribution force at 30th day and 1200th day. The deformation results of δ_{sfyx} and δ_{sfxy} are

TABLE 1: The parameters of structure and foundation.

Structure		Soft foundation	
E	3.425×10^{10} Pa	E_1	1.7546×10^7 Pa
μ	0.167	E_2	1.552×10^7 Pa
—	—	μ	0.31
—	—	η_1	8.139×10^8 Pa*d
—	—	K	1.5391×10^7 Pa
—	—	G_2	6.6969×10^6 Pa
—	—	G_3	5.9237×10^6 Pa



(a)
FIGURE 7: Continued.

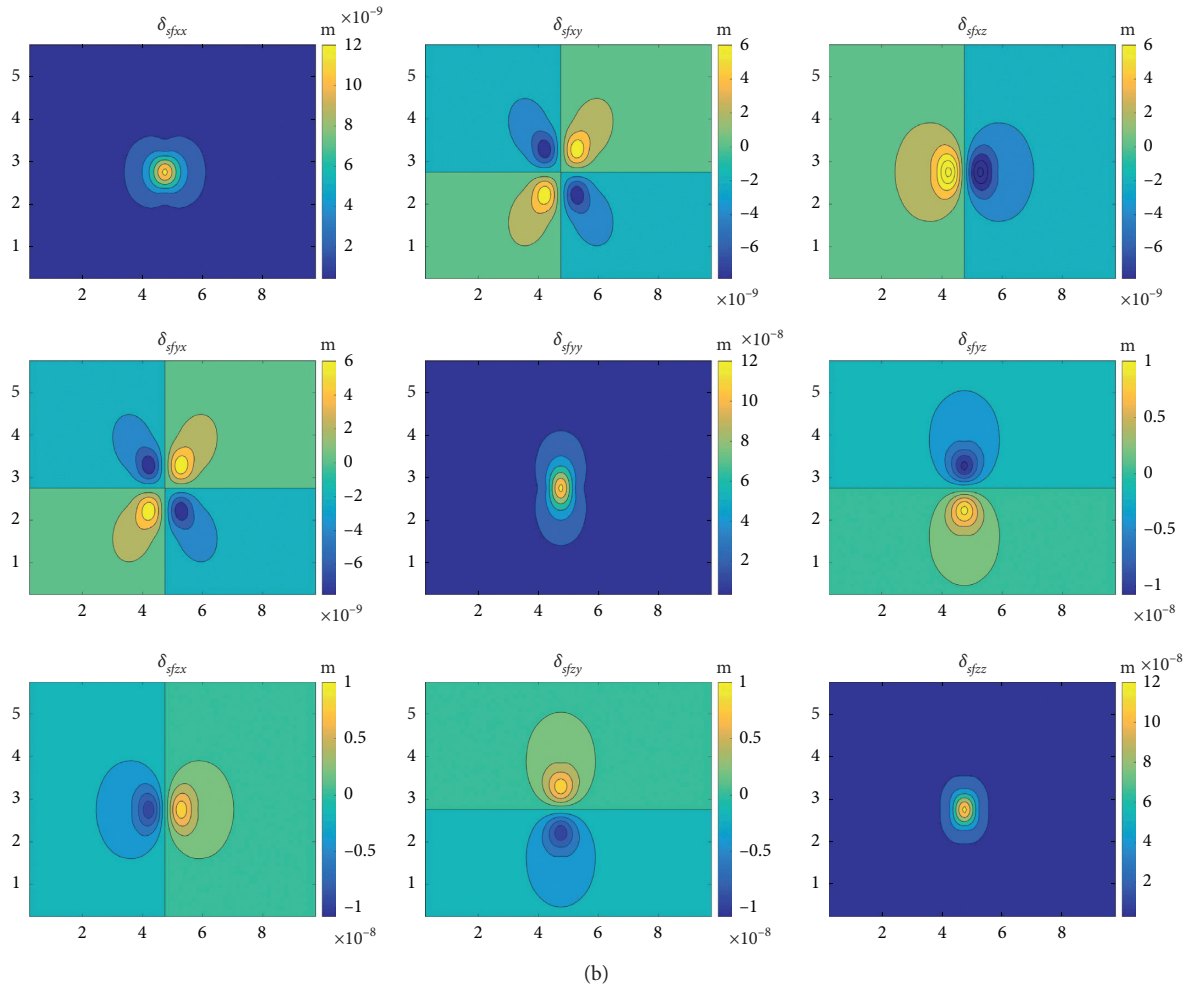


FIGURE 7: The deformation of soft foundation in three directions under unit distribution force. (a) On 30th day. (b) On 1200th day.

center symmetrical about the point of force. The deformation results of δ_{sfxx} , δ_{sfxz} , δ_{sfyy} , δ_{sfyz} , δ_{sfzx} , δ_{sfzy} , and δ_{sfzz} are symmetrical about one axis. The influential sphere of deformation caused by the unit distribution force is restricted from 0 to 3.5 m. This is mainly attributed to the elastic modulus and Poisson's ratio of the soft foundation. Maximum deformation ranges from $7.93e-8m$ at the first step to $1.26e-7m$ at the final step. It shows a 59.52% increment within the time. Overall, the Lee's method can be well used to describe the creep property of soft foundation.

Figure 8 shows the contact forces in three directions by two methods on the 30th day. Figure 9 shows the contact forces in three directions by two methods on the 1200th day. Figure 10 shows the deformation of the center point in the

contact surface. Through the contrastive analysis of our method and AL method, some similarities and differences can be shown:

- (1) From the distribution of contact forces perspective, both of the two methods almost have the same distribution of contact forces. The contact forces in x direction are fan-shaped distribution and focused on the boundary. The contact forces in y direction are symmetrical about x -axis. The contact forces in z direction are basin-shaped distribution. Our method has larger values of corner points than the AL method. The reason behind this scenario may be that the deformation of soft foundation in Lee's method is different with finite method. Overall, contact forces can be well solved by our method.

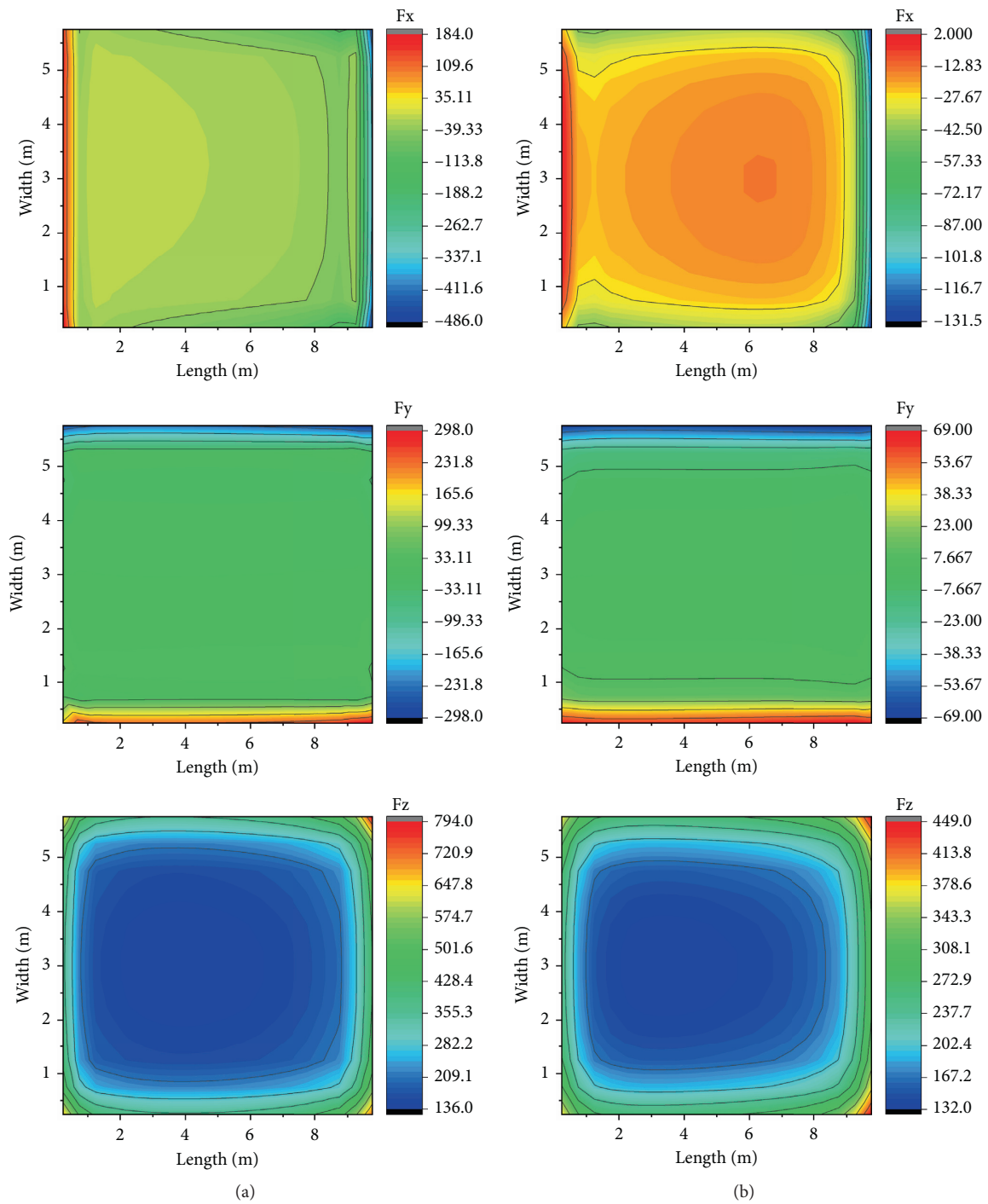


FIGURE 8: Distribution of contact forces in three directions by two methods on 30th day. (a) Our method. (b) Augmented Lagrangian method.

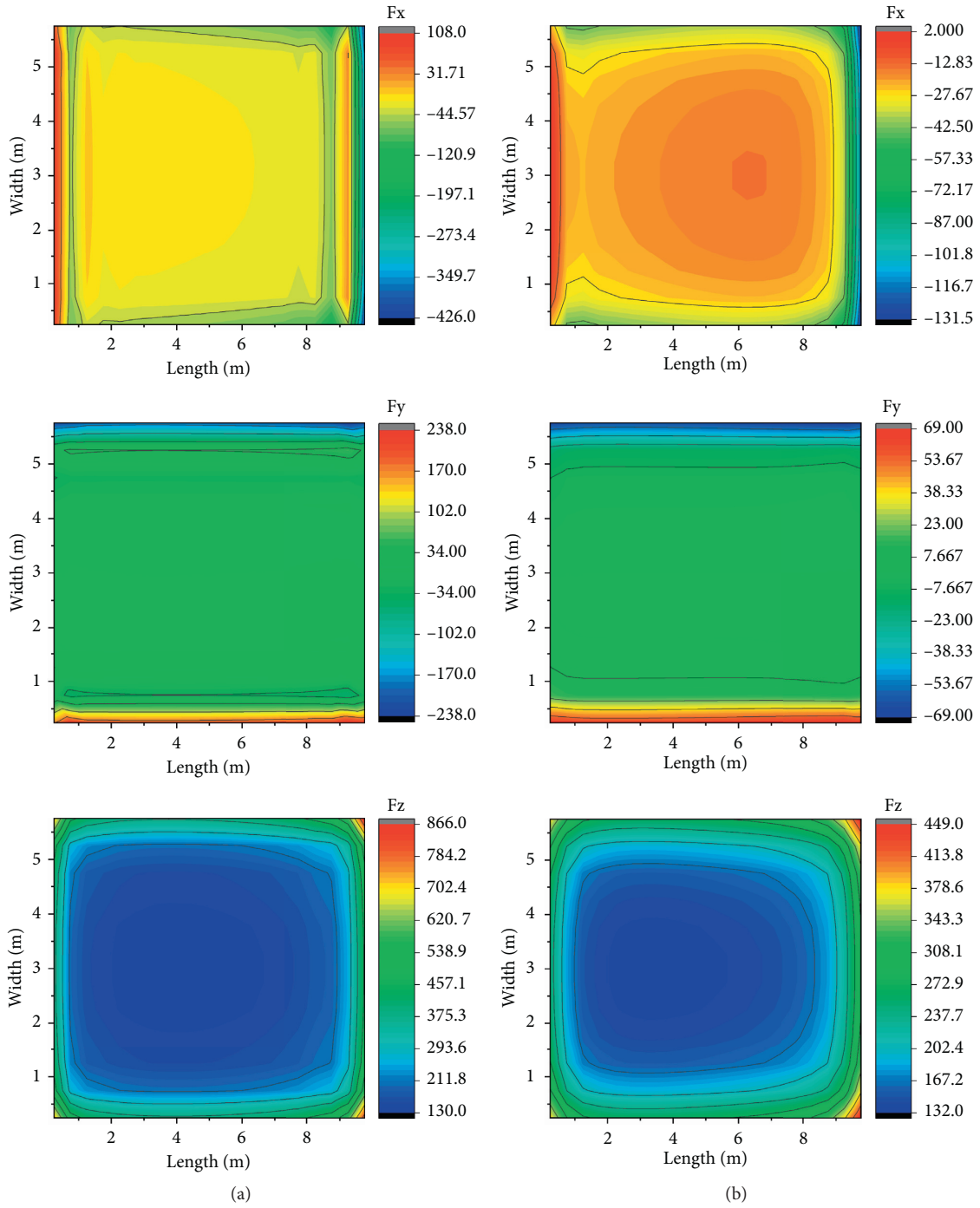


FIGURE 9: Distribution of contact forces in three directions by two methods on 1200th day. (a) Our method. (b) Augmented Lagrangian method.

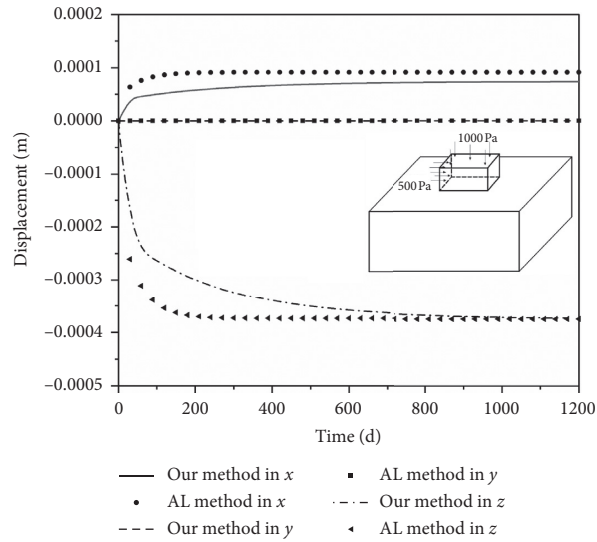


FIGURE 10: Deformation of the center point in the contact surface.

- (2) From the creep property perspective, our method shows the redistribution of the contact forces. The maximum contact force in z direction increases from 796N to 868N, with 9.01% increment. However, the maximum contact forces in x and y directions, respectively, decrease from 464N to 410N and 286N to 236N, with 13.17% and 21.19% reduction.
- (3) From deformations perspective, the displacements of our method are more viscous than the AL method with time changing. Both of them almost have the same final settlement displacement and displacement in x direction.

The difference between our method and the AL method is mainly influenced by the solution of foundation. The AL method is based on the finite element method and related to the size of the foundation model. The analytical method is based on the Laplace transformation and irrelevant to the size of the foundation model. Therefore, the results are influenced by two reasons: (1) the principle of calculation; (2) the size of foundation model. The heavy loading combination and large size of the foundation model can make these differences not obvious. In this example, the external loads are in x and z directions and the length, width, and height of the foundation are three times of the structure. The results show good agreement in the final settlement displacement and displacement in x and z directions with the AL method and proposed method, while there exists large difference in y direction.

8.2. Example 2. Example 1 shows that our method has well adaptability. The local disengagement of contact surface is shown in example 2. The basic situation of this example is the same as example 1, but the external forces are different with example 1. The upper surface of the structure is affected by pressure and tension. The pressure acting on the left square (4.5 m*6 m) and right square (4.5 m*6 m) is 10 kPa. The tension acting on the middle square (1.0 m*6 m) is 8.9 kPa.

Figure 11 shows the contact forces in three directions on the 30th and the 1200th day. The contact forces in z direction are directly affected by the external forces. It represents that there are negative contact forces in the middle of the contact surface. It means the local disengagement phenomenon appears. Actually, these negative contact forces in the disengagement area are zeros. By comparing the positive with negative values, the disengagement area can be intuitively found. After the contact forces redistribute, the real contact state and contact forces are explicitly calculated. The total time of the process is usually less than 10 seconds. The deformation of the center point in the contact surface is shown in Figure 12, where the center point is in the disengagement area. The displacement of the point in z direction has creep property. As time increases, the disengagement area will gradually close, and the contact forces will regenerate. The disengagement area does not always exist.

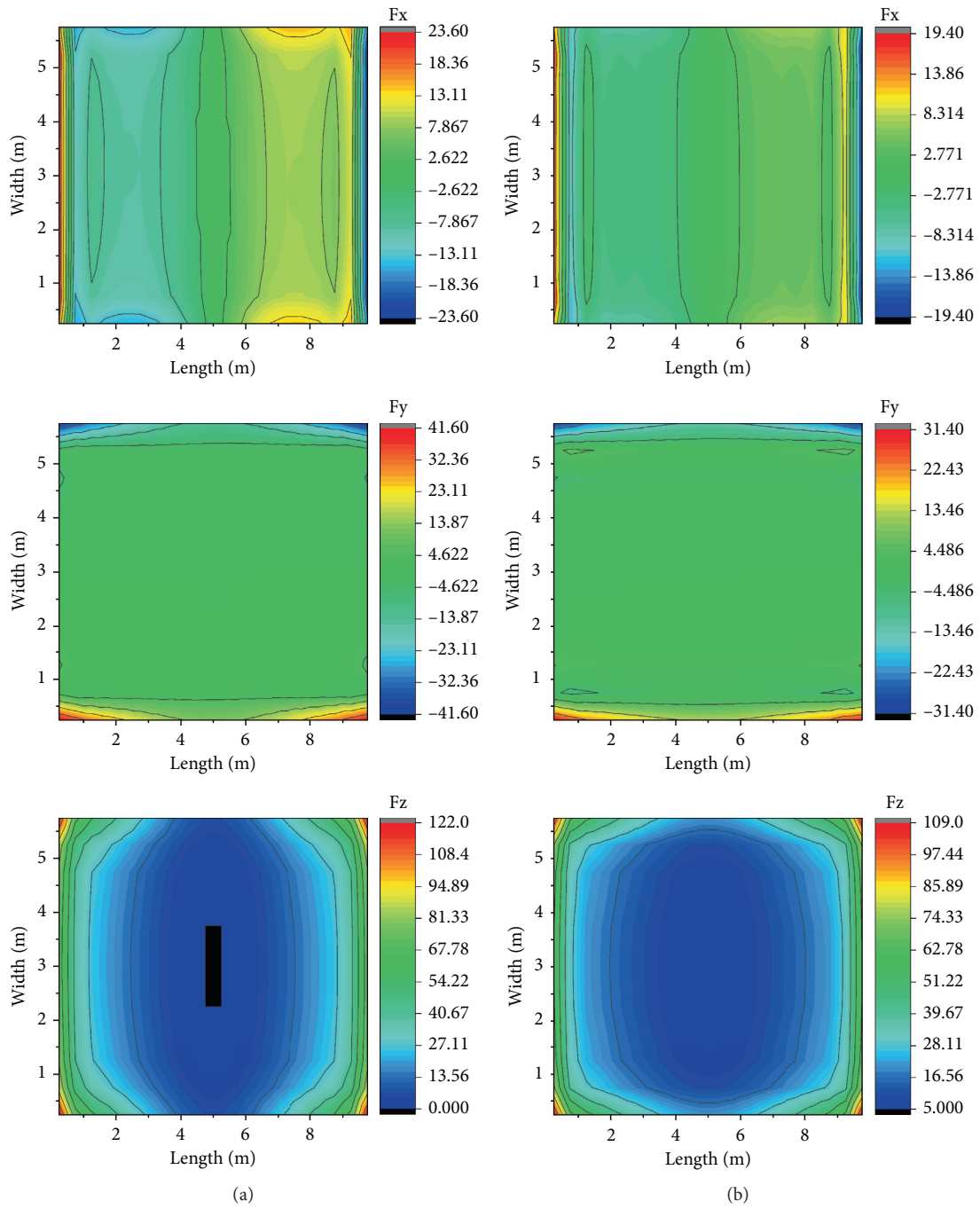


FIGURE 11: Contact forces in three directions. (a) Contact forces at 30th d. (b) Contact forces at 1200th d.

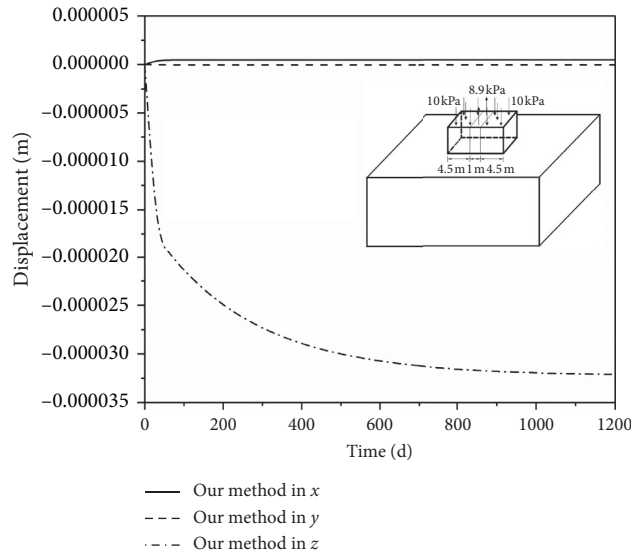


FIGURE 12: Deformation of the center point in the contact surface.

9. Conclusion

This paper reports a methodology to analyze the time affection on a structural soft foundation system. The contact forces are treated as unknown variables and act on the structure and foundation separately. The deformation of structure contains the statically determinate structural deformation and rigid body displacement. It can be solved by the finite method. The creep deformation of soft foundation is solved by Lee’s method. The final equations are formed by the deformation coordination equations and equilibrium equations. It is solved by the Gaussian elimination with the partial pivoting method. The augmented Lagrangian method is used to verify the accuracy of the method. The following important conclusions are summarized:

- (1) The simulations of contact bodies show that our method shows more viscous than the AL method

with time changing. Our method has larger values of corner points than the AL method.

- (2) This methodology is an explicit calculating method, avoiding the occurrence of iteration non-convergence. It is simpler and more efficient in solving the contact forces compared with the AL method.
- (3) It is shown that our method can directly describe local disengagement of two contact bodies. The redistribution phenomenon of contact forces is well shown with time changing.

Appendix

The analytical solution of viscoelastic deformation based on the Maxwell model can be calculated by MATLAB. The codes are as follows:

<pre> %% in x direction, laplacetransform syms inta1 G2 G3 s K a b fk fi fg x y p1 = inta1/G2; q1 = (G3/G2 + 1)*inta1; xs = 2*(G3 + q1*s)/(1 + p1*s) miu_0 = (3*K - xs)/(6*K + xs) e_0 = 9*K*xs/(6*K + xs) udx_la = (1 + miu_0)/(pi*e_0*a*b)*((1 - miu_0)*fk + miu_0*x*x*fg)/s; udy_la = (1 + miu_0)*miu_0/(pi*e_0*a*b)*x*y*fg/s udz_la = (1+miu_0)*(1 - 2*miu_0)/(2*pi*e_0*a*b)*x*fi/s udx_ila = ilaplace(udx_la, s) udy_ila = ilaplace(udy_la, s) udz_ila = ilaplace(udz_la, s) %% laplace inverse transform syms inta1 G2 G3 s K a b fk fi fg x y t t01 = t; disp -----udx----- udx = subs(udx_ila, [s], [t01]) disp -----udy----- udy = subs(udy_ila, [s], [t01]) disp -----udz----- udz = subs(udz_ila, [s], [t01]) </pre>	<pre> %% in z direction, laplacetransform syms inta1 G2 G3 s K a b fk x y p1 = inta1/G2; q1 = (G3/G2 + 1)*inta1 xs = 2*(G3 + q1*s)/(1 + p1*s) miu_0 = (3*K - xs)/(6*K + xs) e_0 = 9*K*xs/(6*K + xs) wdx_la = (1 + miu_0)*(2*miu_0 - 1)/(2*pi*e_0*a*b)/s*x/((x^2 + y^2)^(1/2))*fk wdy_la = (1 + miu_0)*(2*miu_0 - 1)/(2*pi*e_0*a*b)/s*y/((x^2 + y^2)^(1/2))*fk wdz_la = (1 - miu_0*miu_0)/(a*b*pi*e_0)/s*fk wdx_ila = ilaplace(wdx_la, s) wdy_ila = ilaplace(wdy_la, s) wdz_ila = ilaplace(wdz_la, s) %% laplace inverse transform syms inta1 G2 G3 s K a b fk x y t t01 = t; disp -----wdx----- wdx = subs(wdx_ila, [s], [t01]) disp -----wdy----- wdy = subs(wdy_ila, [s], [t01]) disp -----wdz----- wdz = subs(wdz_ila, [s], [t01]) </pre>
---	--

Data Availability

The data used to support the findings of this study are included in the article.

Conflicts of Interest

The authors declare that there are no conflicts of interest regarding the publication of this paper.

Acknowledgments

This work was supported by the National Natural Science Foundation of China (no. 51579089).

References

- [1] N. O. Mohamad, C. E. Razali, A. A. Hadi et al., "Challenges in construction over soft soil - case studies in Malaysia," *IOP Conference Series: Materials Science and Engineering*, vol. 136, Article ID 0, 2016.
- [2] A. D. KR, "Soil mechanics and foundation engineering," 2006.
- [3] L. Zhang, Q. Yang, and Y. Liu, "Long-term stability analysis of the left bank abutment slope at Jinping I hydropower station," *Journal of Rock Mechanics and Geotechnical Engineering*, vol. 8, no. 3, pp. 398–404, 2016.
- [4] R. Wang, W. Xu, Y. Meng, H. Chen, and Z. Zhou, "Numerical analysis of long-term stability of left bank abutment high slope at Jinping I hydropower station," *Yanshilixue Yu Gongcheng Xuebao/Chinese Journal of Rock Mechanics and Engineering*, vol. 33, no. s1, pp. 3105–3113, 2014.
- [5] H. Hertz, "Über die berührung fester Elastischer Körper," *Journal für die reine und angewandte Mathematik (Crelles Journal)*, vol. 92, pp. 156–171, 1981.
- [6] A. Signorini, "Questioni di elasticità non linearizzata e semilinearizzata," *Rendiconti di Matematica e delle sue Applicazioni*, vol. 18, no. 5, pp. 95–139, 1959.
- [7] M. S. Kaschiev and K. Mikhajlov, "A beam resting on a tensionless Winkler foundation," *Computers & Structures*, vol. 55, no. 2, pp. 261–264, 1995.
- [8] D.-S. Yang and C. M. Wang, "Dynamic response and stability of an inclined Euler beam under a moving vertical concentrated load," *Engineering Structures*, vol. 186, pp. 243–254, 2019.
- [9] Z. Dimitrovová, "Complete semi-analytical solution for a uniformly moving mass on a beam on a two-parameter viscoelastic foundation with non-homogeneous initial conditions," *International Journal of Mechanical Sciences*, vol. 144, pp. 283–311, 2018.
- [10] A. Francavilla and O. C. Zienkiewicz, "A note on numerical computation of elastic contact problems," *International Journal for Numerical Methods in Engineering*, vol. 9, no. 4, pp. 913–924, 1975.
- [11] A. Klarbring, "A mathematical programming approach to three-dimensional contact problems with friction," *Computer Methods in Applied Mechanics and Engineering*, vol. 58, no. 2, pp. 175–200, 1986.
- [12] A. Klarbring and G. Björkman, "A mathematical programming approach to contact problems with friction and varying contact surface," *Computers & Structures*, vol. 30, no. 5, pp. 1185–1198, 1988.
- [13] D. G. Luenberger and Y. Ye, *Linear and Nonlinear Programming*, Springer, Berlin, Germany, 1984.
- [14] J. C. Simo and T. A. Laursen, "An augmented Lagrangian treatment of contact problems involving friction," *Computers & Structures*, vol. 42, no. 1, pp. 97–116, 1992.
- [15] R. E. Goodman, R. L. Taylor, and T. L. Brekke, "A model for the mechanics of jointed rock," *Journal of Soil Mechanics & Foundations Div*, vol. 94, no. 3, pp. 637–659, 1968.
- [16] J. Machalová and H. Netuka, "Solution of contact problems for nonlinear Gao beam and obstacle," *Journal of Applied Mathematics*, vol. 2015, pp. 1–12, Article ID 420649, 2015.
- [17] J. Machalová and H. Netuka, "Solution of contact problems for Gao beam and elastic foundation," *Mathematics and Mechanics of Solids*, vol. 23, no. 3, pp. 473–488, 2018.
- [18] D. Gao, J. Machalová, and H. Netuka, "Mixed finite element solutions to contact problems of nonlinear Gao beam on elastic foundation," *Nonlinear Analysis: Real World Applications*, vol. 22, pp. 537–550, Elsevier, Amsterdam, Netherlands, 2015.
- [19] K. Terzaghi, "Theoretical soil mechanics," 1943.
- [20] M. A. Biot, "General theory of three-dimensional consolidation," *Journal of Applied Physics*, vol. 12, no. 2, pp. 155–164, 1941.
- [21] Y. Chen, G. Chen, and X. Xie, "Weak Galerkin finite element method for Biot's consolidation problem," *Journal of Computational and Applied Mathematics*, vol. 330, pp. 398–416, 2018.
- [22] M. Borregales, K. Kumar, F. A. Radu, C. Rodrigo, and F. J. Gaspar, "A partially parallel-in-time fixed-stress splitting method for Biot's consolidation model," *Computers & Mathematics with Applications*, vol. 77, no. 6, pp. 1466–1478, 2019.
- [23] L. Wang, Y. Xu, X. Xia, and A. Zhou, "Semi-analytical solutions to the two-dimensional plane strain consolidation for unsaturated soil with the lateral semi-permeable drainage boundary under time-dependent loading," *Computers and Geotechnics*, vol. 124, Article ID 103562, 2020.
- [24] J. Mitchell and A. Singh, "General stress-strain-time function for soils," *ASCE*, vol. 94, no. 1, pp. 21–46, 1968.
- [25] F. Cavalieri, A. A. Correia, H. Crowley, and R. Pinho, "Dynamic soil-structure interaction models for fragility characterisation of buildings with shallow foundations," *Soil Dynamics and Earthquake Engineering*, vol. 132, Article ID 106004, 2020.
- [26] Z. Chang, H. Gao, F. Huang, J. Chen, J. Huang, and Z. Guo, "Study on the creep behaviours and the improved burgers model of a loess landslide considering matric suction," *Natural Hazards*, vol. 103, no. 1, pp. 1479–1497, 2020.
- [27] X. Li, M. Huang, and L. Wang, "Bounding surface elastoviscoplastic constitutive model for rheological behaviors of soft clays," *Chinese Journal of Rock Mechanics and Engineering*, vol. 26, no. 7, pp. 1393–1401, 2007.
- [28] V. M. G. Zapata, E. B. Jaramillo, and A. O. Lopez, "Implementation of a model of elastoviscoplastic consolidation behavior in Flac 3D," *Computers and Geotechnics*, vol. 98, pp. 132–143, 2018.
- [29] E. H. Lee, "Stress analysis in visco-elastic bodies," *Quarterly of Applied Mathematics*, vol. 13, no. 2, pp. 183–190, 1955.
- [30] M. Müser and V. L. Popov, "Contact mechanics and friction: physical principles and applications," *Tribology Letters*, vol. 40, no. 3, p. 395, 2010.
- [31] Q. Kan, W. Yan, G. Kang, and Q. Sun, "Oliver-pharr indentation method in determining elastic moduli of shape memory alloys-A phase transformable material," *Journal of the Mechanics and Physics of Solids*, vol. 61, no. 10, pp. 2015–2033, 2013.